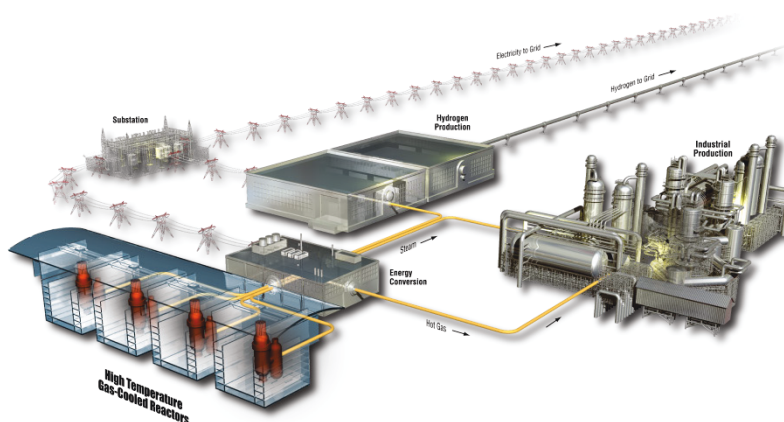


AGR-2 Irradiated Test Train Preliminary Inspection and Disassembly First Look

Scott Ploger, Paul Demkowicz, Jason Harp

May 2015

The INL is a
U.S. Department of Energy
National Laboratory
operated by
Battelle Energy Alliance



DISCLAIMER

This information was prepared as an account of work sponsored by an agency of the U.S. Government. Neither the U.S. Government nor any agency thereof, nor any of their employees, makes any warranty, expressed or implied, or assumes any legal liability or responsibility for the accuracy, completeness, or usefulness, of any information, apparatus, product, or process disclosed, or represents that its use would not infringe privately owned rights. References herein to any specific commercial product, process, or service by trade name, trade mark, manufacturer, or otherwise, does not necessarily constitute or imply its endorsement, recommendation, or favoring by the U.S. Government or any agency thereof. The views and opinions of authors expressed herein do not necessarily state or reflect those of the U.S. Government or any agency thereof.

AGR-2 Irradiated Test Train Preliminary Inspection and Disassembly First Look

Scott Ploger, Paul Demkowicz, Jason Harp

May 2015

**Idaho National Laboratory
INL ART TDO Program
Idaho Falls, Idaho 83415**

<http://www.inl.gov>

**Prepared for the
U.S. Department of Energy
Office of Nuclear Energy
Under DOE Idaho Operations Office
Contract DE-AC07-05ID14517**

ART Program

AGR-2 Irradiated Test Train Preliminary Inspection and Disassembly First Look

INL/EXT-15-34997

May 2015

Author:



Scott Ploger

5-19-2015
Date

Reviewed by:



Francine Rice

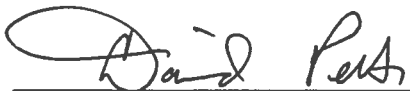
5-20-2015
Date

Approved by:




Paul Demkowicz
ART TRISO Fuels PIE Technical Lead

5/19/15
Date



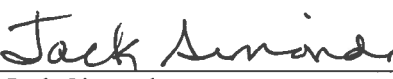
David Petti
Director, ART Technology Development Office

5/19/15
Date



Kirk Bailey
ART Quality Assurance

5-19-2015
Date



Jack Simonds
Program Manager, ART Fuels

05/19/2015
Date

SUMMARY

The AGR-2 irradiation experiment began in June 2010 and was completed in October 2013. The test train was shipped to the Materials and Fuels Complex in July 2014 for post-irradiation examination (PIE). The first PIE activities included nondestructive examination of the test train, followed by disassembly of the test train and individual capsules and detailed inspection of the capsule contents, including the fuel compacts and their graphite fuel holders. Dimensional metrology was then performed on the compacts, graphite holders, and steel capsule shells. AGR-2 disassembly and metrology were performed with the same equipment used successfully on AGR-1 test train components.

Gamma spectrometry of the intact test train gave a preliminary look at the condition of the interior components. No evidence of damage to compacts or graphite components was evident from the isotopic and gross gamma scans.

Disassembly of the AGR-2 test train and its capsules was conducted rapidly and efficiently by employing techniques refined during the AGR-1 disassembly campaign. Only one major difficulty was encountered while separating the test train into capsules when thermocouples (of larger diameter than used in AGR-1) and gas lines jammed inside the through tubes of the upper capsules, which required new tooling for extraction. Disassembly of individual capsules was straightforward with only a few minor complications. On the whole, AGR-2 capsule structural components appeared less brittle than their AGR-1 counterparts.

Compacts from AGR-2 Capsules 2, 3, 5, and 6 were in very good condition upon removal. Only relatively minor damage or markings were visible using high resolution photographic inspection. Compact dimensional measurements indicated radial shrinkage between 0.8 to 1.7%, with the greatest shrinkage observed on Capsule 2 compacts that were irradiated at higher temperature. Length shrinkage ranged from 0.1 to 0.9%, with by far the lowest axial shrinkage on Capsule 3 compacts—possibly as a consequence of lower packing fraction. Differences in fast neutron fluence among compacts from these four capsules had no obvious effect on radial and axial shrinkage. (The AGR-2 experiment included Capsule 1 containing French compacts and Capsule 4 with compacts made at Oak Ridge National Laboratory using South African fuel particles. Information on these two batches of AGR-2 fuel compacts is confined to restricted Appendices A and B because of proprietary information limitations.)

The AGR-2 boronated graphite holders were in very good condition upon extraction although minor damage occurred to one holder during disassembly. Two other holders were slightly damaged when subsequently handled for metrology imaging. Graphite holder outer diameters expanded in Capsules 2 through 5 by approximately 0.1 to 0.5%, with the least expansion in the hottest Capsule 2 holder. By contrast, the graphite holders from end Capsules 1 and 6 exhibited diametral shrinkage of 0.2 to 0.6% with significantly greater shrinkage near the top and bottom of the AGR-2 test train (regions of lowest neutron fluence). The dramatic difference in diametral change behavior between the interior four graphite holders and the two holders at the ends of the test train is not clearly related to B₄C concentration. The diameters of holder holes for fuel compacts generally also enlarged in Capsules 2 through 5.

Bore gauge measurements indicated significant reductions of inner diameters in AGR-2 capsule shells. Rather than irradiation-induced deformation, these measurements reflected accumulation of unknown deposits on interior shell liner surfaces. Similar deposits were also found on interior surfaces of capsule heads and capsule floors, as well as on some graphite holder surfaces. The AGR-2 shell liner deposits are consistent in thickness with those measured inside AGR-1 shells.

No quantitative requirements on measurement uncertainty were specified for AGR-2 components to allow for potential degradation during the 3.5-year interval following the AGR-1 metrology campaign, as well as from the extensive remote handling to place the contaminated equipment into storage and return it to service. Nevertheless, performance checks with in-cell standards indicated that the demanding AGR-1 uncertainty requirements were still satisfied during the AGR-2 campaign.

ACKNOWLEDGEMENTS

The authors wish to extend their appreciation to Cad Christensen, Jeffrey McCanch, Les Scott, Brian Simmons, and Katelyn Wachs at the Idaho National Laboratory's Hot Fuel Examination Facility for their competence, cooperation, care, and patience in coordinating and performing the post-irradiation examination tasks described in this report.

CONTENTS

SUMMARY	v
ACKNOWLEDGEMENTS	vi
ACRONYMS	xiii
1. INTRODUCTION	1
2. AGR-2 RECEIPT AND NONDESTRUCTIVE TESTING	5
2.1 Receipt and Inspection of AGR-2 Test Train.....	5
2.2 AGR-2 Test Train Gamma Scanning	6
3. AGR-2 DISASSEMBLY	8
3.1 Basic Disassembly Equipment.....	8
3.2 Capsule Separation.....	9
3.3 Capsule Disassembly	11
4. METROLOGY	16
4.1 Metrology Equipment	16
4.2 Fuel Compact Inspections	18
4.3 AGR-2 Compact Dimensional Changes	21
4.4 Graphite Holder Inspections	28
4.5 Graphite Holder Dimensional Changes	33
4.5.1 Metrology Results from Capsule 1 Graphite Holder	35
4.5.2 Metrology Results from Capsule 2 Graphite Holder	36
4.5.3 Metrology Results from Capsule 3 Graphite Holder	38
4.5.4 Metrology Results from Capsule 4 Graphite Holder	40
4.5.5 Metrology Results from Capsule 5 Graphite Holder	41
4.5.6 Metrology Results from Capsule 6 Graphite Holder	42
4.5.7 Graphite Holder Comparisons	44
4.6 Capsule Shell Findings.....	45
5. CONCLUSIONS	49
6. REFERENCES	50
Appendix A Proprietary Results on Capsule 1 Fuel Compacts	51
Appendix B Proprietary Results on Capsule 4 Fuel Compacts.....	52

FIGURES

Figure 1. X-radiographs of U.S. UCO (compact LEU09-OP2-Z002, left) and UO2 (compact LEU11-OP2-Z018, right) compacts taken from the same compact lots used in the AGR-2 irradiation. Images taken from Hunn et al. 2010c.....	2
--	---

Figure 2. Cross-sectional diagram of an AGR-2 capsule (viewed from top).....	3
Figure 3. Numbering scheme for AGR-2 compacts in Capsule 1 (left) and Capsules 2-6 (right).	4
Figure 4. AGR-2 test train in a hot cell at the Hot Fuel Examination Facility.	5
Figure 5. Attachment of gamma scanning fixture to top of AGR-2 test train.....	5
Figure 6. Activation product (Co-60) and fission product (Cs-137) intensity from gamma scanning of the AGR-2 test train Stack 1 and Stack 3. Note that data from Capsules 4 and 1 have been omitted from the plot. The region from 160 to 175 cm represents the test train tail piece.....	7
Figure 7. Activation product (Co-60) and fission product (Cs-137) intensity from gamma scanning of the AGR-2 test train Stack 2 and Stack 3. Note that data from Capsules 4 and 1 have been omitted from the plot. The test train tail was not scanned when Stack 2 and 3 were scanned.....	7
Figure 8. Slide table with disassembly and metrology equipment.....	8
Figure 9. Rail-mounted left vise, support cradle, and right vise, plus several tools for capsule disassembly.....	8
Figure 10. Circumferential cuts made to separate capsules and to disassemble each capsule.....	9
Figure 11. Separating the upper capsule from remainder of AGR-2 test train.	9
Figure 12. Using two wedges to pry Capsule 6 (under toggle clamp) away from Capsule 5.....	10
Figure 13. Forcing vises apart with a jacking screw to separate Capsule 6 (in left vise).	10
Figure 14. TC leads and gas lines pulled from the lower test train during separation of Capsule 5.....	11
Figure 15. Bottom of AGR-2 Capsule 2 following floor separation.....	12
Figure 16. Arrangement for removing capsule shells.	12
Figure 17. Mirror view of prying a through tube away from a holder base with a rod and special fixture.....	13
Figure 18. Cutting stuck thermocouples and gas lines between capsule head and graphite holder.....	13
Figure 19. Pushing a stack of compacts into the aluminum fuel holder.	14
Figure 20. Moving the aluminum compact holder from the shell replacement spacer onto the twin roller table.....	14
Figure 21. Fuel compact being loaded from twin roller table into its individual compact container.	15
Figure 22. AGR noncontact metrology system during remote qualification.	17
Figure 23. Performing a verification on the small bore gauge (used in graphite holder holes).	17
Figure 24. Typical appearance of irradiated AGR-2 fuel compacts (2-2-3 at left, 3-3-2 at right).	18
Figure 25. Two sides of accidentally dropped Compact 6-2-2.	19
Figure 26. Chipped top corners on Compact 2-4-1 (left) and Compact 5-4-1 (right).	19
Figure 27. Axially oriented abrasions on the 240° (left) and 90° (right) sides of Compact 5-1-3.	20
Figure 28. Axial marks from apparent abrasion near the bottoms of Compacts 5-1-2 (left) and 3-2-3 (right).	21
Figure 29. Shallow transverse and angled marks on Compacts 6-4-2 (left) and 6-4-3 (right).	21

Figure 30. Example of analyzed compact image (here Compact 6-2-3).....	22
Figure 31. Average diameter changes among fuel compacts from AGR-2 Capsules 6, 5, 3, and 2.	25
Figure 32. Average length changes among AGR-2 compacts from Capsules 6, 5, 3, and 2.	25
Figure 33. Length change versus diameter change for compacts from Capsules 2, 3, 5, and 6.....	26
Figure 34. Percentage changes in compact diameter versus time-average volume-average temperature.	27
Figure 35. Percentage changes in compact length versus time-average volume-average temperature.	27
Figure 36. Average compact diameter changes versus calculated fast neutron fluence ($E >$ 0.18 MeV).....	28
Figure 37. Average compact length changes versus calculated fast neutron fluence ($E >$ 0.18 MeV).....	28
Figure 38. Holder 1 before separation from head assembly (top image, bottom end at right) and after head separation (bottom image, top end at right).	29
Figure 39. Holder 2, before (top) and after (bottom) head separation, bottom ends on right side.....	30
Figure 40. Thick deposit patches (top) and handling fracture on Holder 3, bottom ends on right side.....	31
Figure 41. 0° azimuth of Holder 4, bottom end on right side (upper image) and bottom end left (lower image).....	32
Figure 42. 120° azimuth of Holder 5 (top) and 240° azimuth (bottom), bottom ends on right side.....	32
Figure 43. Two azimuths of Holder 6, bottom end to right (upper image) and bottom end to left (lower image).....	33
Figure 44. Example of an analyzed graphite holder image with blue lines at diameter measurement locations.	34
Figure 45. Small bore gauge before inserting probe tip into Holder 1.	34
Figure 46. Individual OD measurements from 0° composite image of Capsule 1 graphite holder.	35
Figure 47. Bore gauge measurements inside Holder 1 holes after unloading fuel compacts.....	36
Figure 48. OD measurements from 240° azimuth image of the Capsule 2 graphite holder.	37
Figure 49. Hole IDs measured inside the Capsule 2 graphite holder (all $\pm 0.0214 \text{ mm}$).	38
Figure 50. OD measurements from 120° azimuth image of the Capsule 3 graphite holder (excluding top two measurements enlarged by crack).....	39
Figure 51. Hole IDs measured inside the Capsule 3 graphite holder (all $\pm 0.0214 \text{ mm}$).	39
Figure 52. OD measurements from 0° azimuth image of the Capsule 4 graphite holder.	40
Figure 53. Hole IDs measured inside the Capsule 4 graphite holder (all $\pm 0.0214 \text{ mm}$).	41
Figure 54. OD measurements from 120° azimuth image of the Capsule 5 graphite holder.	41
Figure 55. Hole IDs measured inside the Capsule 5 graphite holder (all $\pm 0.0214 \text{ mm}$).	42
Figure 56. OD measurements from 0° azimuth image of the Capsule 6 graphite holder.	43
Figure 57. Hole IDs measured inside the Capsule 6 graphite holder (all $\pm 0.0214 \text{ mm}$).	43

Figure 58. Graphite holder ODs as a function of elevation within the AGR-2 test train.....	44
Figure 59. Relative changes in ODs of AGR-2 graphite holders during irradiation.....	44
Figure 60. ODs of AGR-1 graphite holders after irradiation (Holder 4 broken during disassembly).	45
Figure 61. AGR-2 capsule shell ID being measured by large bore gauge.	45
Figure 62. ID reductions (all± 0.0160 mm) inside AGR-2 capsule shells.	46
Figure 63. Deposits of unknown material throughout interiors of AGR-2 Shell 3 (left) and Shell 2 (right).	47
Figure 64. Dark deposit patches on insides of AGR-2 Capsule 2 head (left) and Capsule 6 floor (right).	48

TABLES

Table 1. Select characteristics of AGR-2 capsules.	2
Table 2. Dimensional changes (mm) and associated standard deviations (σ) from AGR-2 Capsule 2.	23
Table 3. Dimensional changes (mm) and associated standard deviations (σ) from AGR-2 Capsule 3.	23
Table 4. Dimensional changes (mm) and associated standard deviations (σ) from AGR-2 Capsule 5.	24
Table 5. Dimensional changes (mm) and associated standard deviations (σ) from AGR-2 Capsule 6.	24
Table 6. Exterior metrology results from the AGR-2 Capsule 1 graphite holder.	35
Table 7. Hole diameters in Capsule 1 graphite holder (drawing tolerances 12.598 to 12.675 mm).	36
Table 8. Exterior metrology results from the Capsule 2 graphite holder.	37
Table 9. Hole diameters in Capsule 2 graphite holder (drawing tolerances 12.370 to 12.446 mm).	37
Table 10. Exterior metrology results from AGR-2 Capsule 3 graphite holder.	38
Table 11. Hole diameters in Capsule 3 graphite holder (drawing tolerances 12.344 to 12.421 mm).	39
Table 12. Exterior metrology results from AGR-2 Capsule 4 graphite holder.	40
Table 13. Hole diameters in Capsule 4 graphite holder (drawing tolerances 12.319 to 12.395 mm).	40
Table 14. Exterior metrology results from AGR-2 Capsule 5 graphite holder.	41
Table 15. Hole diameters in Capsule 5 graphite holder (drawing tolerances 12.395 to 12.446 mm).	42
Table 16. Exterior metrology results from AGR-2 Capsule 6 graphite holder.	42
Table 17. Hole diameters in Capsule 6 graphite holder (drawing tolerances 12.395 to 12.446 mm).	43
Table 18. Capsule shell ID measurements and changes from as-fabricated values.	46

ACRONYMS

AGR	Advanced Gas Reactor
ART	Advanced Reactor Technologies
ATR	Advanced Test Reactor
CEA	Commissariat à l'énergie atomique
HFEF	Hot Fuel Examination Facility
ID	inner diameter
INL	Idaho National Laboratory
LED	light-emitting diode
NIST	National Institute of Standards and Technology
OD	outer diameter
ORNL	Oak Ridge National Laboratory
PGS	Precision Gamma Scanner
PIE	post-irradiation examination
SST	stainless steel
TAVA	time-average volume-average
TC	thermocouple
TRISO	tristructural isotropic
VHTR	very high temperature reactor

AGR-2 Irradiated Test Train Preliminary Inspection and Disassembly First Look

1. INTRODUCTION

The Advanced Gas Reactor (AGR) Fuel Development and Qualification Program was established to perform the requisite research and development on tristructural isotropic (TRISO) coated particle high-temperature gas-cooled reactor fuel to support deployment of a high temperature gas-cooled reactor (HTGR) as part of the Advanced Reactor Technologies (ART) Program. The overarching goal is to provide a baseline fuel qualification data set to support licensing and operation of a HTGR. Achieving these goals involves the elements of fuel fabrication, irradiation, post-irradiation examination (PIE) and safety testing, fuel performance modeling, and fission product transport (PLN-3636, Rev. 2, 2012).

A series of fuel irradiation experiments are in progress at the Advanced Test Reactor (ATR) at Idaho National Laboratory (INL). These experiments are intended to provide data on fuel performance under irradiation, support fuel process development, qualify the fuel for operating and accident conditions, provide irradiated fuel for safety testing, and support the development of fuel performance and fission product transport models. The first of these irradiation experiments, AGR-1, began in the ATR in December 2006 and was completed in November 2009. This experiment was intended to act as a shakedown test of the multi-capsule design and to provide early data on fuel performance for use in fuel fabrication process refinement along with samples for post-irradiation safety testing. The second irradiation experiment, AGR-2, began in June 2010 and ended on October 16, 2013, after 559 effective full power days in the ATR, achieving a peak burnup in the U.S. fuel capsules of 13.2% fissions per initial heavy metal atom. The AGR-2 irradiation experiment was designed to provide fuel performance data for coated particles industrially fabricated on an engineering scale pilot line using a 150-mm (6-inch) diameter coater. The AGR-2 test train included six independent capsules containing fuel compacts made from particles with kernels of either uranium carbide/uranium oxide (known as UCO) or uranium oxide (UO₂). The AGR-2 fuel, test train, and experiment description are summarized in the AGR-2 Test Plan (Collin 2011). Actual AGR-2 irradiation conditions and accumulated neutron exposures are presented in the AGR-2 Irradiation Test Final As-Run Report (Collin 2014).

As discussed below, the AGR-2 experiment included Capsule 1 containing French compacts and Capsule 4 with compacts made at Oak Ridge National Laboratory (ORNL) with South African fuel particles. Information on these two batches of AGR-2 fuel compacts and associated PIE results are confined to restricted Appendices A and B because of proprietary information limitations. Two different types of fuel kernels were used in the remaining four AGR-2 capsules: (1) low enriched UCO with a mean diameter of 426.7 μm and U enrichment of 14.03%; and (2) low enriched UO₂ with a mean diameter of 507.7 μm and U enrichment of 9.60%. Both sets of kernels were fabricated at Babcock and Wilcox Nuclear Operations Group, where the TRISO coatings were also applied. The coating process conditions were derived from the production of the AGR-1 Variant 3 fuel.

The coated particles for AGR-2 Capsules 2, 3, 5, and 6 were formed into right cylindrical compacts (approximately 25-mm long and 12.3 mm in diameter) at ORNL. The compact matrix material is composed of a mixture of graphite and a thermosetting epoxy resin. The same compacting process was used for the UCO and UO₂ particles, and it was similar to the AGR-1 process. Figure 1 shows x-radiographs of the two types of compacts, where the 37% packing fraction of the UCO compact is conspicuously higher than the 23% packing fraction of the UO₂ compact (Collin 2011). The AGR-2 compacts had much thinner fuel-free zones at the axial ends of the compacts (end caps) compared to the AGR-1 compacts.

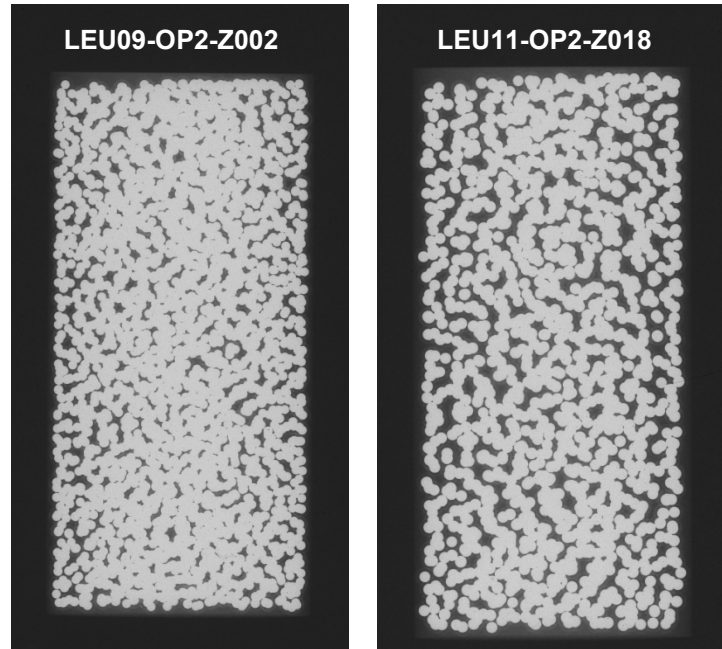


Figure 1. X-radiographs of U.S. UCO (compact LEU09-OP2-Z002, left) and UO₂ (compact LEU11-OP2-Z018, right) compacts taken from the same compact lots used in the AGR-2 irradiation. Images taken from Hunn et al. 2010c.

The basic design of the AGR-2 test train was very similar to that of the AGR-1 experiment. Each of the six capsules was independently controlled for temperature and independently monitored for fission product release. Each capsule was approximately 150 mm (6 inches) in length and 36 mm (1.4 inches) in diameter. Each AGR-2 capsule contained a specific fuel type. Table 1 lists the fuel in each AGR-2 capsule, along with other important characteristics. The capsules are listed in Table 1 in the same physical arrangement that they were placed in the reactor (i.e., Capsule 6 is at the top of the test train). Four of the capsules contained U.S. UCO or UO₂ fuel. Capsule 4 contained UO₂ fuel compacts fabricated at ORNL using coated particles from South Africa while Capsule 1 contained 50-mm long compacts containing UO₂ coated particles and fabricated by Commissariat à l'énergie atomique (CEA) in France. The Capsule 4 compacts have similar dimensions to the U.S. compacts while the Capsule 1 compacts are slightly wider as well as approximately twice as long.

Table 1. Select characteristics of AGR-2 capsules.

Capsule	Fuel Type^a	Graphite Holder Boron Carbide Content (w/o)^a	As-fabricated Radial Control Gap (mm)
6	United States, UCO kernels	4.83	0.635
5	United States, UCO kernels	5.75	0.394
4	South Africa, UO ₂ kernels	4.92	0.787
3	United States, UO ₂ kernels	4.92	0.787
2	United States, UCO kernels	5.75	0.686
1	France, UO ₂ kernels	4.29	0.635

a. Collin 2011.

Capsules 2 through 6 each contained a total of twelve compacts in three stacks while Capsule 1 contained six compacts. A cross-sectional view of an AGR-2 capsule is shown in Figure 2. The capsules

consisted of a graphite fuel holder with holes machined for insertion of fuel compacts, thermocouples (TCs), encapsulated melt and flux wires, and niobium through tubes to pass gas lines and TC leads from lower capsules in the test train. The graphite fuel holders contained boron carbide (B_4C) as a burnable poison to provide power leveling during the early stages of irradiation and provide a more uniform particle power level throughout the experiment. Initial weight percentages of B_4C are listed in Table 1. Stacks 1 and 2 were oriented closer to the reactor core than Stack 3 (see Figure 2), which would have produced much higher neutron fluxes in Stacks 1 and 2. To partially counteract this effect, a combination of hafnium and stainless steel shrouds surrounded the graphite holder to provide a more uniform neutron flux during the experiment. The entire assembly was encapsulated in a stainless steel (SST) outer shell. As listed in Table 1, gaps of different sizes were created between the graphite holders and the capsule shell liners to aid in temperature control. Nubs were placed around each shell to center the test train within the B-12 cavity in the ATR with a double row facing the core center.

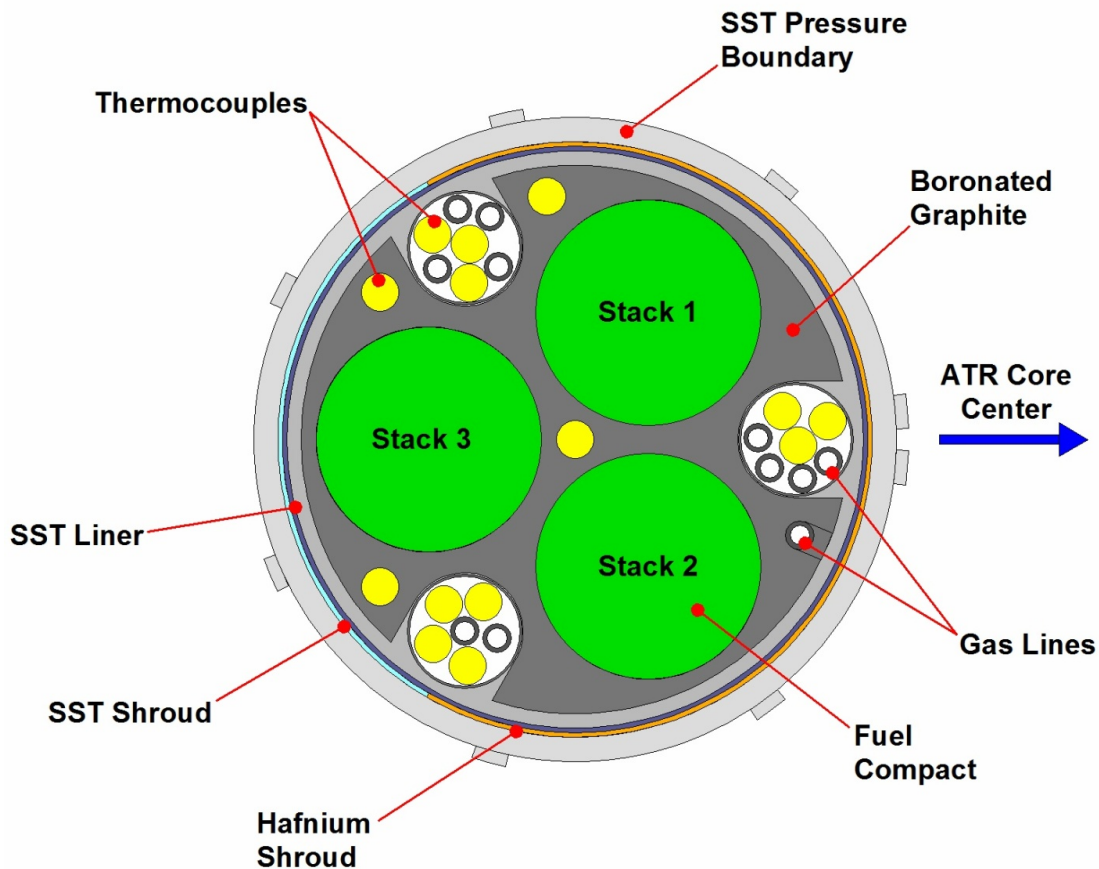


Figure 2. Cross-sectional diagram of an AGR-2 capsule (viewed from top).

A numbering system was developed to uniquely identify each fuel compact in the test train. This is based on the specific capsule, level, and stack number. Figure 3 identifies the stack and position (or level) numbers in a particular capsule. For example, Compact 6-4-1 refers to the compact in Capsule 6 at the top (Level 4) of Stack 1.

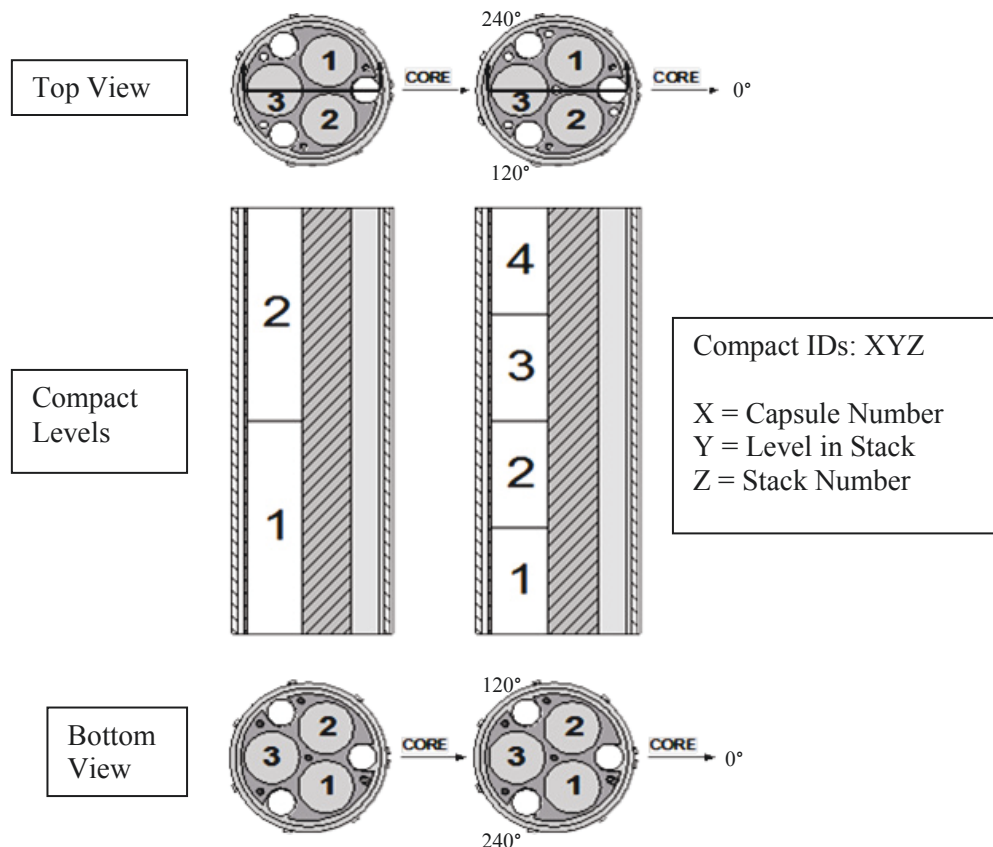


Figure 3. Numbering scheme for AGR-2 compacts in Capsule 1 (left) and Capsules 2-6 (right).

The TCs used in the test train are Type N. The TCs were inserted into holes drilled in the graphite fuel holder at various locations. Capsules 1–5 had two TCs each, while the top capsule (Capsule 6) had five TCs. Each capsule contained a melt wire package containing two pure beryllium wires (Capsules 1, 3, 4, 5, and 6) or a single nickel wire (Capsule 2), which were encapsulated in vanadium and placed in a hole drilled at the centerline of the graphite holder. These will be used to indicate if the temperature of the capsule (at the location of the melt wires) exceeded 1287°C (beryllium wires) or 1455°C (nickel wire). Each capsule also contains three different flux wires (pure Fe, V-0.1%Co, and pure Nb), all of which were encapsulated in sealed vanadium tubes and placed around the periphery of the graphite holder. The measured activity in the wires after irradiation will be used to calculate the neutron fluence for the different neutron energy ranges covered by the three flux wires.

The AGR-2 test train was shipped to the Materials and Fuels Complex in July 2014 for post-irradiation examination (PIE). The first PIE activities included nondestructive examination of the test train, followed by disassembly of the test train and individual capsules and detailed inspection of the capsule contents, including the fuel compacts and the graphite fuel holders. AGR-2 disassembly was conducted with the same equipment that disassembled the AGR-1 test train and its components. Dimensional metrology of the compacts, graphite holders, and steel capsule shells was performed with the same equipment used successfully on similarly sized AGR-1 components: a custom machine vision system (for outer diameters and lengths) and conventional bore gauges (for inner diameters).

2. AGR-2 RECEIPT AND NONDESTRUCTIVE TESTING

2.1 Receipt and Inspection of AGR-2 Test Train

The AGR-2 test train was received from the ATR in July 2014 and visually inspected at the Materials and Fuels Complex Hot Fuel Examination Facility (HFEF). After extracting the test train from the experiment basket that centered the test train inside the shipping cask, examination of the test train exterior with binoculars revealed only superficial scuff marks from sizing and handling. A fixture for vertically suspending the test train was then attached for gamma scanning. The test train, its experiment basket, and the gamma scanning fixture are shown in Figure 4.

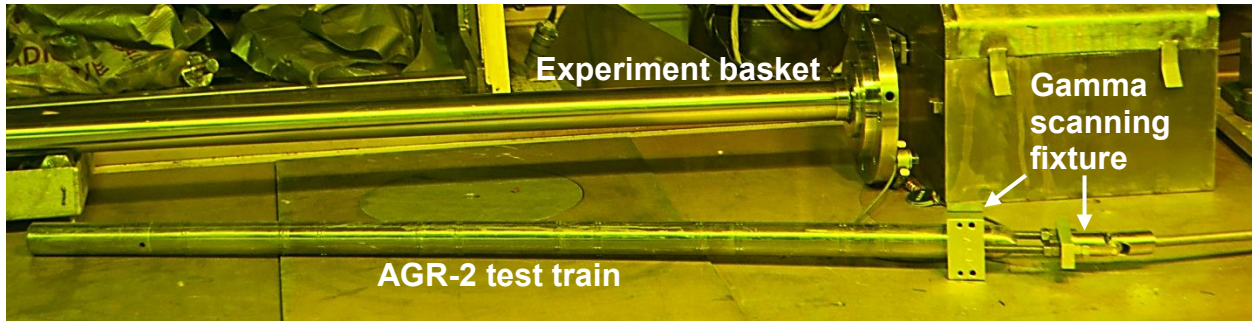


Figure 4. AGR-2 test train in a hot cell at the Hot Fuel Examination Facility.

Figure 5 presents a close-up view of the top of the AGR-2 test train after the gamma scanning fixture was attached. The distortion is readily apparent in Figure 5 where the leadout (for gas lines and instrument wires) was severed during length sizing at ATR to fit the test train into the shipping cask. Although the leadout stub was severely deformed, no significant distortion extended past the nubs into the uppermost AGR-2 capsule shell.

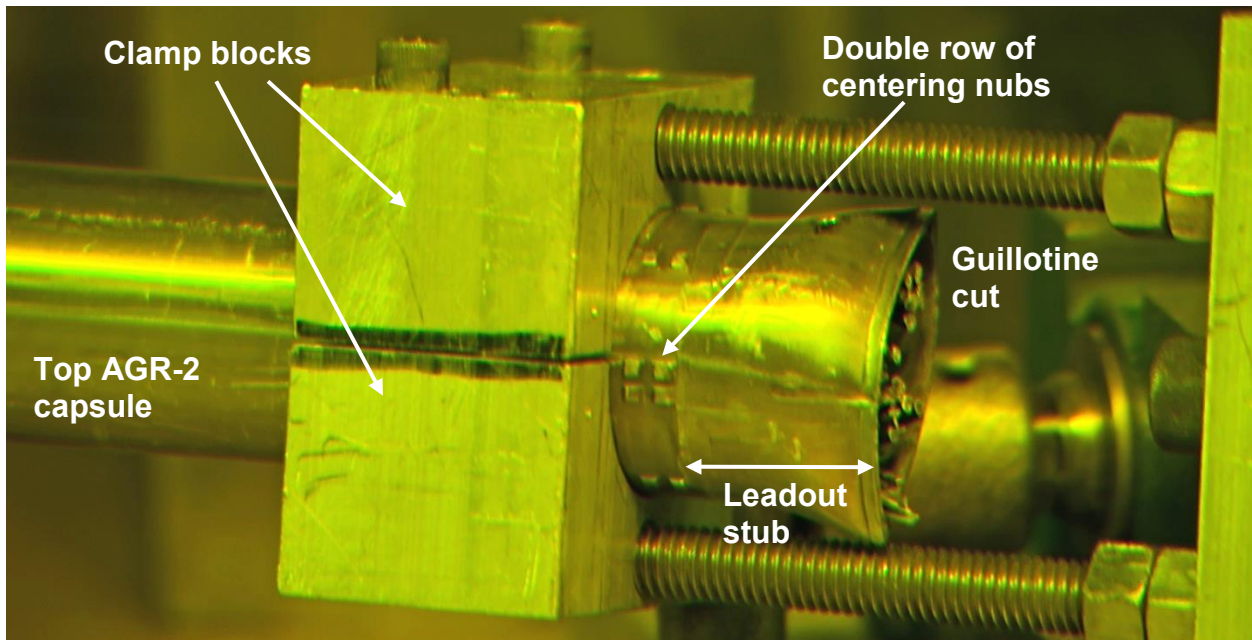


Figure 5. Attachment of gamma scanning fixture to top of AGR-2 test train.

2.2 AGR-2 Test Train Gamma Scanning

Following receipt and visual inspection, the intact AGR-2 test train was examined using the HFEF Precision Gamma Scanner (PGS) to identify interior components, including the fuel compacts, and to determine if any damage or shifting of components within the capsules had occurred. The test train was suspended vertically in front of the PGS collimator (fixed 2.22-cm width with an adjustable opening height that can be set between 0 and 0.254 cm) during scanning. The centerline of the test train was established by taking a horizontal scan of the test train with a vertical collimator orientation to establish the edges of the test train using the Co-60 activation product in the stainless steel. The test train was then scanned with the collimator in a horizontal orientation in two off-axis sweeps that captured Stack 1 of the fuel compacts and part of Stack 3 in one sweep and Stack 2 and part of Stack 3 in the other sweep. The double nubs on the exterior of the test train that indicated core center in ATR were used to visually align the rotation of the test train with the PGS collimator (see Figure 5). To prevent the highly activated steel components of the test train from overwhelming the detector, scans were performed with the collimator closed down to a 0.0254-cm width, but scans were taken in 0.254-cm axial increments. Thus only 10% of the test train was actually counted.

Spectra from the scans were analyzed for activation products from the structural materials (Co-60, Mn-54, Nb-94, Hf-175, Hf-181), fission products from the fuel compacts (Cs-134, Cs-137, Ce/Pr-144, etc.), and activation products from the thermocouples, melt wires and flux wire packages (Co-60, Nb-94, Ta-182). Special attention was given to the regions adjacent to the expected location of the fuel compacts, where the presence of fission products might indicate whether deterioration of graphite spacers allowed fuel compacts to shift axially. No TCs, melt wires or flux wire packages were observed in the test train data. This may be due to the high activation product signal from the test train, but such small items could also have been in the gaps between incremental scans. Nothing unexpected was observed in the fission product distribution. In general, the fission products appeared to be retained in approximately 10.16-cm long sections of the test train at regular intervals indicating no shifting of the compacts during irradiation. Occasionally the fission product signal dropped significantly between scans. This is due to the collimator opening and increment size mismatch, and it occurred when the collimator was focused on the area between two compacts. (AGR-2 compacts had very small fuel-free end caps.)

The intensity of Co-60 and Cs-137 from the test train scans (Capsules 6, 5, 3, and 2) is shown in Figure 6 and Figure 7. (Data from Capsule 4 and Capsule 1 were excluded from these figures due to proprietary information limitations.) Nothing unexpected was observed in the test train gamma scans. The attenuation seen in Capsule 6 between 68.3 and 71.4 cm is due to shielding from the fixture that holds the test train in the PGS. Capsule 3 is UO₂ fuel that had a lower fission density than the UCO fuel in the other capsules. The intensity from other fission products generally resembles the trends shown by the Cs-137. The spikes in the Co-60 activity indicate the solid metal heads and floors of each capsule. Note that the fuel compacts will be gamma scanned after removal from the capsules in order to quantify fission product inventories.

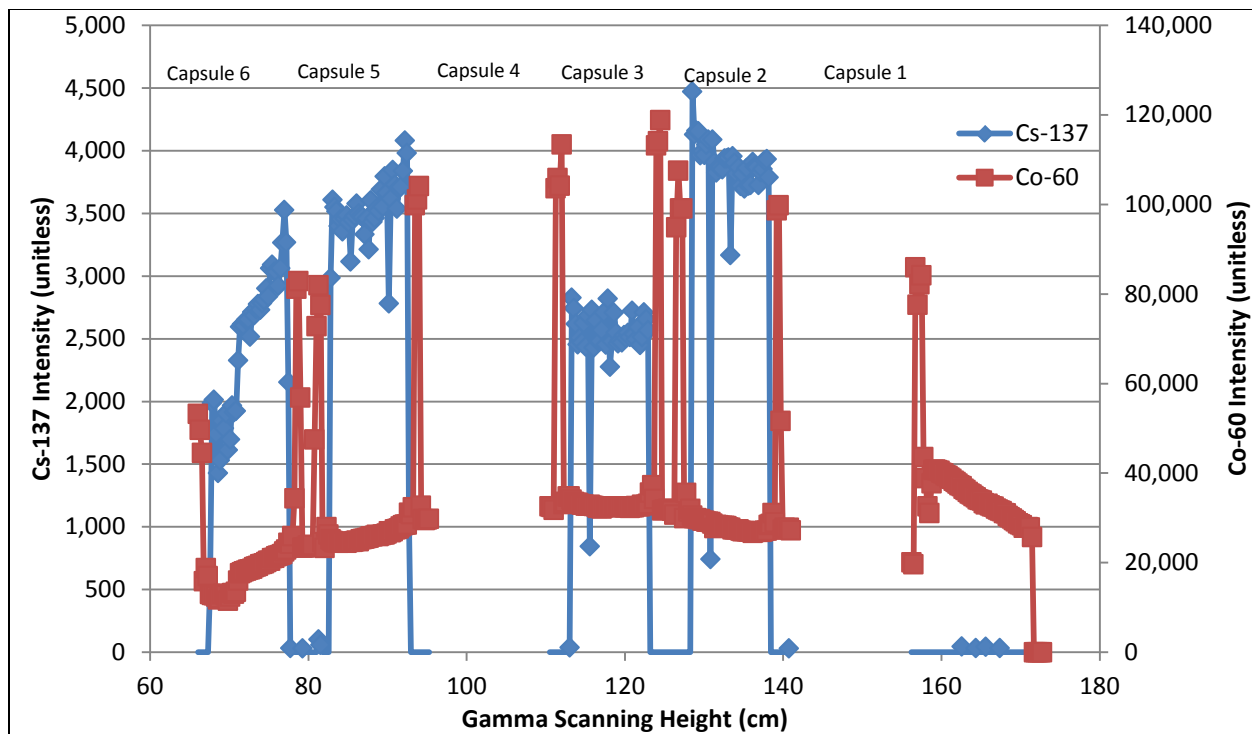


Figure 6. Activation product (Co-60) and fission product (Cs-137) intensity from gamma scanning of the AGR-2 test train Stack 1 and Stack 3. Note that data from Capsules 4 and 1 have been omitted from the plot. The region from 160 to 175 cm represents the test train tail piece.

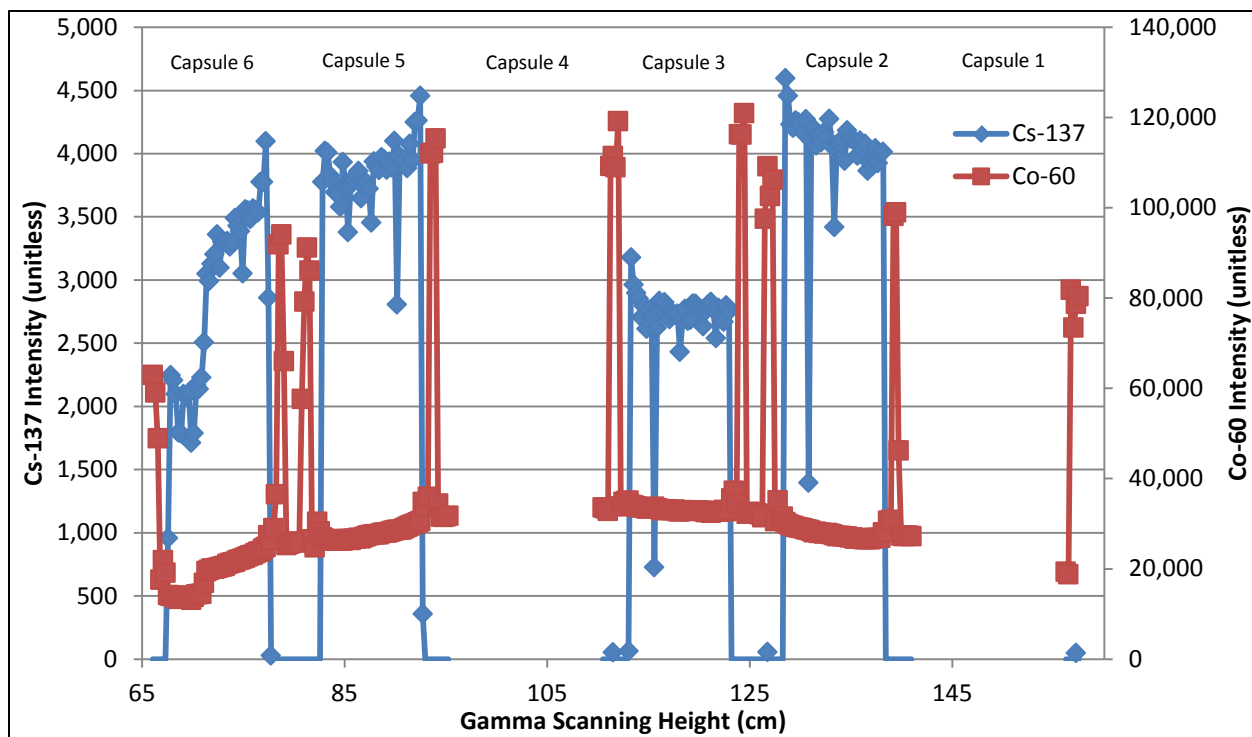


Figure 7. Activation product (Co-60) and fission product (Cs-137) intensity from gamma scanning of the AGR-2 test train Stack 2 and Stack 3. Note that data from Capsules 4 and 1 have been omitted from the plot. The test train tail was not scanned when Stack 2 and 3 were scanned.

3. AGR-2 DISASSEMBLY

3.1 Basic Disassembly Equipment

As with AGR-1 disassembly, the platform for AGR-2 disassembly operations was the slide table displayed in Figure 8, which was positioned at Window 3M at the HFEF main hot cell. It was used both to separate the test train into six individual capsules and to disassemble each capsule. Circumferential cuts were made on the test train's stainless steel outer shell with a modified Tri-Tool® portable tubing lathe attached to the carriage rail of the slide table. The cutter and motor were mounted on a plate that could pivot from vertical to horizontal when the cutter was inactive to create more room on the left side of the table. Remote handling tools such as the clamp vises and support cradle (shown in Figure 9) were mounted on twin slide rails to hold the test train and its components on a fixed axis. The clamp vises were also employed to support and move a variety of handling tools during disassembly and metrology. These tools included devices for separating and extracting capsule components such as fuel compacts. Additional tool and fixture descriptions are provided below in the context of specific operations.

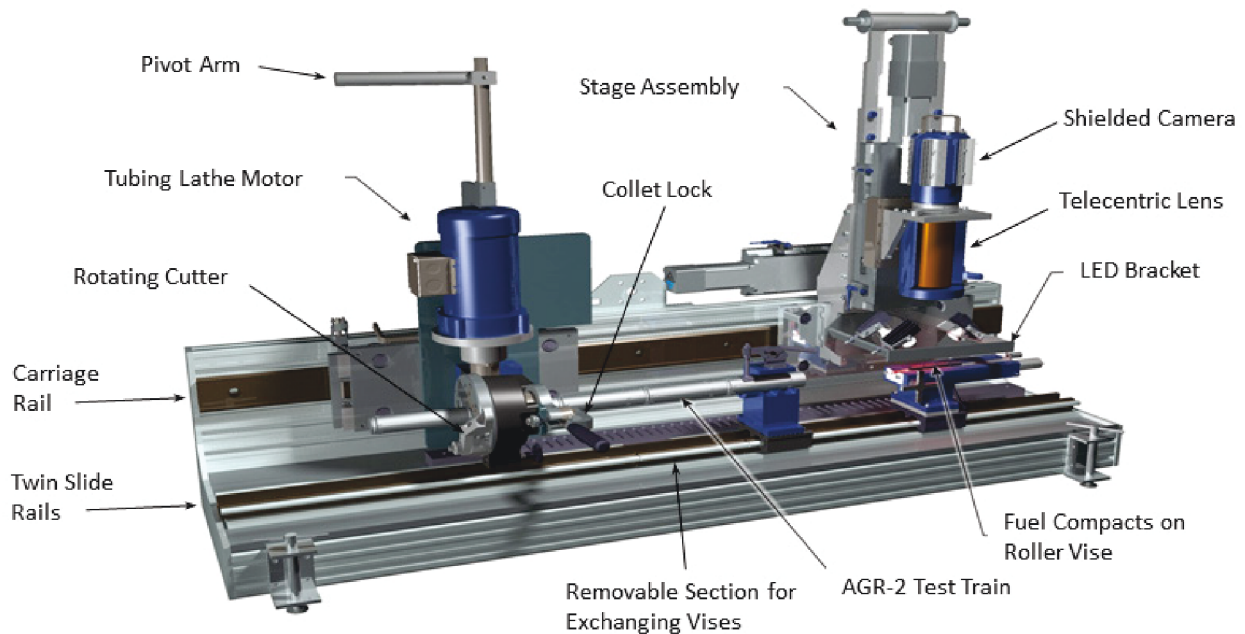


Figure 8. Slide table with disassembly and metrology equipment.

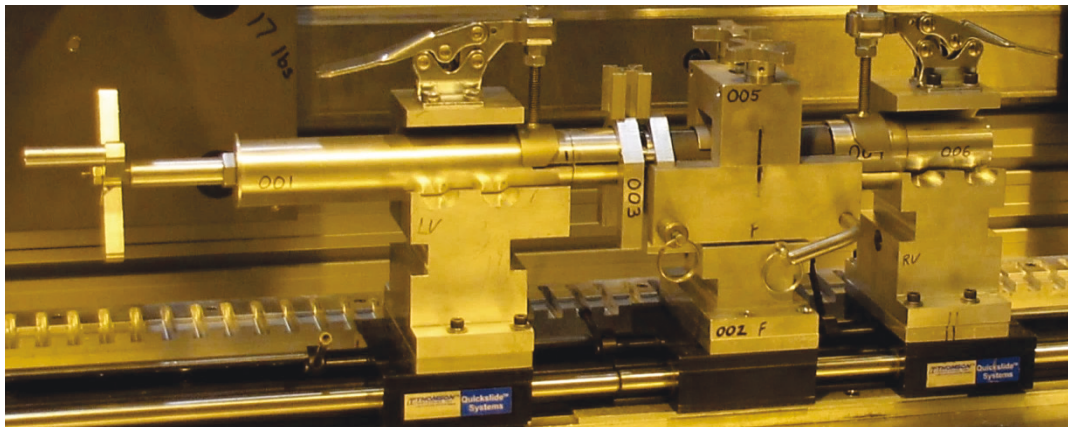


Figure 9. Rail-mounted left vise, support cradle, and right vise, plus several tools for capsule disassembly.

3.2 Capsule Separation

Test train disassembly activities were initiated on August 11, 2014, per HFEF Laboratory Instruction No. 0031 (Scott 2014). The first cut made with the tubing lathe removed the short leadout stub on top of the test train. Because the leadout stub had been deformed by the guillotine cut (see Figure 5), a slightly deeper cut was needed to penetrate the entire shell circumference here than to sever other shell locations.

The approach for dividing the test train into individual capsules involved making a single circumferential cut near each capsule head, as diagrammed in Figure 10 and shown in Figure 11. Although the cuts themselves were straightforward, separating topmost Capsule 6 and then Capsule 5 from the lower test train proved very difficult. Following each cut, the plan was to pull the loose capsule shell over the TCs and gas lines from lower capsules that passed inside the through tubes by moving the left vice away from the cutter while the test train remained locked in the collet (see Figure 11). This approach worked well for separating the lower four AGR-2 capsules, as well as for all of the AGR-1 capsules. However, the AGR-2 TCs were of substantially larger diameter than those in the AGR-1 experiment, and there was very little free space inside the through tubes of the uppermost AGR-2 capsules when the test train was assembled. Consequently, the TC leads and gas lines in the upper capsules promptly jammed when tugged during disassembly.

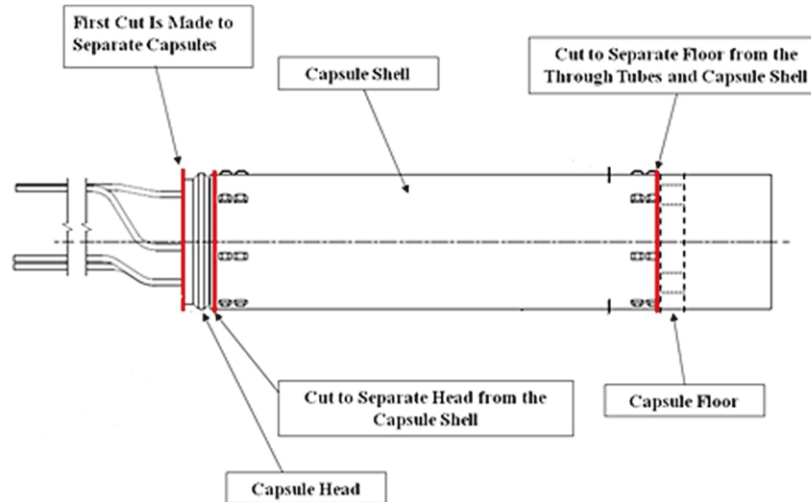


Figure 10. Circumferential cuts made to separate capsules and to disassemble each capsule.

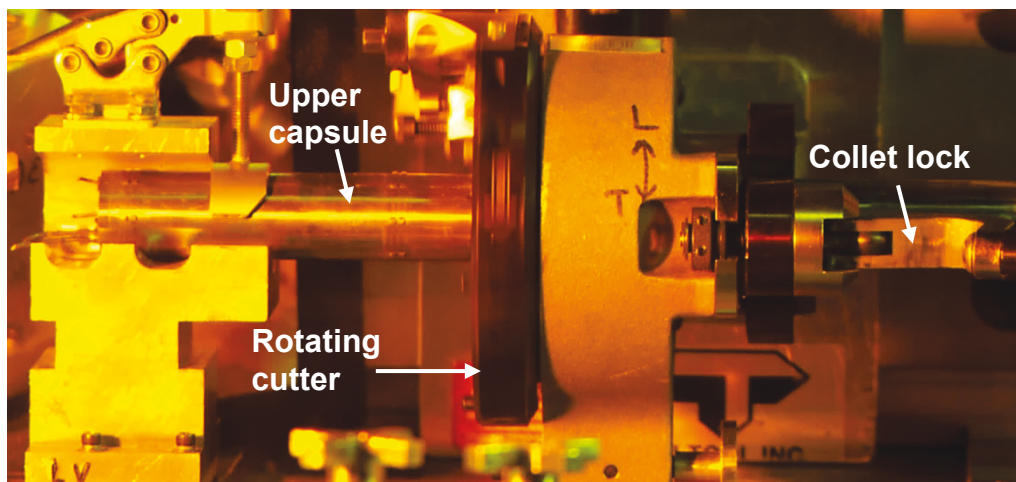


Figure 11. Separating the upper capsule from remainder of AGR-2 test train.

Several wedges of varying thickness were then used to enlarge the opening to several centimeters, as depicted in Figure 12. Because a large separation force continued to be necessary, the lower test train was removed from the cutter collet and locked in the right vise. An attempt was made with two pry bars (one shown at bottom of Figure 12) to further separate Capsule 6 by levering the vises apart, but slippage occurred under the toggle clamps and one of the pry bars began to bend. Consequently, an extra clamp was added outside each vise and a jacking screw was employed to supply the separation force, as displayed in Figure 13. This arrangement successfully widened the gap, although a “cheater bar” had to be added to enable a manipulator to turn the star wheel on the jacking screw. The bundles of TC leads and gas lines were ultimately extracted from the bottom of Capsule 6, as originally intended.

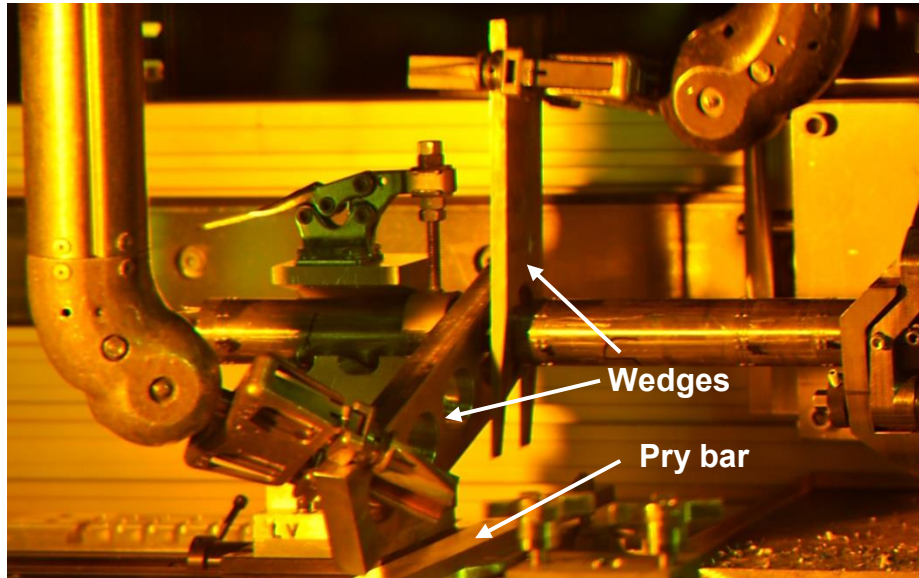


Figure 12. Using two wedges to pry Capsule 6 (under toggle clamp) away from Capsule 5.

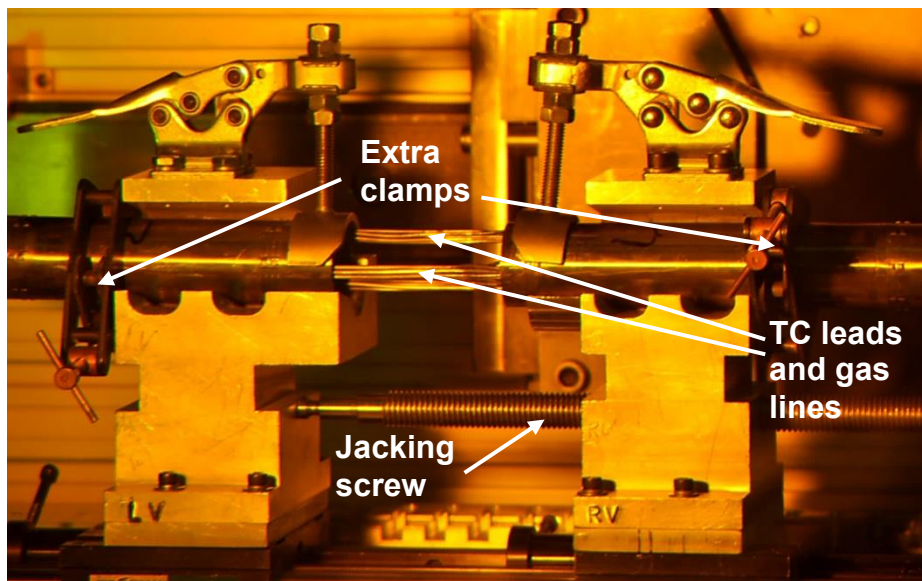


Figure 13. Forcing vises apart with a jacking screw to separate Capsule 6 (in left vise).

Capsule 5 was separated from the lower test train in much the same fashion as Capsule 6. However, the bundles of TC leads and gas lines became completely jammed inside the Capsule 5 through tubes during the wedging step. With additional separation by the jacking screw, it became evident that the bundles were being pulled from the lower test train rather than sliding through the Capsule 5 through tubes, as demonstrated by Figure 14. These bundles had to be clipped to free Capsule 5, leaving many of the leads and lines still jammed inside this capsule. Because the through tubes had to be empty for capsule disassembly, a new custom clamp was fabricated to grip each bundle for extraction with the aid of the wedges. Some metallic slivers emerged from the bottom of Capsule 5 along with the bundles, but a visual examination of the through tube interiors merely revealed scratches, not tears.

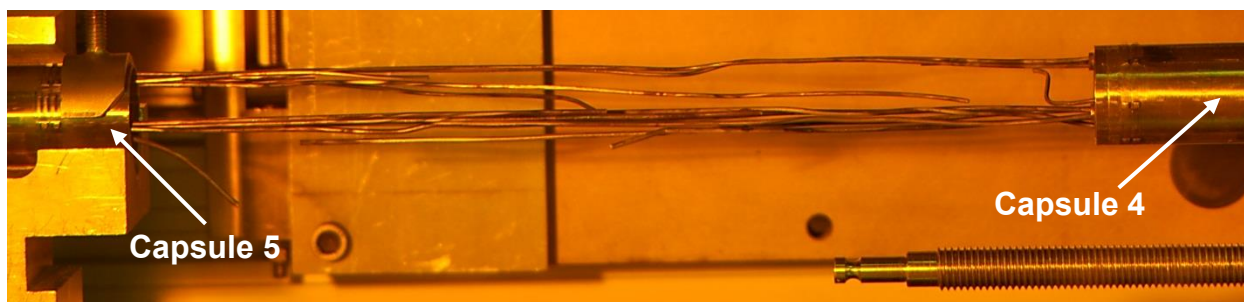


Figure 14. TC leads and gas lines pulled from the lower test train during separation of Capsule 5.

Separation of the lower four capsules proceeded without problems. As each capsule was separated from the test train, the TC leads and gas lines brazed to the capsule head were trimmed and discarded. One surprise was that the AGR-2 niobium gas lines were as difficult to cut as the TC leads. In contrast, the niobium gas lines inside the AGR-1 test train were all found to be extremely brittle (Demkowicz et al. 2011). After trimming the leads and lines, each of the six capsules was placed in a paint can for interim storage. These cans provided easy manipulator access and ample room to later store disassembled capsule components, whenever necessary.

3.3 Capsule Disassembly

Disassembly of AGR-2 capsules was conducted in the following order: Capsules 2, 5, 3, 6, 4, and 1. Early information was desired on Capsules 2 and 5, which were very similar (identical fuel compacts and similar burnup and fast fluence) except for the relatively high average irradiation temperature experienced by Capsule 2 (Demkowicz 2013). The next priority was to contrast performance of the UO₂ kernel fuel in Capsule 3 with the UCO kernel fuel in Capsules 2 and 5.

In most regards, disassembly of individual AGR-2 capsules proceeded smoothly because considerable advantage was taken of lessons learned during AGR-1 capsule disassembly iterations. With minor variations, all of the AGR-2 capsules were disassembled as follows.

The initial step was to make a circumferential cut to remove the capsule floor at the location presented in Figure 10. Wedges were needed to enlarge the opening because the niobium through tubes tended to be bound inside the floor holes, although they were not brazed there to enable axial thermal expansion. Some through tubes pulled out of the floor during the prying while others fractured above the floor, as evidenced in Figure 15. (The protruding through tube in Figure 15 first fractured midway inside this capsule before it was fractured again by flexing the floor.) A thin deposit of varying darkness was found on the inner surfaces of all capsule floors, each of which was then placed into the capsule storage can after inspection. The bottom graphite spacer and Grafoil® disks were photographed and carefully loaded into a pre-labeled container for later gamma counting.

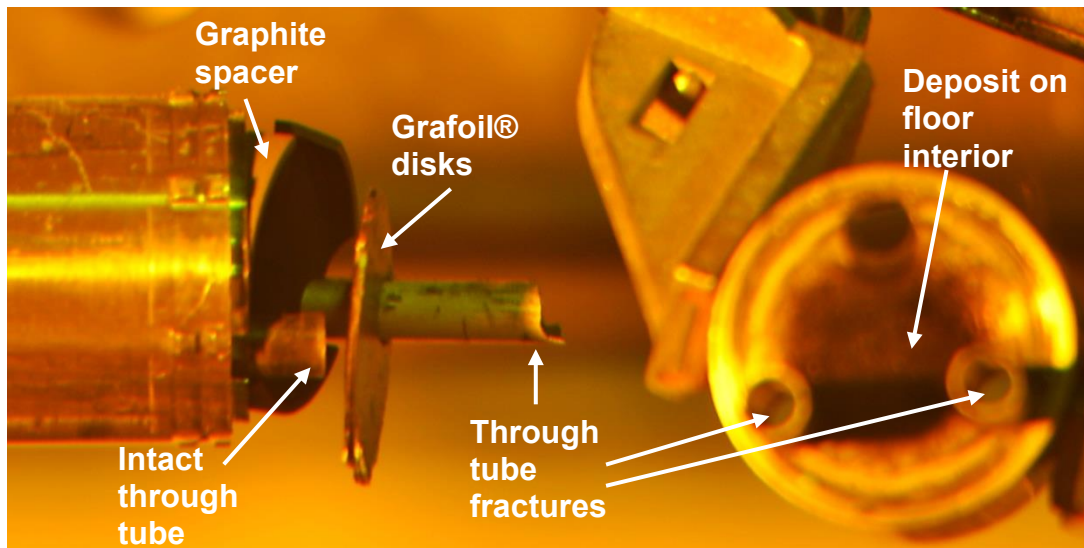


Figure 15. Bottom of AGR-2 Capsule 2 following floor separation.

The next step was to cut through the stainless steel shell just below the capsule head where indicated in Figure 10. At this point the capsule was supported by a rotating fixture whose three prongs were inserted inside the through tubes from the left while the capsule was locked in the cutter collet. Following the head cut, the capsule was extracted from the lathe collet and held in the support cradle, as shown in Figure 16. The head separator was then engaged to both the capsule head and the rotating fixture, after which, the support cradle was pried to the right, pulling the shell over the graphite holder and through tubes. After removal from the support cradle, the interior of the shell was examined and photographed for the presence of deposits, as discussed in Section 4.6. After lifting off the head separator, the graphite holder was rotated in 120° increments for photo-visual inspections. As with shell interiors, graphite holders also exhibited deposits of unknown material in varying amounts (see Section 4.4).

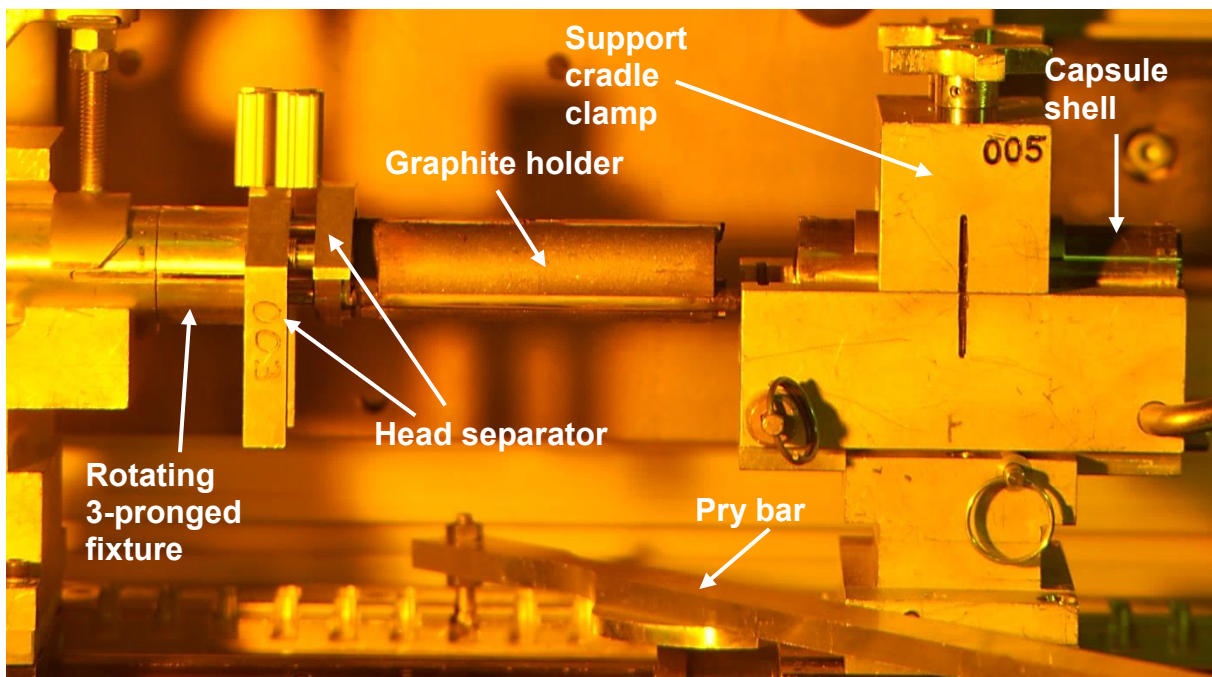


Figure 16. Arrangement for removing capsule shells.

The next major goal was separating the head and the metallic components brazed to it (through tubes, TCs, and gas lines) from the graphite holder. (Unlike the molybdenum AGR-1 through tubes, none of the niobium AGR-2 through tubes pulled free of the capsule head brazes during disassembly.) The plan was to do the head separation in much the same manner as the shell removal, using the head separator after clamping the holder in the support cradle. However, the springs on the support cradle clamp were not sufficiently strong to overcome through tube friction against the graphite holder plus adhesion of TC leads and gas lines inside the holder. Accordingly, the through tubes were first broken off near the head as illustrated in Figure 17, where the support cradle clamp was replaced by a special clamp with an open slot at the top, which still firmly held the graphite holder and capsule head. The three prongs on the rotating capsule support fixture were withdrawn until the prongs only engaged the short portions of the through tubes inside the capsule head (see Figure 18). A pry rod was then inserted into the through tube via an aligned guide slot and then lifted up, which generally bent the through tube near the head. Some of the niobium through tubes were sufficiently brittle to promptly fracture, while others were still ductile and had to be flexed up and down to break them.

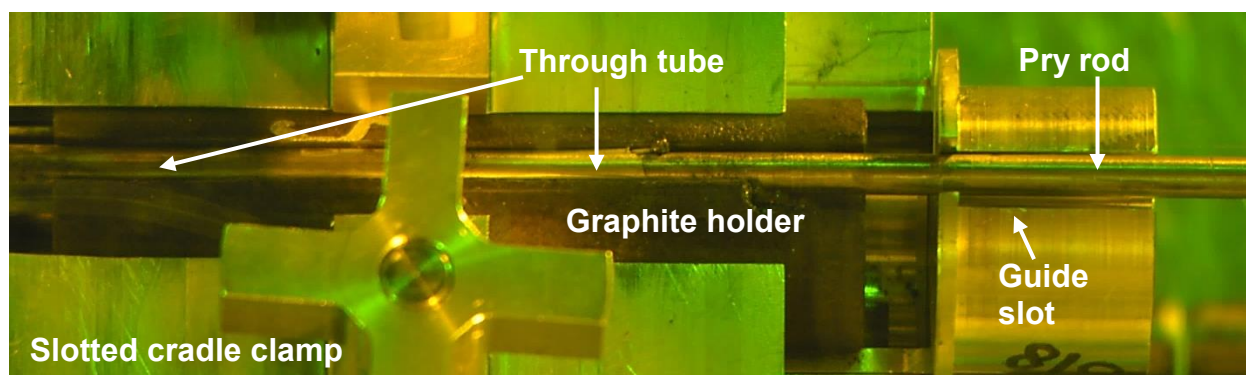


Figure 17. Mirror view of prying a through tube away from a holder base with a rod and special fixture.

After all three tubes had been broken off, the guide slot fixture was removed and the shell replacement spacer (see Figure 18) was installed under the graphite holder. The slotted cradle clamp was also replaced by the regular spring-loaded cradle clamp block. Any TCs and gas lines that were bound inside the holder were then cut with a short hacksaw blade, as displayed in Figure 18. The inside of the head served as a blade guide, which in most cases limited damage to the nearby Grafoil® disks to abrasion marks. At this point, the capsule head and through tube stubs were grabbed with manipulator fingers to separate them from the graphite holder. Head interiors all exhibited a thin deposit, much like the deposits seen on the floor interiors. The two upper Grafoil® disks and the upper graphite spacer were removed with tweezers and placed in a pre-labeled container for gamma counting.

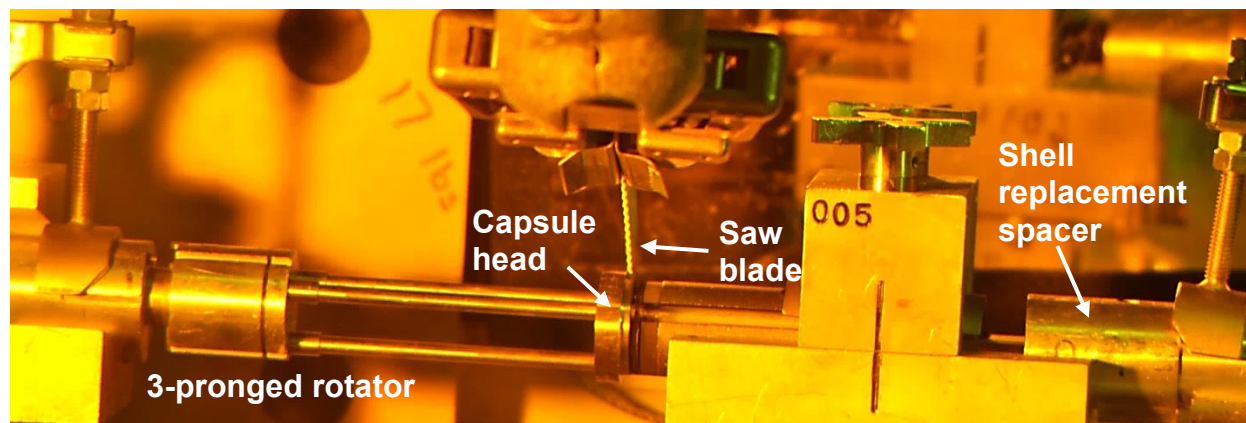


Figure 18. Cutting stuck thermocouples and gas lines between capsule head and graphite holder.

Access was now open to both ends of the graphite holder for unloading fuel compacts into an aluminum holder with three chamfered holes of approximately the same size and spacing as in the graphite holders. As shown in Figure 19, the left end of the aluminum holder fit inside the shell replacement spacer to abut the bottom (right) end of the graphite holder. A force gauge fixture with three holes on its right end was mounted in the left vise, and a pushrod was installed into the fixture hole matching the stack of compacts to be unloaded. While the support cradle and right vise were locked to the rails and while the left vise was moved to the right, the pushing force was monitored to detect any jamming of the compact stacks. No significant pushing force was noticed while pushing out the vast majority of the stacks. However, a peak force of 62 N (14 lb) was needed to move Stack 1 from Holder 1, and 53 N (12 lb) was ultimately required to move Stack 3 from Holder 5. Additional discussion regarding Capsule 5 compacts is presented in Section 4.2. Unloading behavior of Capsule 1 compacts is discussed only in restricted Appendix A due to proprietary information considerations.

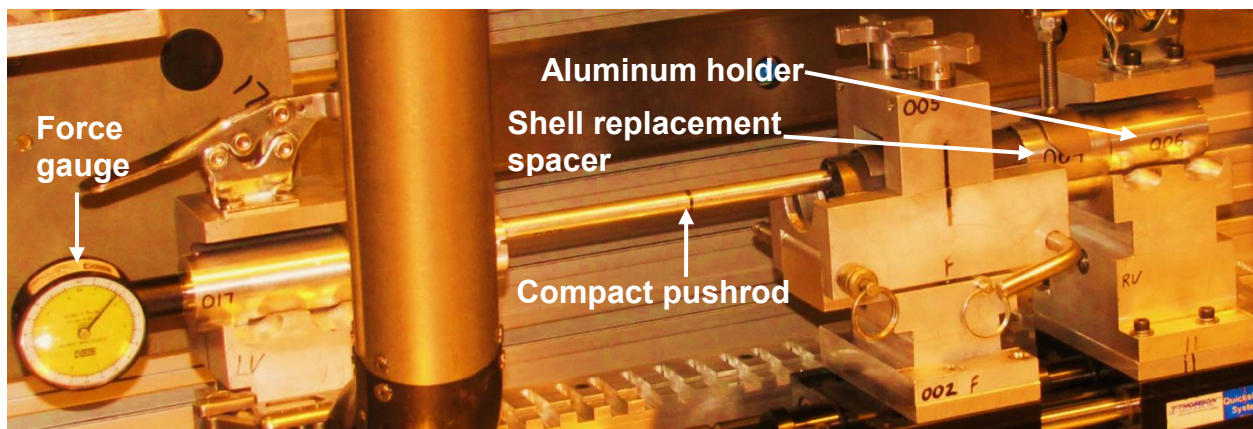


Figure 19. Pushing a stack of compacts into the aluminum fuel holder.

After removing the right vise, the “3-rod compact pusher” was loaded into the left vise and used to move the aluminum holder (full of compacts) away from the graphite holder and onto the roller trolley, as indicated in Figure 20. At this point of the disassembly sequence, it was convenient to measure the inner diameters of the holder holes. The force gauge fixture was again loaded into the left vise, but the pushrod in Figure 20 was replaced with the smaller bore gauge, as discussed in Section 4.5. After the holes were measured, each graphite holder was tilted for collection of loose flux wires and then placed in its own pre-labeled container for interim storage before gamma scanning.

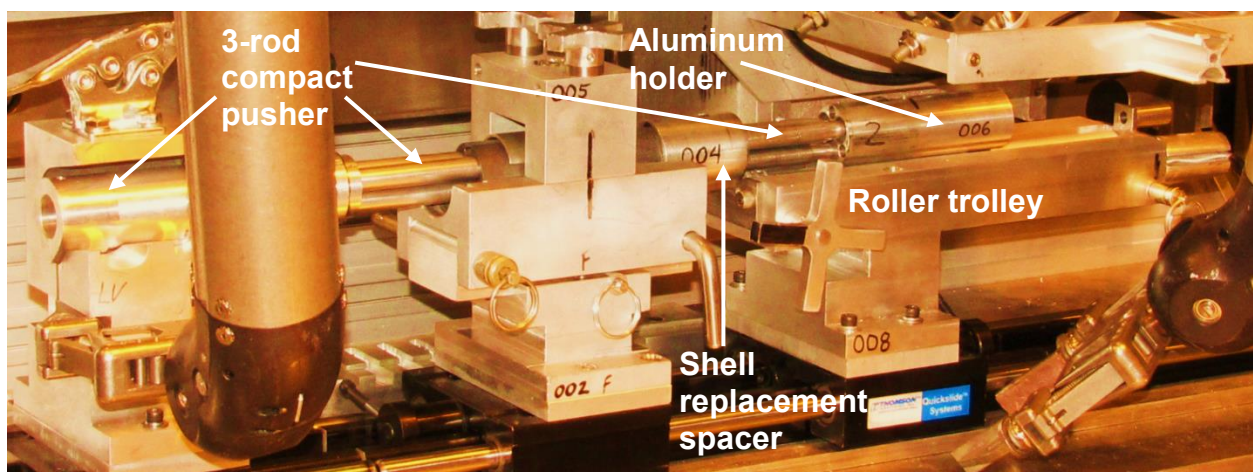


Figure 20. Moving the aluminum compact holder from the shell replacement spacer onto the twin roller table.

The last major step in capsule disassembly is depicted in Figure 21, where individual fuel compacts were examined and placed in containers. A rod (not shown) pushed compacts from the aluminum holder onto the roller trolley. There each compact was rotated for an initial visual inspection by rotating the star wheel, which in turn spun the twin rollers until the entire lateral surface was examined. Few noteworthy items were observed through the hot cell window with a spotting scope (pending higher resolution images taken later with the metrology camera, which are discussed in Section 4.2). A conventional putty knife was employed to gently slide the compact into a modified aluminum Swagelok® container (each with an engraved identifier). The Swagelok® cap on one end of each container was welded shut and the compact top (aimed upward in the reactor) was loaded toward the welded end to preserve axial orientation. The container holder was then pivoted upright for loading soft packing material and for securing the container with another Swagelok® cap.

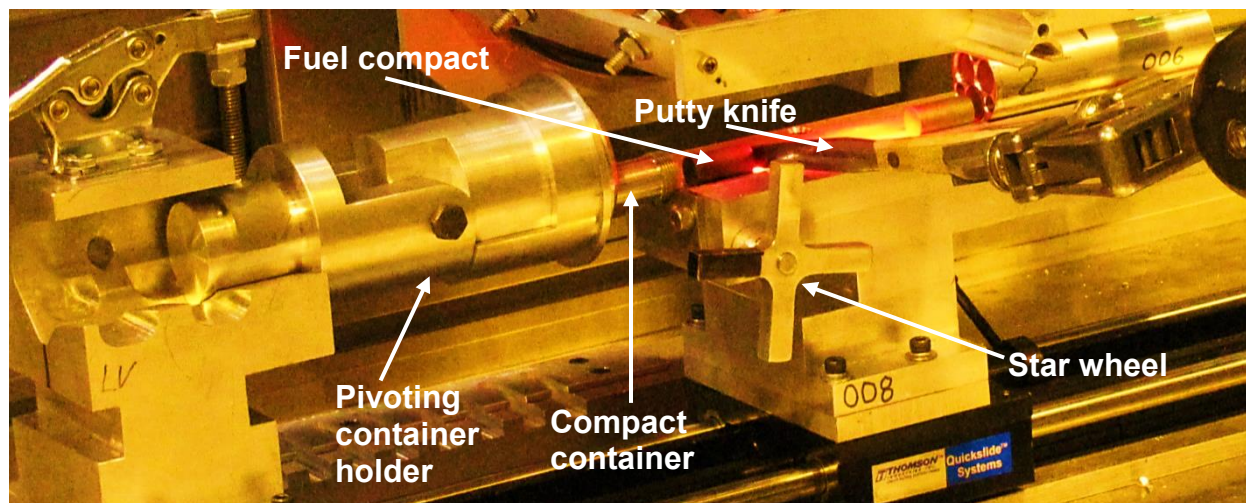


Figure 21. Fuel compact being loaded from twin roller table into its individual compact container.

All melt wires, two stuck flux wires, and the few severed remnants of TCs and gas lines in the graphite holders have not been removed at the time of this writing. However, these items will be extracted after HFEF gamma scanning is completed on the graphite holders. Removal of the melt wires will involve coring, which may also be needed to extract the two remaining flux wires. Ultimately each of the graphite holders will be crushed for pneumatic shipment to a different hot cell for additional analyses. Similarly, capsule shells are being cut into pieces in preparation for investigations of fission product deposition, along with capsule heads, capsule floors, and through tubes.

4. METROLOGY

Irradiation-induced dimensional changes of the AGR-2 fuel and surrounding capsule components are important because of the changes in thermal gaps and the effect they may have on the calculated thermal history of the fuel. The two radial gaps of primary interest are between fuel compacts and the graphite fuel holders and between the graphite holders and the lined steel capsule shells. Consequently, the outer diameter (OD) of the fuel compacts and graphite holders and the inner diameter (ID) of the graphite holder fuel holes and the capsule shell were measured. In addition, compact lengths were measured to explore potential relationships between length changes and diameter changes. All AGR-2 metrology activities were conducted in accordance with HFEF Laboratory Instruction No. 0032 (Ploger 2014b).

4.1 Metrology Equipment

A noncontact approach was taken for measuring lengths and diameters of AGR-1 and AGR-2 fuel compacts and their graphite holders during PIE. The primary reason was to obtain external dimensions on these potentially fragile components without risk of damage from probe pressure and without additional handling steps thought necessary for contact measurements. A customized in-cell system based on machine vision principles was selected both to meet dimensional measurement goals and to obtain high resolution inspection images.

Major components of the AGR metrology system are displayed in Figure 22. A shielded 6.6-megapixel camera and shielded telecentric lens (no change in object size over entire depth of focus) were vertically oriented on a radiation-resistant stage assembly. A shutter shield was employed to protect the lens elements and camera electronics from radiation sources beneath them when not actively viewing components. Upper illumination for fuel compacts and graphite holders was provided by three high intensity light-emitting diodes (LEDs). Graphite fuel holders were supported on a fixture for viewing at three azimuths (120° apart). To enhance contrast along their edges, holders were positioned above an aluminum imaging backdrop, which also had a 45° bi-directional mirror for any end views needed of holders and compacts. Compacts were positioned on the roller trolley for imaging at three azimuths. The roller trolley included an LED light pipe for backlighting compact ends.

The LEDs provided sufficient monochromatic illumination to minimize the lens aperture and thus to maximize its depth of focus, which was then adequate to cover the upper half of a graphite holder. The lens horizontal field of view is 35 mm, which converts to a camera pixel size of approximately 12 μm in the object plane. The field of view was large enough for a single image to cover both compact lengths and holder ODs but not the 100-mm length of holders. Six images were consequently taken along the length of each holder and stitched into composites with commercial image processing software, which was also used to extract dimensions. Pixel size was calibrated to images taken of a National Institute of Standards and Technology (NIST)-traceable chrome grid lithographed onto a glass substrate. The glass had a low thermal expansion coefficient to minimize effects of changing ambient temperature in the hot cell, which can vary from 27 to 38°C. Proper system performance was confirmed on check standards when dictated by changing circumstances.

Customized dial indicator-based bore gauges were used to measure the IDs of graphite holders (after removal of fuel compacts) and the inside of stainless steel capsule shells. Commercial ring gauge standards were employed in conjunction with custom support and alignment fixtures to check for calibration drifts, as displayed in Figure 23.

Performance of the entire AGR metrology system was rigorously evaluated during remote qualification in preparation for the AGR-1 metrology (Ploger 2010), using steel standards carefully fabricated to resemble both AGR-1 fuel compacts and AGR-1 graphite holders (nearly identical to AGR-2 counterparts). The reference dimensions of these standards were established with NIST-traceable measurement methods. System performance was further demonstrated by successful completion of the AGR-1 metrology campaign (Demkowicz et al. 2011). The AGR-2 metrology campaign was conducted

with the same equipment (excepting minor replacements), but AGR-1 quantitative performance and calibration requirements were relaxed to allow for potential degradation between campaigns (Ploger 2012).

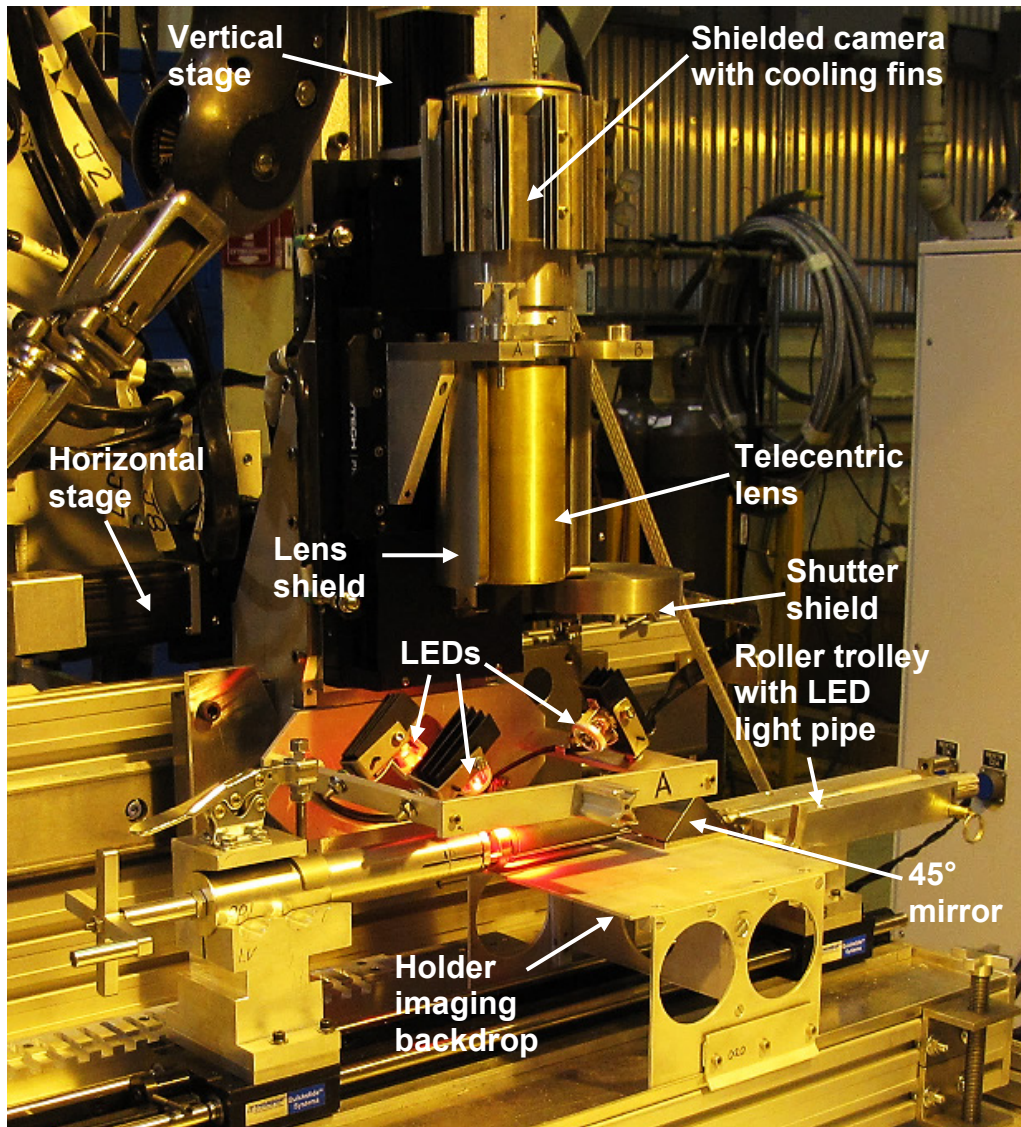


Figure 22. AGR noncontact metrology system during remote qualification.

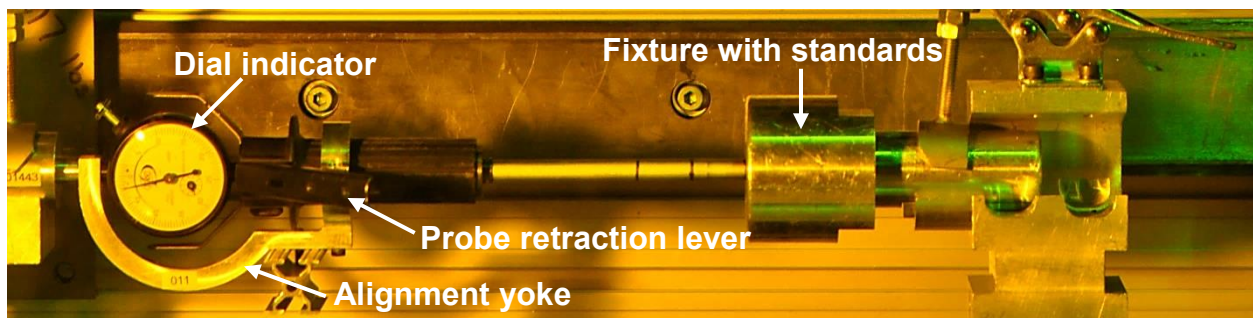


Figure 23. Performing a verification on the small bore gauge (used in graphite holder holes).

4.2 Fuel Compact Inspections

All fuel compacts were extracted intact from AGR-2 Capsules 2, 3, 5, and 6. (Refer to restricted Appendices A and B regarding compacts from Capsules 1 and 4, respectively.) No structural defects related to irradiation were observed, no free fuel particles were detected as compacts were unloaded from their graphite holders, and no cavities were found on compact surfaces from which fuel particles could have been dislodged. Compact images were not obtained when unloaded from the aluminum holder (before loading into individual compact containers) to avoid a relatively high radiation dose to the metrology lens and camera from the multiple radiation sources inside the aluminum holder. Instead, each compact was unloaded from its container horizontally onto the twin roller trolley following completion of all capsule disassembly operations. The compact side initially facing upward (toward the metrology camera) was arbitrarily called the 0° azimuth. After images were obtained at all three azimuths (120° apart), the compact was returned to its container by gentle sliding, as indicated in Figure 21.

Most compact images revealed no conspicuous damage from manual assembly or remote disassembly. Two representative examples of undamaged compacts are presented in Figure 24, where compact sides are highlighted by light reflected off the rollers for contrast when measuring diameters. Note that Capsule 2 compacts contained particles of 873- μm mean diameter (smaller UCO kernels) with a 37% packing fraction, while Capsule 3 compacts contained particles of 953- μm mean diameter (larger UO_2 kernels) and a 23% packing fraction (Collin 2011). As suggested by Figure 24, lateral surfaces on compacts with the lower packing fraction appeared somewhat smoother.

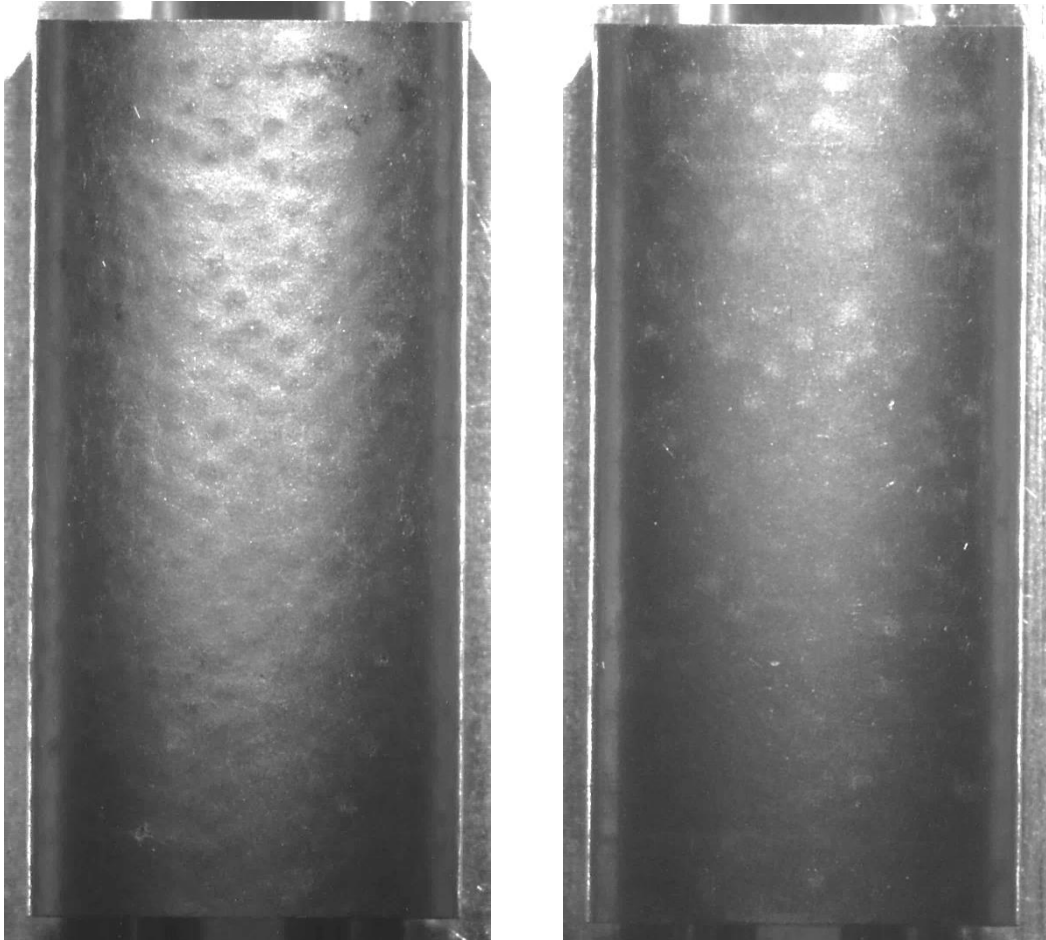


Figure 24. Typical appearance of irradiated AGR-2 fuel compacts (2-2-3 at left, 3-3-2 at right) with top ends in the reactor pointing upward.

Although most compacts from Capsules 2, 3, 5, and 6 exhibited no anomalous features, a small number of compacts from these capsules showed a variety of noteworthy items. Compact 6-2-2 accidentally fell off the roller trolley while unloading it from its container for imaging, and top versus bottom orientation was unfortunately lost in the process. As shown in Figure 25, one corner evidently was chipped when it landed and its sides may have been marred by a tweezer when it was retrieved. However, the transverse anomalies present in Figure 25 (along with images from a couple other AGR-2 compacts) are probably not from handling and may be fabrication artifacts.

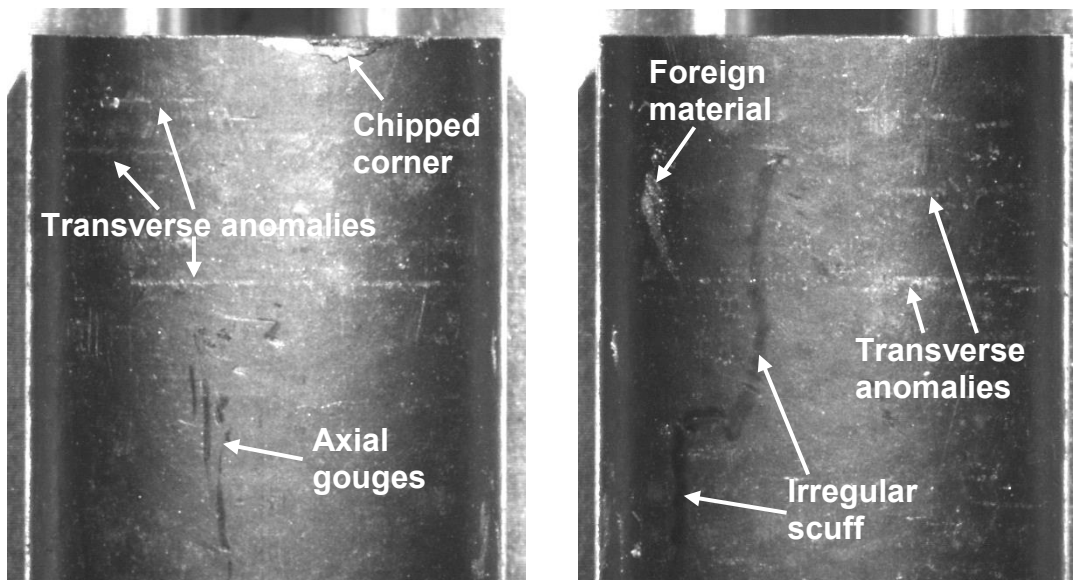


Figure 25. Two sides of accidentally dropped Compact 6-2-2.

A few other compacts revealed chipped top corners that could not be readily attributed to disassembly handling. Two such examples are provided in Figure 26. The top ends were the trailing edges when compacts were pushed from their graphite holders, and the pushrod ends are tapered, so these chipped corners probably did not occur then. Furthermore, the shallow scratch in the left portion of Figure 26 almost certainly initiated at the chip, which suggests that the scratch and possibly the chip occurred when the compact was pushed into its graphite holder during capsule assembly. In any case, these chips are extremely small and confined to the top end caps (no fuel particles), so the integrity of these compacts was never in jeopardy during irradiation.

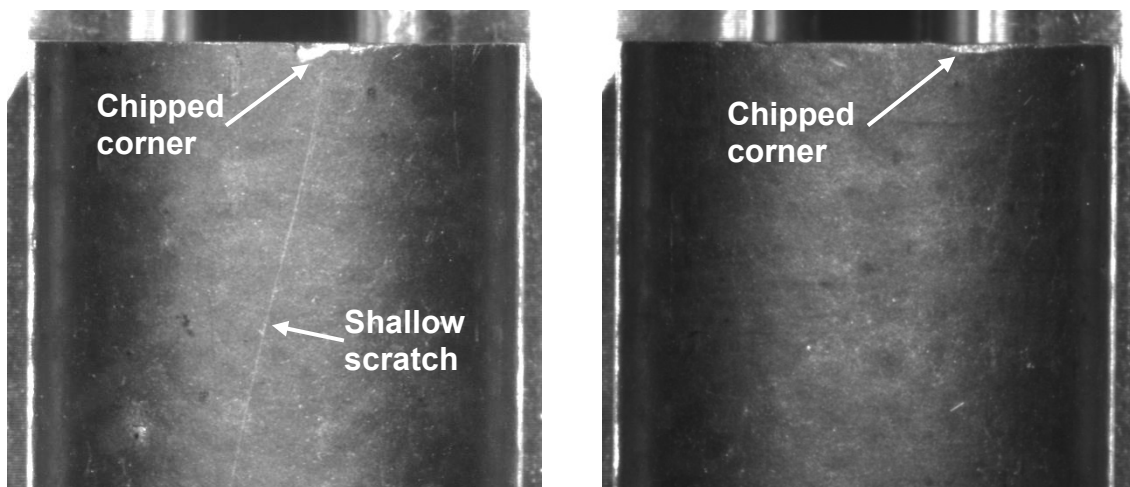


Figure 26. Chipped top corners on Compact 2-4-1 (left) and Compact 5-4-1 (right).

As discussed in Section 3.3, a relatively large force was needed to dislodge Stack 3 compacts from the Capsule 5 graphite holder. However, anomalous features were found only near the bottom of the lowest compact in this stack, at the leading edge when the compacts were pushed from the graphite holder. As indicated in Figure 27, axial abrasions were found on nearly opposite sides of Compact 5-1-3. The 240° side apparently rubbed against the chamfered hole entrance to the aluminum holder when first exiting the graphite holder (44 N of push force initially), slightly chipping the bottom corner in the process. After moving a short distance, the 90° side evidently began to scrape against the aluminum holder (or against abrasive material trapped inside the aluminum hole). The push force probably reached its maximum value of 53 N when the transverse gouges formed (shown in right side of Figure 27).

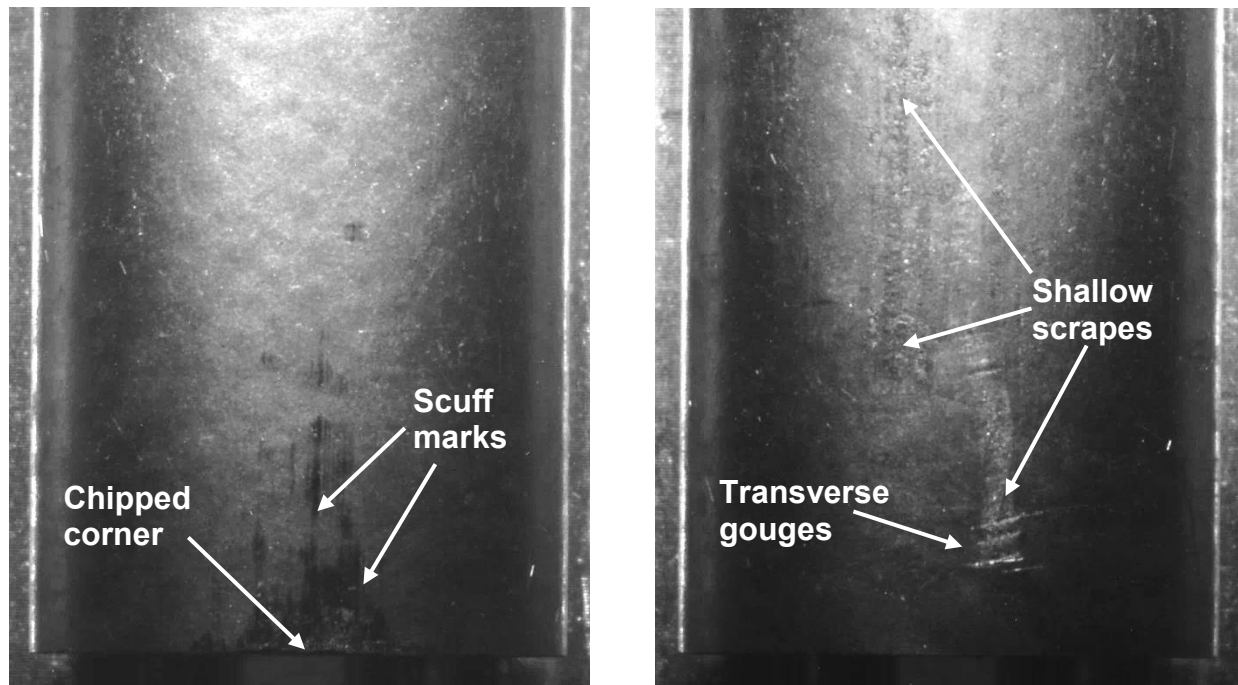


Figure 27. Axially oriented abrasions on the 240° (left) and 90° (right) sides of Compact 5-1-3.

Substantial axially oriented abrasions were found on two additional compacts from Capsules 2, 3, 5, and 6. Dark scuff marks at the bottom of Compact 5-1-2 in the left side of Figure 28 resemble those on Compact 5-1-3 in the left side of Figure 27. Both compacts were at the bottom of Capsule 5 and both scuffs apparently initiated at the leading edges when their stacks were pushed into the aluminum holder (Stack 1 first followed by Stack 2 with bottom Stack 3 last). However, the bottom corner of Compact 5-1-2 was not chipped and the maximum push force for Stack 2 was only 9 N. (Compact 5-1-1 showed no anomalous features, and 0 N push force was monitored when unloading Stack 1.) The reason why Compact 5-1-3 scraped badly is speculative, but one possibility is that the relatively large diameter of Holder 5 induced a misalignment between Stack 3 and the mating hole in the aluminum holder.

The final axially oriented anomaly is the gouge in Compact 3-2-3, which is displayed in the right side of Figure 28. The geometry of this gouge suggests that it formed when the top end of this compact was being loaded initially, such as into its graphite holder during original assembly (small radial clearance) or when nudged into its individual aluminum container for the first time (larger radial clearance). Furthermore, the force gauge read “0” for the entire time this stack of compacts was pushed into the aluminum holder.

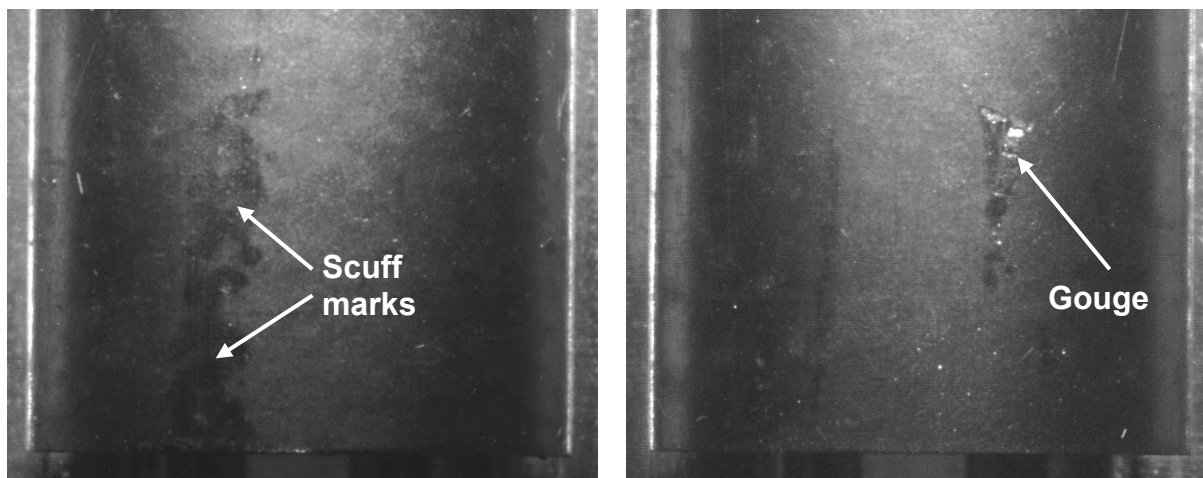


Figure 28. Axial marks from apparent abrasion near the bottoms of Compacts 5-1-2 (left) and 3-2-3 (right).

Some anomalous features were not axially oriented, as depicted in Figure 29. These marks apparently happened in conjunction with compact rotation, the timing of which is unknown so no satisfactory explanation exists. The fact that both of these compacts were at the top of the AGR-2 test train may be coincidental, although Compact 6-4-1 also exhibited a faint transverse mark at mid-length at one azimuth.

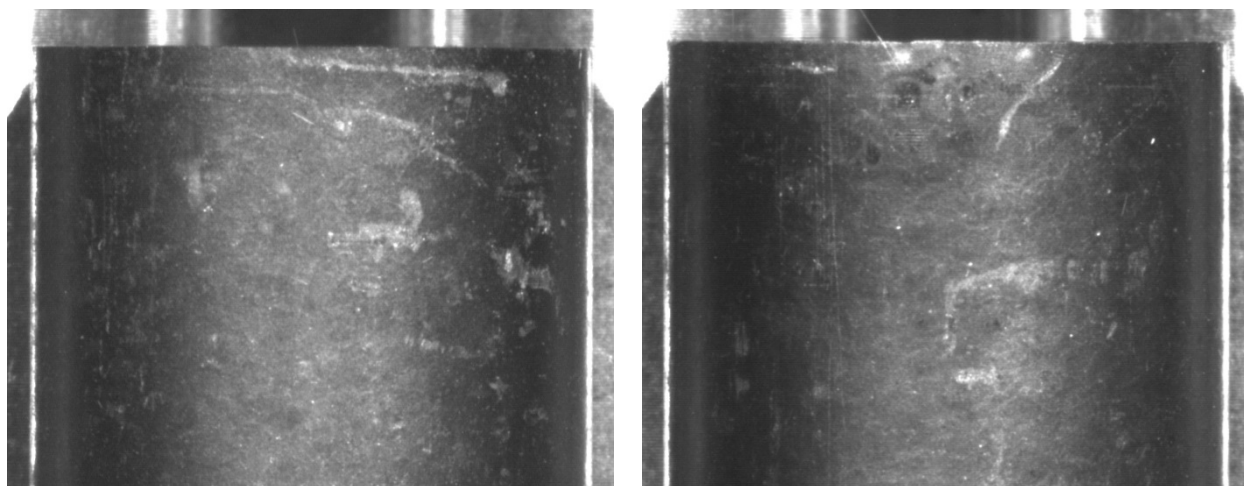


Figure 29. Shallow transverse and angled marks on Compacts 6-4-2 (left) and 6-4-3 (right).

4.3 AGR-2 Compact Dimensional Changes

Diameter and length measurements were obtained from images of AGR-2 fuel compacts where dimensions were based upon carefully calibrated pixel sizes in both horizontal and vertical directions. Due to increasing pincushion distortion toward the telecentric lens periphery, different calibration coefficients were developed for compact diameters and compact lengths using the first image of the line grid standard (taken before the AGR-2 metrology campaign was begun). Two additional images of the line grid standard were taken during the campaign to check for magnification drift from lens browning, which changes the indices of refraction of lens elements. The second grid standard image was taken after compacts from Capsules 2 and 5 were imaged, and no changes to pixel calibration coefficients were found necessary at that time for compact dimensions (as documented on page 57 of INL Laboratory Notebook No. 2283). Thus, the same pair of coefficients was also used to extract dimensions from Capsule 6 compacts. The third image of the grid standard was captured immediately after imaging

Capsule 4 compacts and shortly before imaging compacts from Capsules 3 and 1. Although the compact diameter coefficient was still valid, an adjustment of a single pixel width ($11.7\ \mu\text{m}$ over a 25-mm span) was made for length measurements on compacts from the last three capsules, as documented on page 83 of INL Laboratory Notebook No. 2283. (Compact measurements from Capsule 1 and Capsule 4 are reported in restricted Appendices A and B, respectively, because of proprietary information constraints.)

PAX-it!™ image processing software (Midwest Information Systems, Inc.) was used to extract fuel compact dimensions as detailed in Laboratory Instruction No. 463 (Ploger 2014a). Results from each compact were exported as a Microsoft Excel™ spreadsheet using a custom template. Each spreadsheet includes copies of the unprocessed and analyzed compact images. Compact dimension tables and associated plots below were extracted from these spreadsheets.

Compacts were imaged at three azimuths 120 degrees apart to allow the full external surface to be inspected, but only one of the three azimuths was deemed necessary for dimensional analysis based upon AGR-1 experience (Ploger 2012). The particular image chosen was generally determined by the uniformity of the light reflected off the twin rollers onto compact sides for best diameter measurements. As shown by the horizontal blue lines in Figure 30, six diameter measurements were spaced along the fuel-bearing length of each compact (using the red grid overlay as a guide). Two measurements were made in each of the upper, middle, and lower regions while avoiding non-fueled end caps. Consequently, each compact diameter change entry in the following tables is an average of six measurements.

Compact lengths were measured in three places along compact centers where ends were backlit by a light pipe driven at its maximum current. When compact images were analyzed from Capsules 2 and 5, difficulty was encountered in observing any rounded “crowns” on compact ends. Because the as-fabricated lengths were measured by a contact-based height gauge that was sensitive to crowns, this difficulty caused appreciable scatter in length changes among compacts from each of these two capsules. Consequently, the Capsule 2 and 5 compact images were digitally brightened by the same amount, and the lengths were re-measured. Most average lengths did not change significantly, but the few compacts that initially exhibited extreme length changes were moved closer to values from other compacts in each capsule. Compacts from AGR-2 Capsules 1, 3, 4, and 6 had yet to be imaged at this point of the campaign, so the exposure time was doubled for them. Currents for the upper three LEDs could then be reduced substantially, while the light pipe LED was still operated for maximum brightness, thereby eliminating the necessity for any digital brightening to better detect crowns.

While ORNL made only one length measurement on each compact (Capsules 2 through 6), ORNL reported six diameter values—two orthogonal measurements at top, middle, and bottom elevations (Hunn et al. 2010a, Hunn et al. 2010b). The original ORNL axial positions were not preserved when the compacts were loaded into graphite holders, so local as-fabricated diameters could not be compared axially to PIE diameters. Instead, all six as-fabricated diameters had to be averaged into a single diameter. (The impact of this averaging on comparisons was minimal because as-fabricated compact diameters were reasonably consistent within each capsule.) As-fabricated lengths of AGR-2 fuel compacts exhibited significant variability, even among similar compacts loaded into a single capsule. Consequently, analyses were directed toward relative changes in diameter and length during irradiation. Consequently, for each compact, as-fabricated average measurements were subtracted from PIE average measurements and each difference was then divided by the

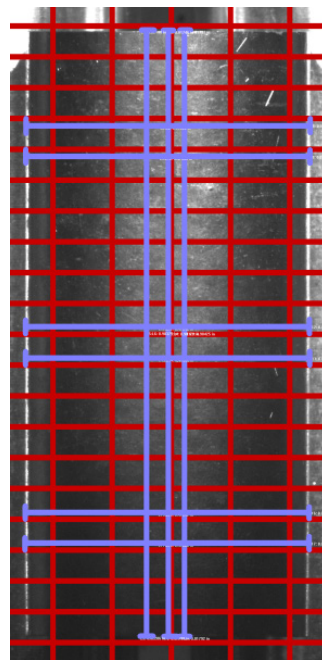


Figure 30. Example of analyzed compact image (here Compact 6-2-3).

corresponding as-fabricated value to generate a percentage change. Summarized compact results from AGR-2 Capsules 2, 3, 5 and 6 are presented in Table 2, Table 3, Table 4, and Table 5, respectively.

Table 2. Dimensional changes and associated standard deviations (σ) from AGR-2 Capsule 2.

Compact ID	As-fabricated dimensions		Average diameter change			Average length change		
	Diameter (mm)	Length (mm)	(mm)	(%)	σ (mm)	(mm)	(%)	σ (mm)
2-1-1	12.288	25.156	-0.162	-1.32%	0.0089	-0.172	-0.68%	0.0069
2-1-2	12.290	25.142	-0.163	-1.33%	0.0089	-0.200	-0.80%	0.0000
2-1-3	12.290	25.115	-0.128	-1.05%	0.0048	-0.189	-0.75%	0.0069
2-2-1	12.288	25.134	-0.187	-1.52%	0.0061	-0.196	-0.78%	0.0069
2-2-2	12.290	25.154	-0.189	-1.54%	0.0061	-0.201	-0.80%	0.0117
2-2-3	12.290	25.151	-0.173	-1.41%	0.0074	-0.221	-0.88%	0.0000
2-3-1	12.288	25.139	-0.197	-1.60%	0.0089	-0.185	-0.74%	0.0000
2-3-2	12.290	25.132	-0.202	-1.65%	0.0064	-0.186	-0.74%	0.0069
2-3-3	12.290	25.142	-0.185	-1.50%	0.0074	-0.220	-0.87%	0.0069
2-4-1	12.288	25.144	-0.181	-1.48%	0.0089	-0.218	-0.87%	0.0069
2-4-2	12.290	25.135	-0.181	-1.47%	0.0097	-0.197	-0.78%	0.0069
2-4-3	12.290	25.158	-0.157	-1.28%	0.0061	-0.228	-0.91%	0.0000

Table 3. Dimensional changes and associated standard deviations (σ) from AGR-2 Capsule 3.

Compact ID	As-fabricated dimensions		Average diameter change			Average length change		
	Diameter (mm)	Length (mm)	(mm)	(%)	σ (mm)	(mm)	(%)	σ (mm)
3-1-1	12.268	25.147	-0.138	-1.12%	0.0046	-0.061	-0.24%	0.0066
3-1-2	12.270	25.180	-0.138	-1.12%	0.0058	-0.032	-0.13%	0.0069
3-1-3	12.273	25.153	-0.132	-1.07%	0.0048	-0.087	-0.35%	0.0069
3-2-1	12.267	25.124	-0.152	-1.24%	0.0048	-0.085	-0.34%	0.0069
3-2-2	12.270	25.132	-0.144	-1.17%	0.0048	-0.050	-0.20%	0.0000
3-2-3	12.273	25.143	-0.141	-1.15%	0.0058	-0.104	-0.41%	0.0069
3-3-1	12.267	25.147	-0.142	-1.16%	0.0061	-0.058	-0.23%	0.0066
3-3-2	12.270	25.130	-0.144	-1.17%	0.0048	-0.037	-0.15%	0.0000
3-3-3	12.270	25.115	-0.144	-1.17%	0.0048	-0.092	-0.37%	0.0000
3-4-1	12.267	25.133	-0.142	-1.16%	0.0061	-0.086	-0.34%	0.0000
3-4-2	12.270	25.126	-0.141	-1.15%	0.0074	-0.083	-0.33%	0.0069
3-4-3	12.270	25.137	-0.138	-1.12%	0.0058	-0.075	-0.30%	0.0069

Table 4. Dimensional changes and associated standard deviations (σ) from AGR-2 Capsule 5.

Compact ID	As-fabricated dimensions		Average diameter change			Average length change		
	Diameter (mm)	Length (mm)	(mm)	(%)	σ (mm)	(mm)	(%)	σ (mm)
5-1-1	12.283	25.132	-0.106	-0.87%	0.0048	-0.120	-0.48%	0.0000
5-1-2	12.285	25.146	-0.118	-0.96%	0.0058	-0.119	-0.47%	0.0069
5-1-3	12.287	25.134	-0.116	-0.94%	0.0058	-0.177	-0.70%	0.0066
5-2-1	12.283	25.133	-0.124	-1.01%	0.0061	-0.117	-0.47%	0.0069
5-2-2	12.285	25.140	-0.131	-1.07%	0.0048	-0.167	-0.67%	0.0069
5-2-3	12.287	25.146	-0.133	-1.08%	0.0089	-0.200	-0.80%	0.0069
5-3-1	12.283	25.217	-0.132	-1.07%	0.0104	-0.163	-0.65%	0.0069
5-3-2	12.285	25.130	-0.133	-1.08%	0.0104	-0.165	-0.66%	0.0117
5-3-3	12.287	25.130	-0.145	-1.18%	0.0089	-0.180	-0.72%	0.0069
5-4-1	12.283	25.135	-0.110	-0.90%	0.0086	-0.131	-0.52%	0.0069
5-4-2	12.285	25.146	-0.123	-1.00%	0.0048	-0.154	-0.61%	0.0069
5-4-3	12.287	25.166	-0.127	-1.03%	0.0061	-0.182	-0.72%	0.0069

Table 5. Dimensional changes (mm) and associated standard deviations (σ) from AGR-2 Capsule 6.

Compact ID	As-fabricated dimensions		Average diameter change			Average length change		
	Diameter (mm)	Length (mm)	(mm)	(%)	σ (mm)	(mm)	(%)	σ (mm)
6-1-1	12.283	25.132	-0.118	-0.96%	0.0046	-0.101	-0.40%	0.0069
6-1-2	12.283	25.135	-0.120	-0.98%	0.0000	-0.147	-0.58%	0.0000
6-1-3	12.283	25.142	-0.112	-0.91%	0.0058	-0.150	-0.60%	0.0069
6-2-1	12.283	25.137	-0.124	-1.01%	0.0061	-0.203	-0.81%	0.0069
6-2-2	12.283	25.137	-0.132	-1.07%	0.0074	-0.153	-0.61%	0.0069
6-2-3	12.283	25.153	-0.124	-1.01%	0.0061	-0.161	-0.64%	0.0069
6-3-1	12.283	25.143	-0.120	-0.98%	0.0074	-0.151	-0.60%	0.0069
6-3-2	12.283	25.109	-0.128	-1.04%	0.0061	-0.163	-0.65%	0.0069
6-3-3	12.283	25.149	-0.124	-1.01%	0.0061	-0.130	-0.52%	0.0069
6-4-1	12.283	25.123	-0.124	-1.01%	0.0094	-0.107	-0.43%	0.0069
6-4-2	12.283	25.133	-0.118	-0.96%	0.0086	-0.110	-0.44%	0.0000
6-4-3	12.283	25.140	-0.114	-0.93%	0.0097	-0.117	-0.46%	0.0000

Average changes in diameter and length from these four tables are plotted according to axial position within the AGR-2 test train in Figure 31 and Figure 32, respectively. Metrology resolution is equal to the 11.7- μm effective pixel size, which (after normalizing to compact diameter or length) corresponds to a potential bias (inaccuracy) in either direction of nearly 0.1% in Figure 31 and nearly 0.05% in Figure 32. This estimate of bias can be conservative for an average, however, because bias errors in individual measurements will often cancel out when combined. A smaller contributor to measurement uncertainty is random error (repeatability), which is estimated by normalizing the standard deviations tabulated above for each average dimensional change to compact diameter or length. The representative error bar in each figure estimates a “combined standard uncertainty” above and below a data point as recommended by

ANSI/NCSL Z540-2-1997. Each estimate of combined uncertainty was calculated by root-sum-squaring the two contributing terms. Note that no coverage factors (e.g., from Student's t-table) have been applied to expand each error bar into a statistical confidence interval. (Although AGR-2 metrology did not have quantitative performance requirements, the error bars in Figure 31 and Figure 32 correspond to approximately 0.015 mm or 0.0006 inch, which is well inside the AGR-1 combined standard uncertainty requirement of ≤ 0.001 inch.)

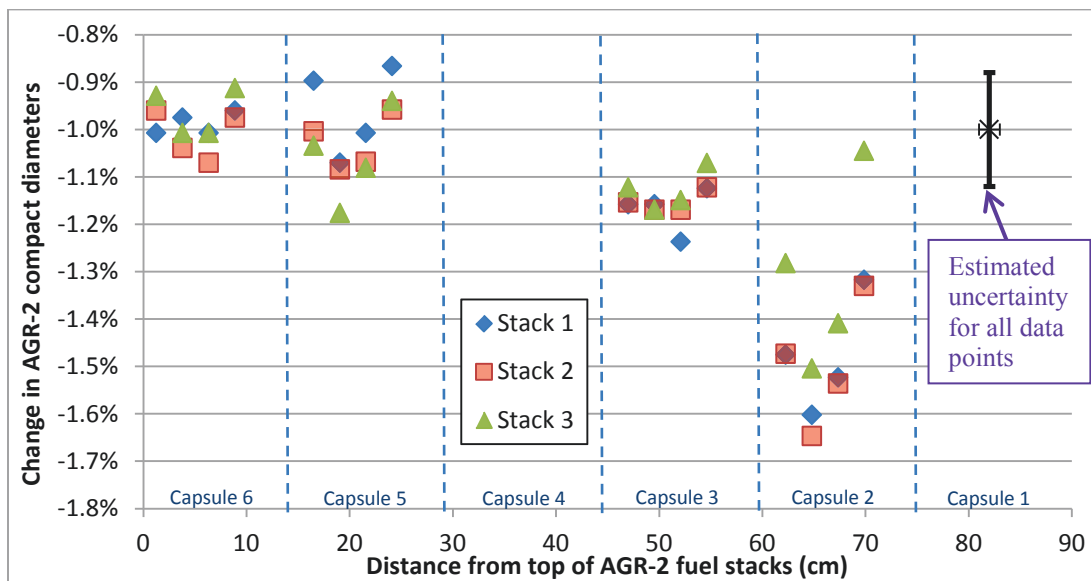


Figure 31. Average diameter changes among fuel compacts from AGR-2 Capsules 6, 5, 3, and 2.

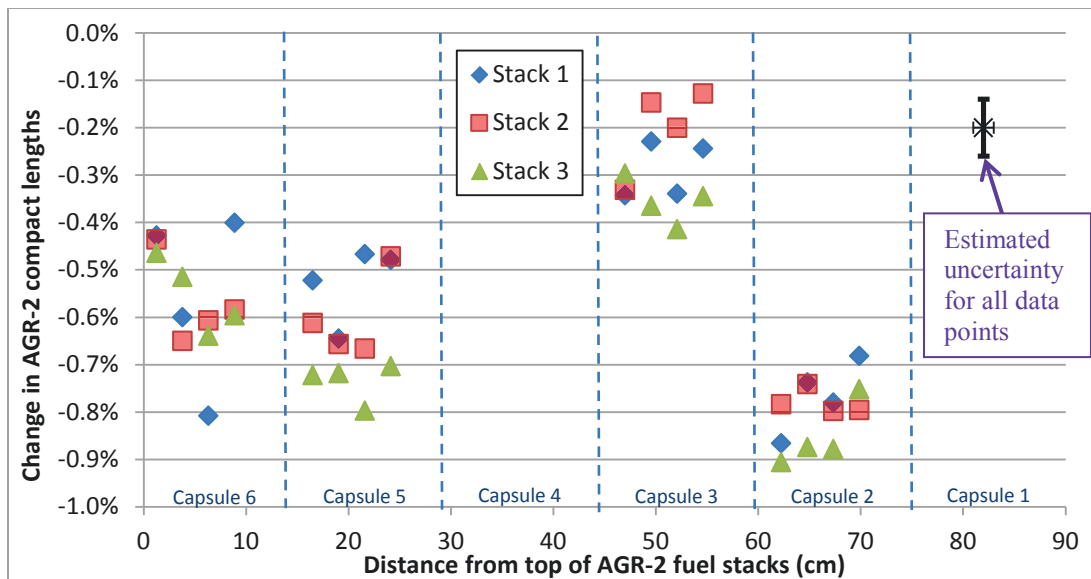
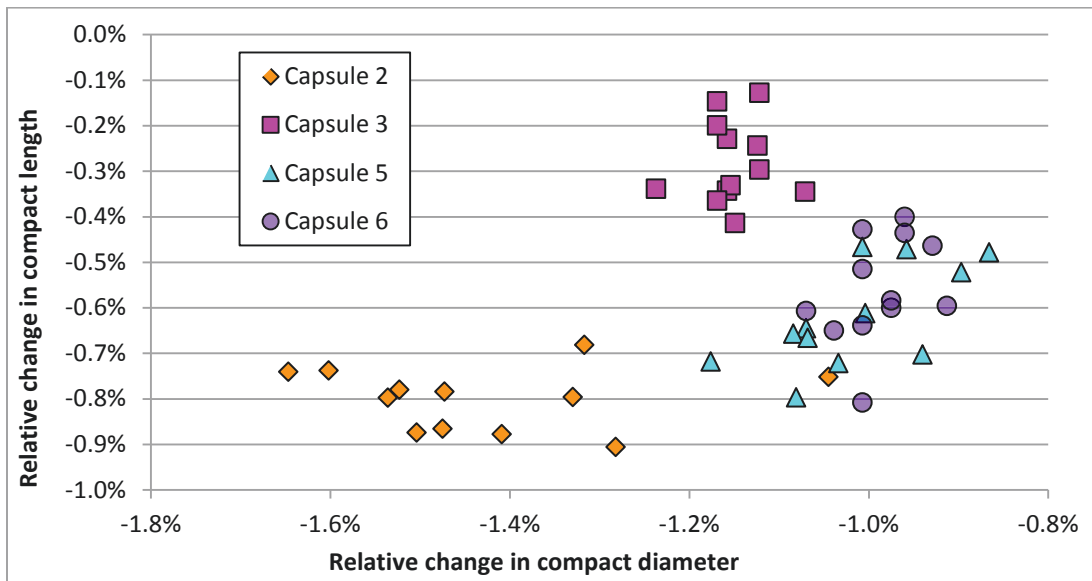


Figure 32. Average length changes among AGR-2 compacts from Capsules 6, 5, 3, and 2.

Because the vertical scale ranges are the same in Figure 31 and Figure 32, uncertainty considerations suggest that more scatter should be visually evident in the relative diameter changes than in the relative length changes. Inspection indicates that this is not always the case, which may reflect having six measurements contribute to each diameter average and merely three for each length average. Another

likely factor is the aforementioned difficulty in detecting crowns on the ends of compacts with the marginal backlighting from the LED light pipe.

All values in Figure 31 and Figure 32 are negative, indicating that all 48 fuel compacts shrank both radially and axially during irradiation. Capsule 2 compacts typically exhibit the most shrinkage in both directions. Capsule 3 compacts reveal slightly more radial shrinkage than compacts from Capsules 6 and 5 but significantly less axial shrinkage among compacts from these four capsules. Another view of the same results is displayed in Figure 33. While dimensional behavior of Capsule 5 and 6 compacts was quite consistent during irradiation, Capsule 2 and Capsule 3 compact results are statistically separate populations, albeit in different directions.



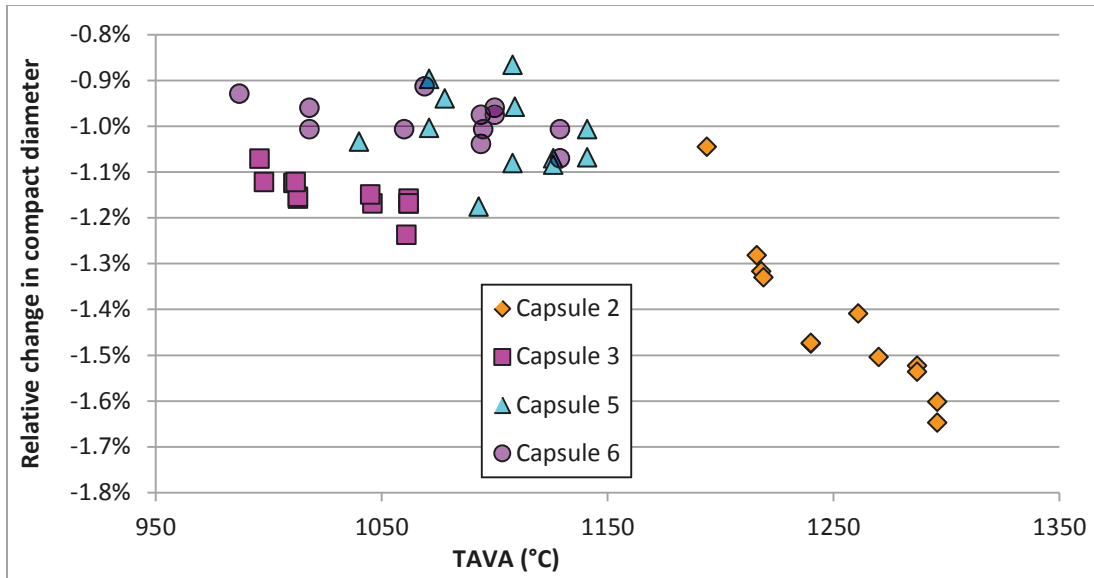


Figure 34. Percentage changes in compact diameter versus time-average volume-average temperature.

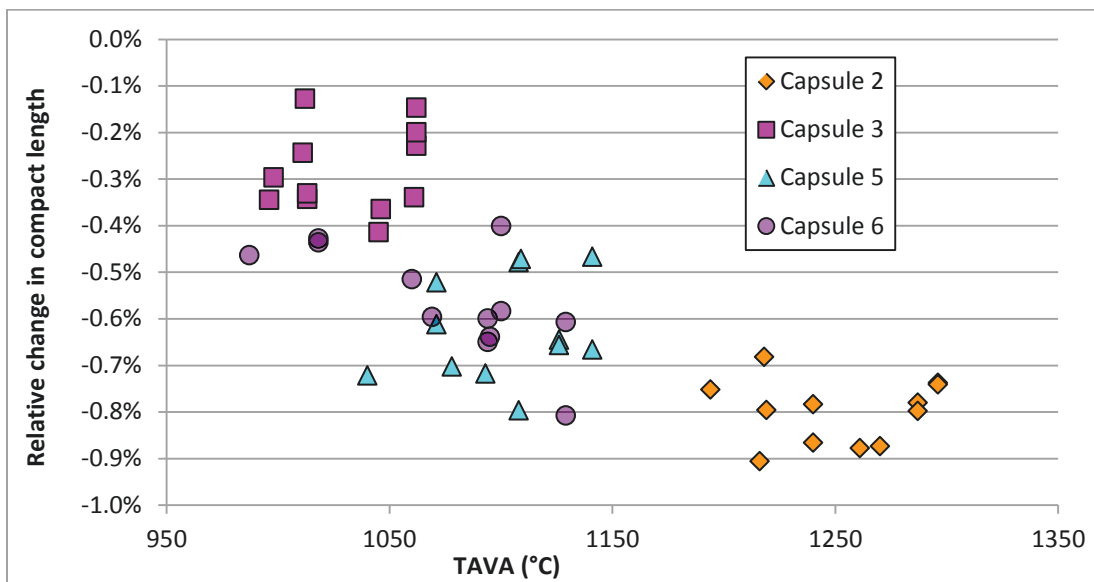


Figure 35. Percentage changes in compact length versus time-average volume-average temperature.

The potential dependence of radial and axial shrinkage on fast neutron fluence (Collin 2014) is investigated in Figure 36 and Figure 37, respectively. No definite relationship is apparent for either diameter changes or length changes when comparing results for compacts of a single fuel type irradiated at similar temperatures. Changes are reasonably consistent within capsules despite the significant fluence difference between Stack 3 (leftmost four data points for each capsule) and Stacks 1 and 2. More importantly, radial and axial shrinkage in compacts from Capsules 5 and 6 are very similar despite the large disparity in fast neutron fluence. Lower fluence Capsule 6 exhibited less shrinkage than higher fluence Capsule 2, but higher irradiation temperature has already been identified as the dominant reason why Capsule 2 compacts shrank more. This is further supported by the comparison between Capsules 5 and 2: Capsule 2 exhibited greater shrinkage in spite of similar fast fluence. As noted previously, Capsule 3 compacts shrank slightly more in the radial direction than Capsule 5 compacts but significantly

less axially. Figure 36 and Figure 37 jointly demonstrate that fast fluence was very similar for these two AGR-2 capsules. This comparison lends some additional credence to a potential influence of the larger particles with a low packing fraction in Capsule 3 compacts, although Capsule 3 compact temperatures were slightly lower on average than Capsule 5 temperatures (see Figure 34 and Figure 35).

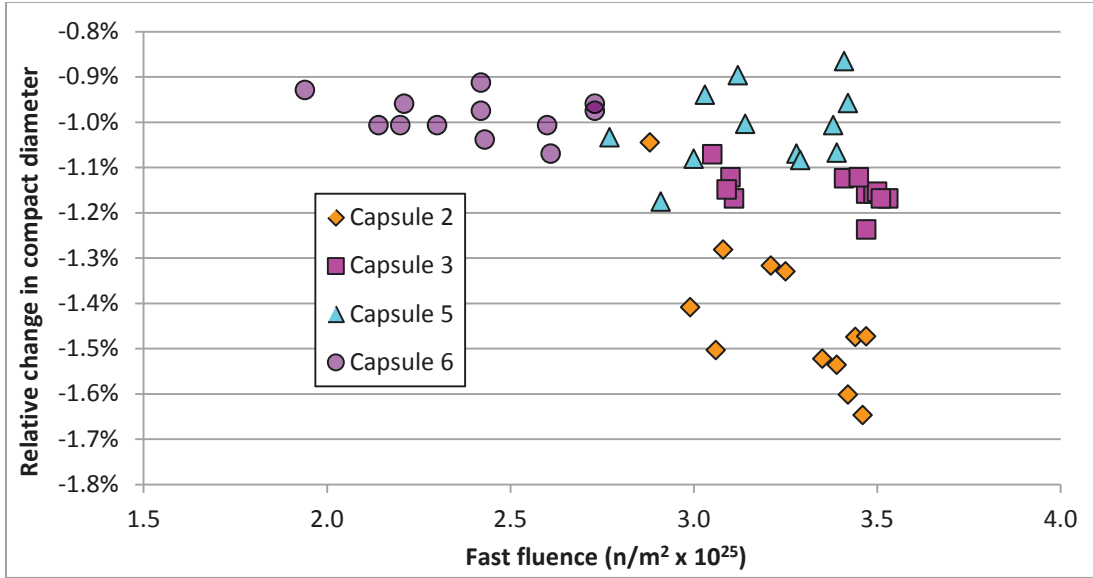


Figure 36. Average compact diameter changes versus calculated fast neutron fluence ($E > 0.18$ MeV).

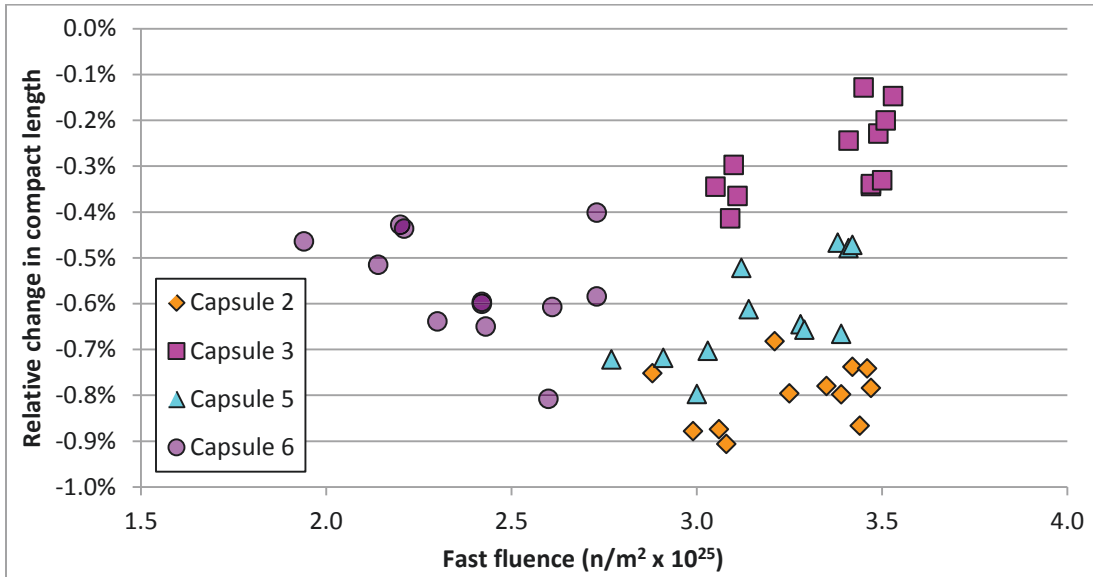


Figure 37. Average compact length changes versus calculated fast neutron fluence ($E > 0.18$ MeV).

4.4 Graphite Holder Inspections

After capsule shell removal, each graphite holder was daubed on the 0° azimuth (facing core center during irradiation; see Figure 3) with a bright marker at the bottom end. This reference mark clearly and conveniently established both azimuthal and axial orientations during subsequent manipulator handling operations, eliminating the need to carefully examine holder ends to determine orientations. Holder sides were photographed in color with a zoom lens through the hot cell window in 120° increments for full

surface coverage. This was done mainly to document the condition of holders before any subsequent disassembly damage, but it also proved helpful for highlighting some features such as deposit patterns.

Higher resolution black and white images were taken later with the metrology camera at three azimuths (approximately 120° apart). These images were primarily intended for extraction of accurate OD measurements. However, to diminish radiation dose to the camera and lens, these images were captured after unloading fuel compacts, so any damage from separating the upper head assembly (including through tubes, TCs, and gas lines) from holders could also be documented. Azimuths of the metrology images below generally were chosen to illustrate the worst of any such damage. Empty separated holders were supported by a fixture whose three prongs were approximately the same diameter as the through tubes, but aligning the through tube slots with the prongs could be difficult so damage occasionally occurred when loading holders onto the fixture. Six metrology images were obtained from each holder at each azimuth for a full-length composite because considerable overlap between images was needed for successful stitching. Overlapped regions appear slightly darker in the composites below. Holder inspection results that follow are presented in numerical order because the initial inspections and later metrology imaging were not performed in the same sequence to accommodate gamma scanning.

Through-window and metrology images of Holder 1 are respectively presented in the top and bottom of Figure 38. Patches of discoloration or thin deposits were found, but essentially just on the side shown. The discontinuity at mid-length in the top image occurred during fabrication because this holder was lathed from both ends. The patches are barely discernable in the lower image, but broken out regions can be easily seen along the 120° through tube slot. Such regions being located toward the top holder end typically indicates that the niobium through tube was ductile and flattened there when bent rather than incurring a brittle fracture. The through tube then had to be flexed up and down to ultimately induce a fracture.

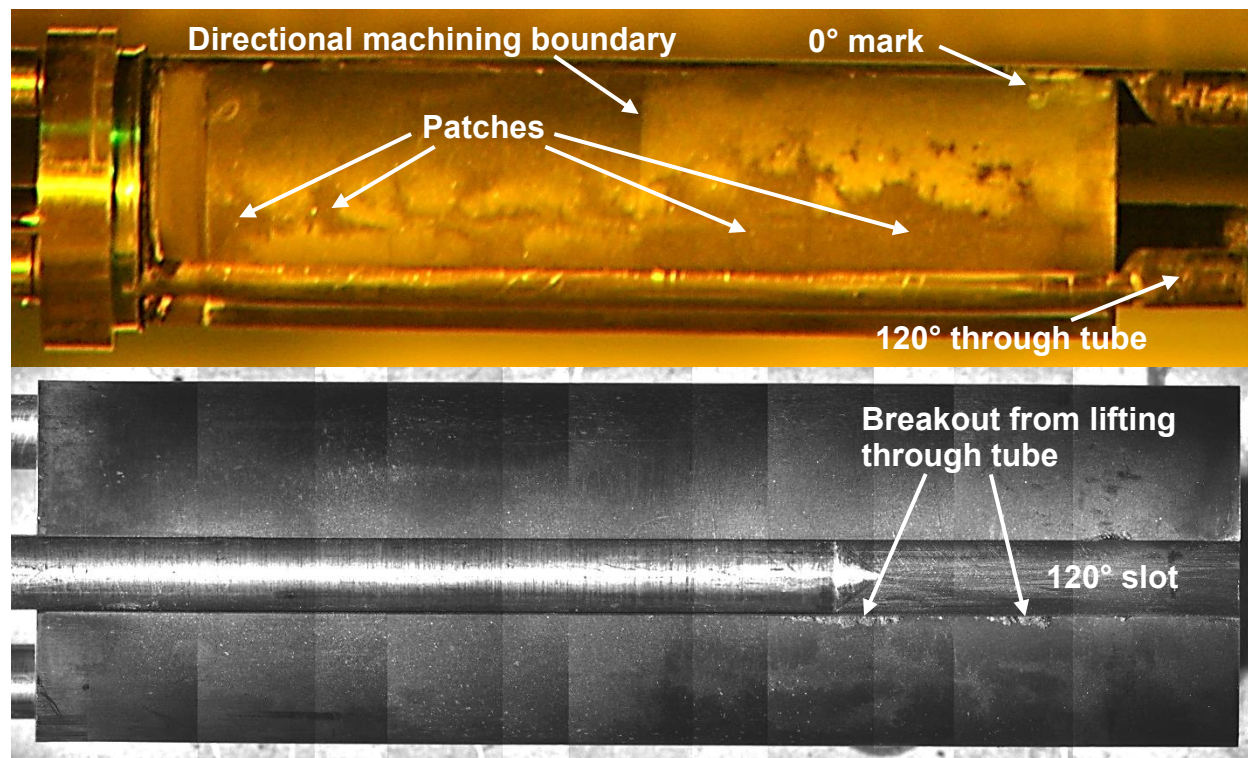


Figure 38. Holder 1 before separation from head assembly (top image, bottom end at right) and after head separation (bottom image, top end at right).

Two views of Holder 2 are provided in Figure 39. Although not obvious in these images, the anomalous regions had a smoother texture (no pits where B₄C fragments broke out during machining) and thus were deposits of unknown material rather than mere discolorations. Deposits were more apparent at the top end. They were virtually absent elsewhere except for loose flakes along the broken upper (0°) through tube (top image) that may have been scraped loose when the capsule shell was removed. These small flakes fell off the holder when it was rotated to inspect other sides, but they were collected in an underlying pan under the holder for analyses of fission product content along with the rest of the capsule components. The guide slot in the through tube prying fixture had to be aligned before inserting the pry rod (see Figure 17) with the aid of a mirror. The alignment fixture rotated while the clamp star wheels were tightened (before the 120° through tube was lifted), resulting in the damage in the bottom image. Nevertheless, the fingernail-shaped holder piece and tinier broken out fragments were caught in the pan for eventual fission product analyses.

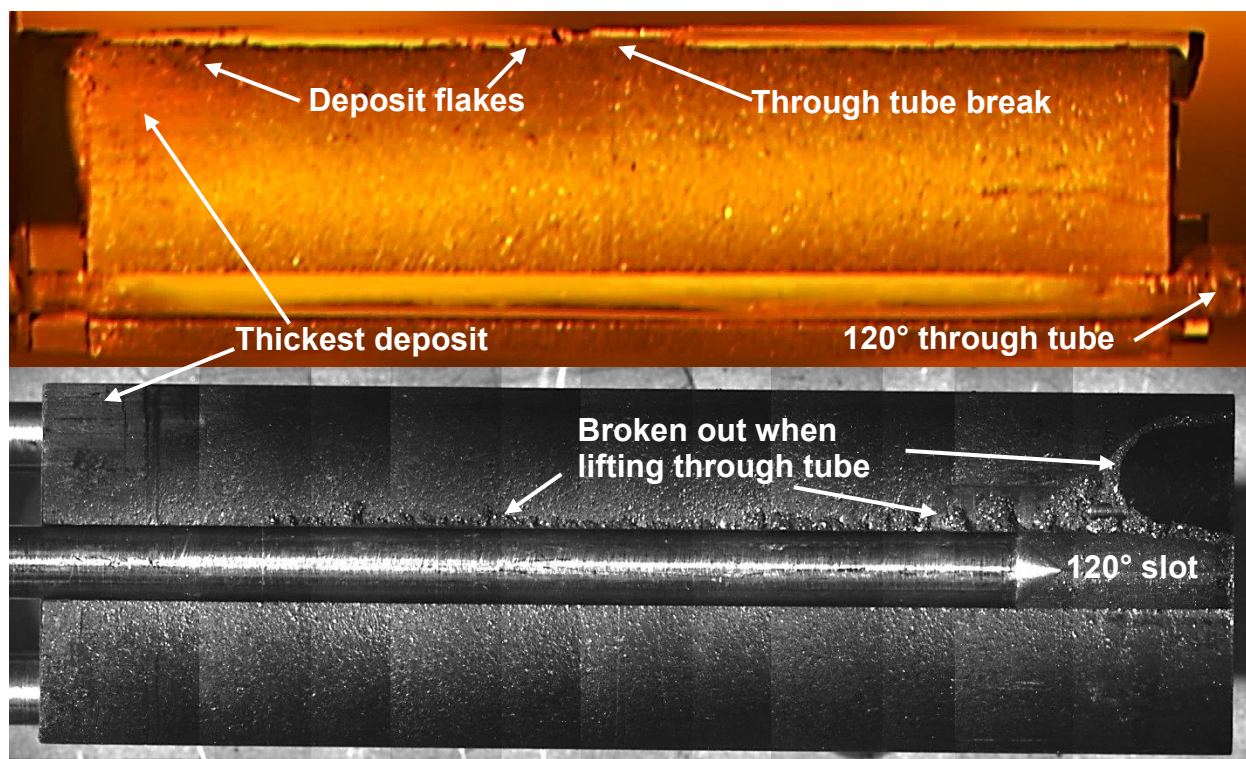


Figure 39. Holder 2, before (top) and after (bottom) head separation, bottom ends on right side.

The thickest patches of unknown deposit among AGR-2 holders were observed on Holder 3. As demonstrated in the upper portion of Figure 40, the patches were concentrated toward the top end with relatively little elsewhere. Deposit flakes found along the 0° through tube were loose and again fell into the pan when this holder was rotated to inspect its other sides. When the bottom graphite disk broke is unknown because its missing portions were not found after floor removal or shell removal, so the disk damage may have occurred during capsule assembly. The damage to Holder 3 in the bottom portion of Figure 40 occurred because the 240° through tube was ductile and flattened near the head when it was lifted, which broke out a small piece to expose a TC that remained inside the holder after hacksawing. The large fracture happened after disassembly when the holder was pushed onto the 3-prong fixture for taking metrology images. No material broke off Holder 3 during this incident, but the fracture did not close completely, which artificially enlarged diameter measurements near the top of Holder 3 as discussed in Section 4.5. Nevertheless, an increase in diameter is also evident near the top of Holder 3 in the bottom portion of Figure 40, which cannot be attributed to the fracture. Deposit patches near the holder top likely

contributed to this conspicuous flaring, but actual swelling during irradiation may also have been a key factor.

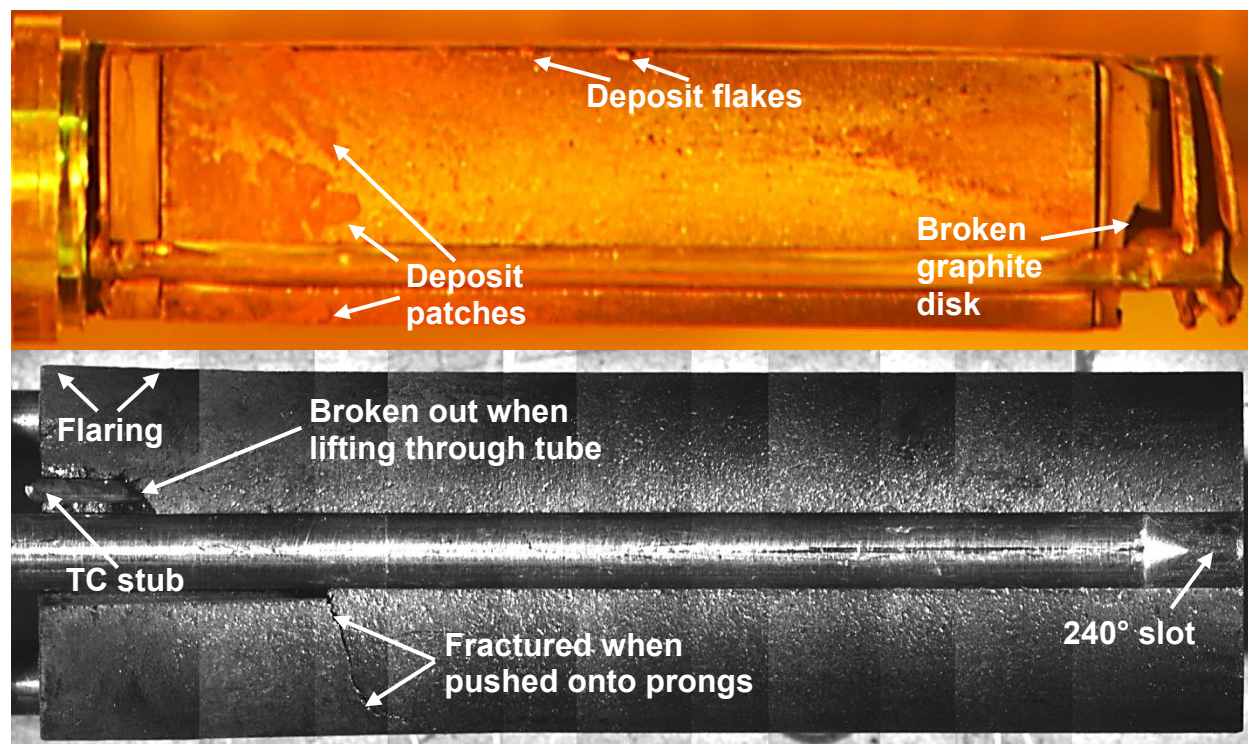


Figure 40. Thick deposit patches (top) and handling fracture on Holder 3, bottom ends on right side.

Unknown material deposits were generally confined to the top end of Holder 4, as suggested in the upper image of Figure 41. Another feature of interest in this image is the row of small protrusions along the 120° through tube. They were evidently created when gas lines and TC leads from the lower capsules in the test train were partially pulled through the through tubes during removal of Capsule 5 (see Figure 14). (Some damage also occurred to the interior of the through tubes because they had to be reamed extensively before the rotator prongs could be inserted.) The only significant disassembly damage to Holder 4 was the narrow piece that broke out to expose the gas exit line hole (lower image in Figure 41). When lifted, the 0° through tube flattened near the head, rather than incurring a brittle fracture, and had to be flexed several times before it finally broke. The flattened region caught against the side of the through tube slot during the flexing process.

The camera used to take pictures through the hot cell window was temporarily unavailable immediately after the Capsule 5 shell was removed, so no images could be obtained when Holder 5 was initially inspected. According to inspection notes, Holder 5 had several small patches of dark deposit near mid-length on two sides, with no other significant features at this point of the disassembly. Figure 42 reveals that handling damage through metrology imaging was minor on Holder 5. The upper image shows a TC hole exposed where the 120° through tube flattened and subsequent flexing broke out one side of the slot. As well as a short crack from lifting the 240° through tube, the lower image depicts two axial gouges that apparently were created by burrs when the shell was removed. Such burrs probably formed when other capsule shells were cut, but such conspicuous scratches may have occurred only on Holder 5 because of its relatively large OD.

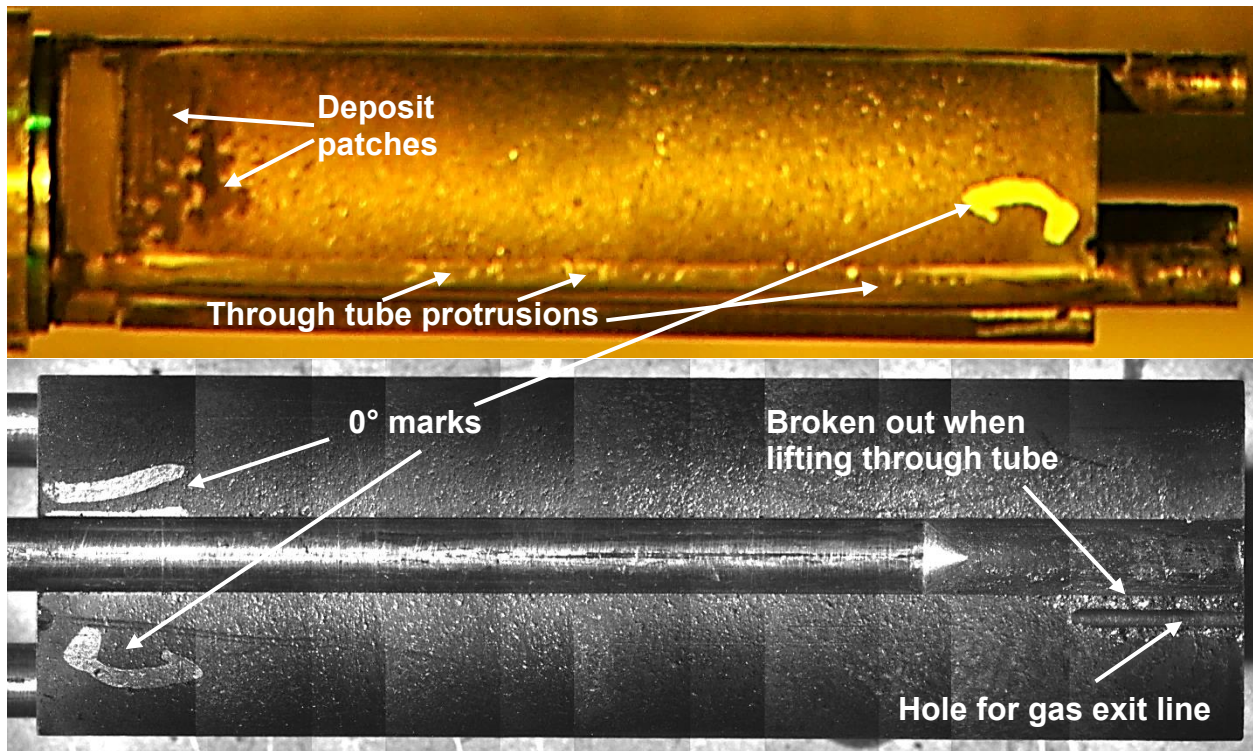


Figure 41. 0° azimuth of Holder 4, bottom end on right side (upper image) and bottom end left (lower image).

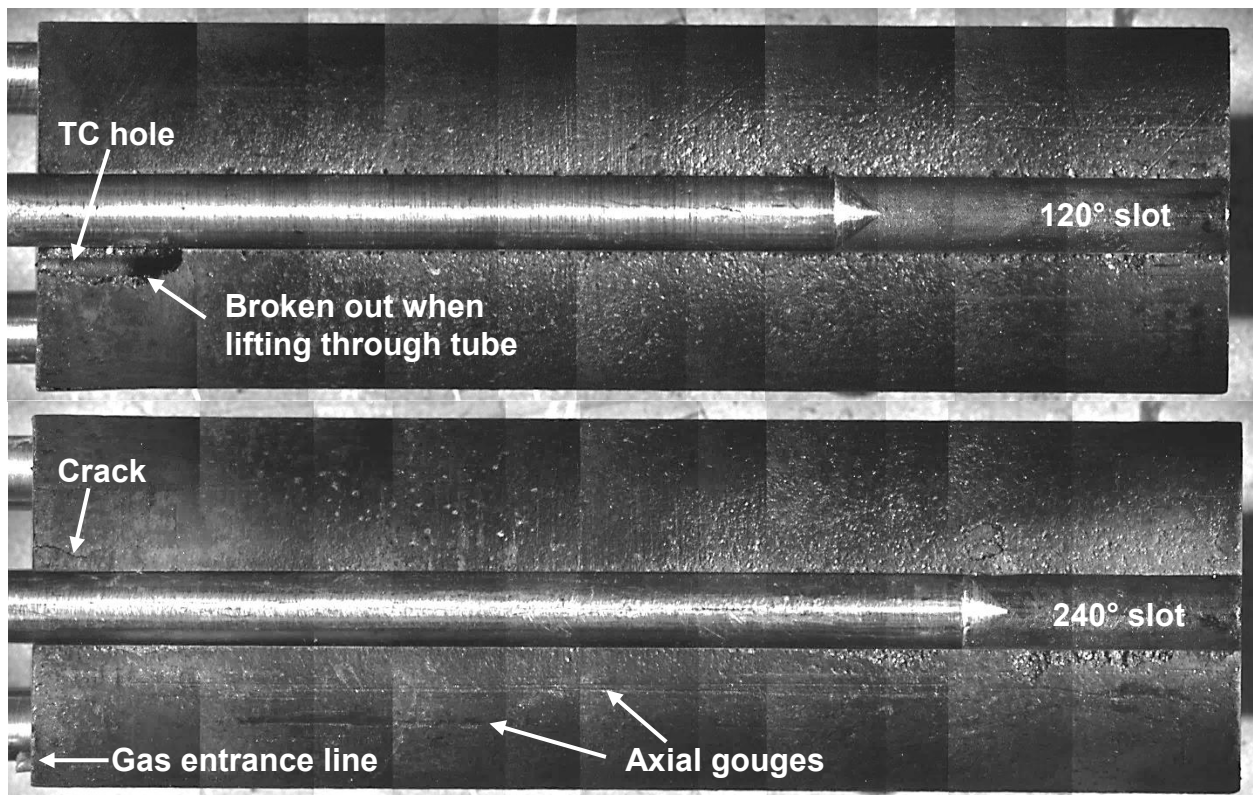


Figure 42. 120° azimuth of Holder 5 (top) and 240° azimuth (bottom), bottom ends on right side.

Holder 6 exhibited thin deposit patches or discolorations near the top end on all sides. As revealed in the upper portion of Figure 43, a ridge of small protrusions was found along the 120° through tube, which evidently formed when TC leads and gas lines were pulled from it. The through tubes had to be reamed before Capsule 6 could be loaded onto the 3-pronged rotating fixture, and wedges were needed to withdraw the prongs before removing the through tubes. The upper image further indicates that both the 0° and 240° through tubes were fractured before prying them upward during disassembly. Both through tubes fractured near the head (apparently during floor separation), which suggests that they were relatively brittle compared to most other AGR-2 through tubes. The lower portion of Figure 43 shows a thumbnail-sized piece broken off the top end when Holder 6 was loaded onto the 3-pronged fixture. It was captured in the pan as with all other holder fragments.

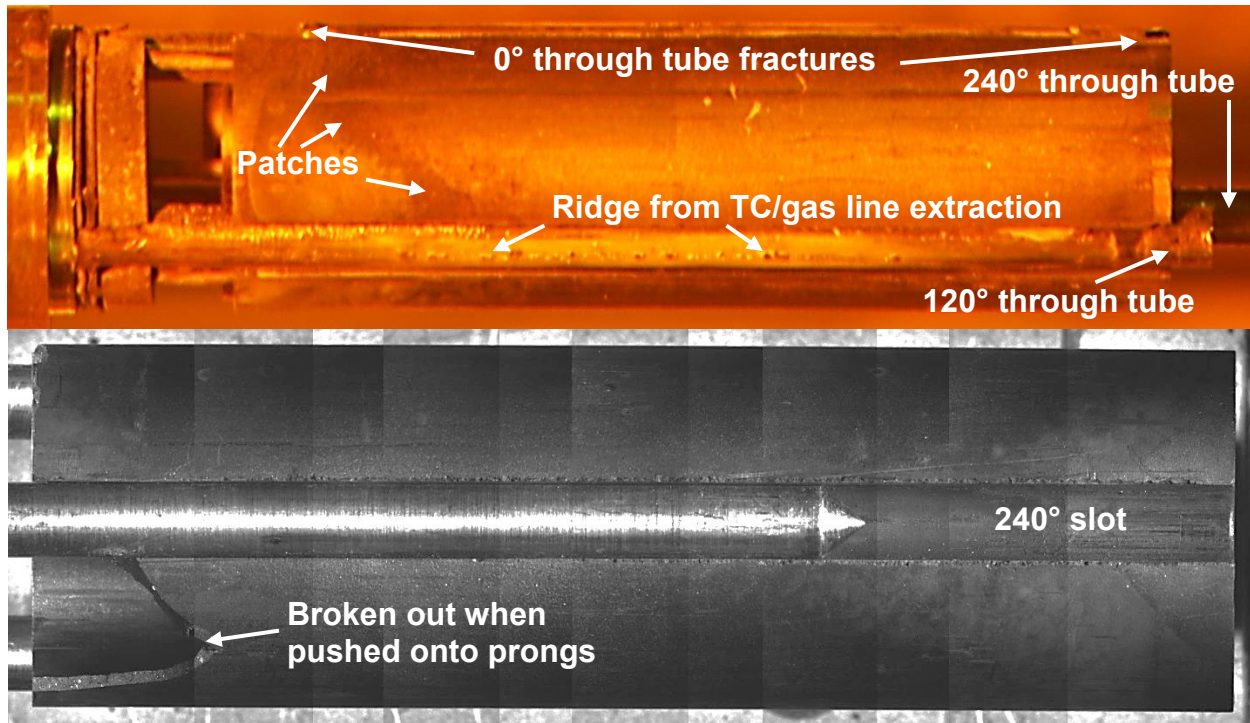


Figure 43. Two azimuths of Holder 6, bottom end to right (upper image) and bottom end to left (lower image).

4.5 Graphite Holder Dimensional Changes

ODs were extracted from composite images of all AGR-2 graphite holders. Each holder was imaged at three azimuths facing the camera (120 degrees apart) for inspecting the full external surface. However, only one of the three images was measured, where the azimuth analyzed was generally selected to avoid any pieces broken out before imaging. As with compact images, OD resolution is limited by the pixel width on the digital images (11.7 μm). As displayed in Figure 44, a total of eight diameter measurements (vertical blue lines) were made outside overlapped regions in the stitched composite. Specific locations were chosen such that two measurements were made over positions occupied by each of the four compacts. (Two measurements were made over each of the upper and lower halves of the long Capsule 1 compacts—see Figure 3.)

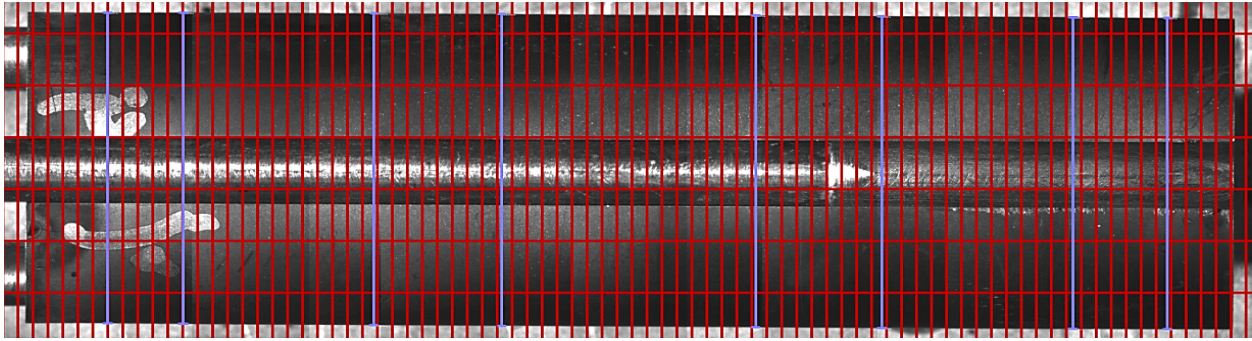


Figure 44. Example of an analyzed graphite holder image with blue lines at diameter measurement locations.

Holder diameter data are tabulated below in terms of absolute PIE diameter, diameter changes from as-fabricated diameters, and percentage changes. As-fabricated dimensions were extracted from the Inspection Data Traveler for Work Order 09-208 under which the AGR-2 graphite holders were fabricated. Only one pre-irradiation measurement was made of the OD of each holder (position not recorded), so whether there originally was any significant variability along the length of any holder is unknown.

IDs of holder holes were measured after removal of fuel compacts using a commercial bore gauge with three self-centering probes (retractable to prevent gouging). As shown in Figure 45, the bore gauge handle was centered in a fixture (mounted in a vise to the left outside the field of view) while each graphite holder was rigidly mounted in support cradle, which jointly prevented significant misalignment errors. The dial indicator was read through the hot cell window with the aid of binoculars. While probes were retracted, the bore gauge was moved to different axial positions by sliding one fixture along the disassembly table rails. Depth positions inside the holder were dictated by fiducial marks placed on the bore gauge shaft. After all four readings were made along each hole, the entire sequence was repeated to confirm repeatability (particularly the absence of graphite dust on probe anvils). Thus each ID value tabulated below represents an average of two readings at each hole position.

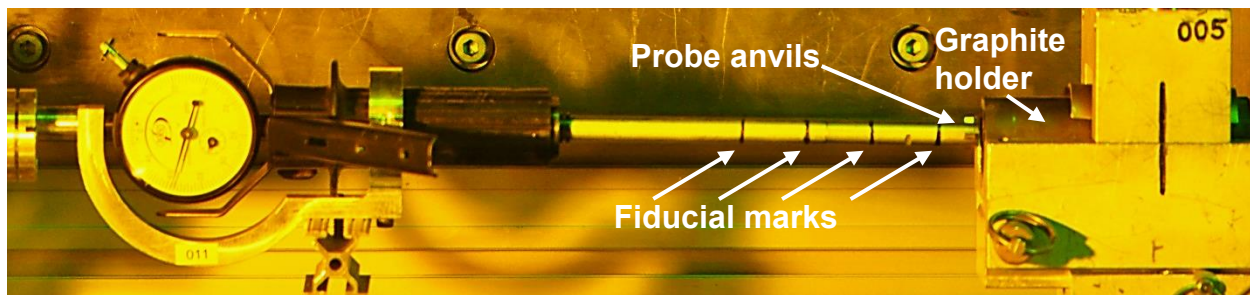


Figure 45. Small bore gauge before inserting probe tip into Holder 1.

All small bore gauge readings were relative to the 12.446-mm (0.4900-inch) ring gauge standard. Before any readings were taken on any AGR-2 holder, the bore gauge dial was rotated once to “0” with the probes extended inside the standard to null the gauge. The dial was then locked and not rotated again. However, multiple readings were taken inside the standard before and after the three holes in each holder were measured to compute an average bias (zero drift) for each set of holder measurements. Each absolute ID value was then calculated by adding the average bore gauge reading from each position to the standard value and finally subtracting the average bias value.

Ideally, the absolute hole ID results from PIE could be compared to as-fabricated IDs to determine changes during irradiation. Unfortunately, the as-fabricated information on AGR-2 graphite holder holes is not adequate for this purpose. Instead of making an as-fabricated measurement in each hole with either

a bore gauge or inner micrometer, pin gauges of successively smaller diameter were tried in all three holes until a single pin gauge would slide all the way through all three holes. The diameter of this pin gauge was recorded as the as-fabricated ID of all three holes, which was deemed sufficient to verify that drawing tolerances were met. Furthermore, each hole was bored from both holder ends so a small misalignment step could occur at mid-length, and the inspector confirmed that a larger pin gauge would often hang up at this point. Consequently, from the standpoint of radial gaps, hole IDs in each holder were probably somewhat larger than the recorded value by unknown amounts. Under these circumstances, PIE hole IDs can merely be compared to the drawing tolerance range for each AGR-2 holder.

4.5.1 Metrology Results from Capsule 1 Graphite Holder

OD findings from metrology on a Capsule 1 graphite holder image (0° azimuth facing camera) are summarized in Table 6 and plotted in Figure 46. Holder 1 was measured as 30.66 mm in diameter after fabrication, but at an unknown axial location. Negative change values in Table 6 indicate shrinkage from the as-fabricated measurement. Figure 46 reveals that somewhat more shrinkage was measured toward the ends of Holder 1, especially near its bottom (the bottom of the AGR-2 test train).

Table 6. Exterior metrology results from the AGR-2 Capsule 1 graphite holder.

Distance from Holder Top (cm)	OD (mm)	OD Change (mm)	% Change
0.56	30.548	-0.112	-0.366%
1.35	30.571	-0.089	-0.290%
2.95	30.606	-0.054	-0.175%
4.01	30.595	-0.065	-0.213%
6.15	30.606	-0.054	-0.175%
7.24	30.595	-0.065	-0.213%
8.84	30.536	-0.124	-0.403%
9.45	30.501	-0.159	-0.517%
Axial Average	30.570 ($\sigma = 0.036$)	-0.090	-0.294%

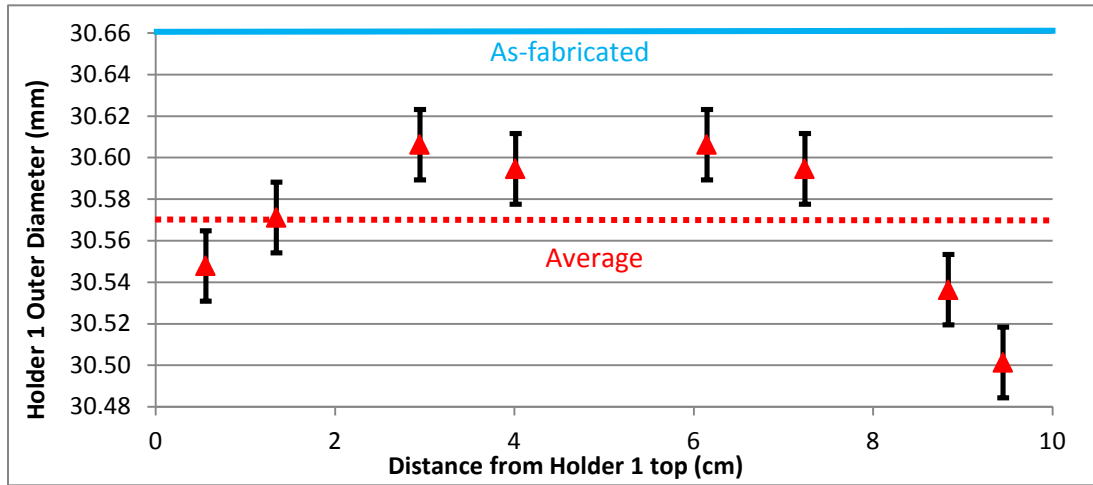


Figure 46. Individual OD measurements from 0° composite image of Capsule 1 graphite holder.

The error bars in Figure 46 are a combined standard uncertainty that equals ± 0.017 mm, which is the root-sum-square of a bias term and a repeatability term. The potential bias is estimated as the pixel width at the object plane (0.0117 mm), as for compact ODs. However, whereas the compact repeatability term was obtained from the standard deviation for each average compact OD (see Section 4.3), the data points in Figure 46 represent individual measurements without standard deviations. Accordingly, ten independent OD measurements were made near the middle of a composite image of the steel holder check

standard, which produced a standard deviation of 0.0124 mm as a defensible estimate of the repeatability for a single holder OD measurement. Error bars of the same magnitude thus appear in OD plots below for the other five AGR-2 graphite holders. (Note that 0.017 mm equals 0.00067 inch, which would satisfy the $\text{AGR-1} \leq 0.001$ -inch combined standard uncertainty requirement with ample margin.)

Hole diameters measured by bore gauge in Holder 1 are presented in Table 7 and plotted in Figure 47. All values are within the drawing tolerances so no firm conclusion can be drawn on hole shrinkage or expansion. However, the profile of Figure 47 resembles that of the Holder 1 OD in Figure 46, with the smallest values for all three holes near the bottom of Holder 1. Because the Holder 1 OD definitely shrank the most at this position, shrinkage of the holes also seems likely here (possibly along their entire length).

Table 7. Hole diameters in Capsule 1 graphite holder (drawing tolerances 12.598 to 12.675 mm).

Axial Position (cm from top)	Hole 1 (mm)	Hole 2 (mm)	Hole 3 (mm)
1.27	12.657	12.657	12.650
3.81	12.657	12.657	12.657
6.35	12.657	12.650	12.644
8.89	12.644	12.638	12.638
Hole Averages	12.654	12.651	12.647
Grand Average	12.6505 mm ($\sigma = 0.0073$ mm)		

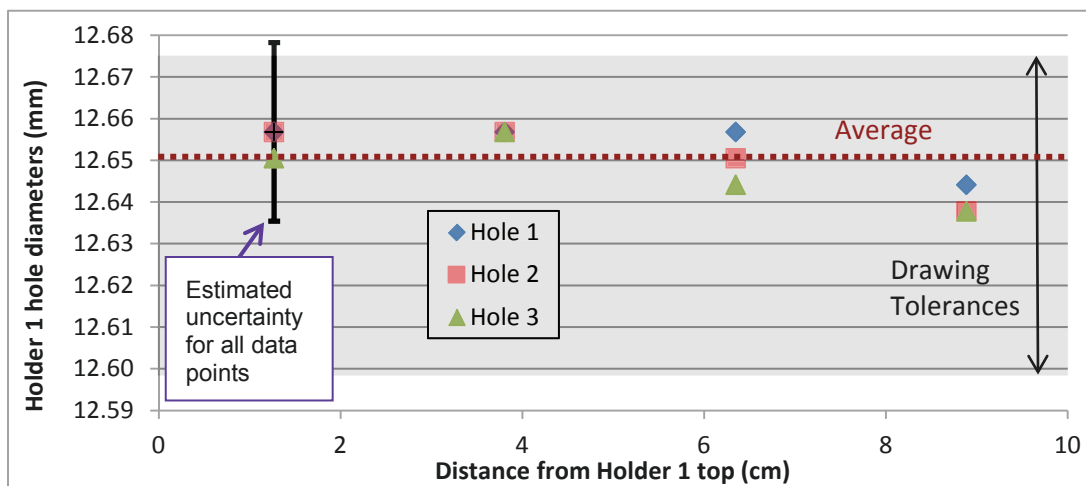


Figure 47. Bore gauge measurements inside Holder 1 holes after unloading fuel compacts.

The error bar in Figure 47 is a ± 0.0214 -mm combined standard uncertainty ($< \pm 0.0254$ -mm AGR-1 requirement). It applies to all 12 data points and was estimated by root-sum-squaring a bias term and a repeatability term. The bias term is the bore gauge's resolution—the dial indicator's 0.0005-inch (0.0125-mm) graduation spacing. This value also represented the amount by which the ring gauge standard checks often changed before and after measurements were made on a given holder. The 0.0174-mm repeatability term is the standard deviation of ten independent readings in the standard where the standard, the AGR-2 bore gauge, and the bore gauge centering guide were unloaded and reloaded between readings. Error bars of the same magnitude appear in hole ID plots below for other holders.

4.5.2 Metrology Results from Capsule 2 Graphite Holder

OD findings from a Holder 2 composite image (240° azimuth up) are summarized in Table 8 and plotted in Figure 48. Holder 2 had an as-fabricated OD of 30.65 mm. Expansion during irradiation is

indicated by the positive values for diameter change in Table 8. More expansion occurred toward the ends of Holder 2.

Table 8. Exterior metrology results from the Capsule 2 graphite holder.

Distance from Holder Top (cm)	OD (mm)	OD Change (mm)	% Change
0.94	30.688	0.038	0.123%
1.32	30.688	0.038	0.123%
2.82	30.676	0.026	0.085%
4.06	30.665	0.015	0.048%
6.12	30.665	0.015	0.048%
7.24	30.676	0.026	0.085%
8.89	30.699	0.049	0.161%
9.14	30.699	0.049	0.161%
Axial Average	30.682 ($\sigma = 0.013$)	0.032	0.104%

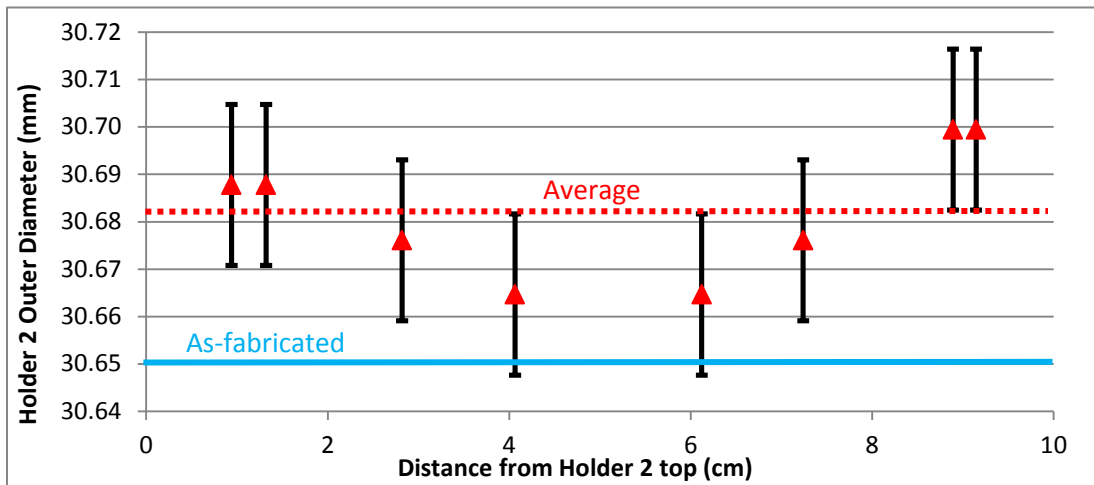


Figure 48. OD measurements from 240° azimuth image of the Capsule 2 graphite holder.

Hole diameters inside Holder 2 are presented in Table 9 and plotted in Figure 49. All measurements are inside drawing tolerances, so it is not clear whether Holder 2 hole sizes changed during irradiation.

Table 9. Hole diameters in Capsule 2 graphite holder (drawing tolerances 12.370 to 12.446 mm).

Axial Position (cm from top)	Hole 1 (mm)	Hole 2 (mm)	Hole 3 (mm)
1.27	12.421	12.427	12.433
3.81	12.433	12.433	12.427
6.35	12.433	12.433	12.421
8.89	12.433	12.433	12.446
Hole Averages	12.430	12.432	12.432
Grand Average	12.4312 mm ($\sigma = 0.0065$ mm)		

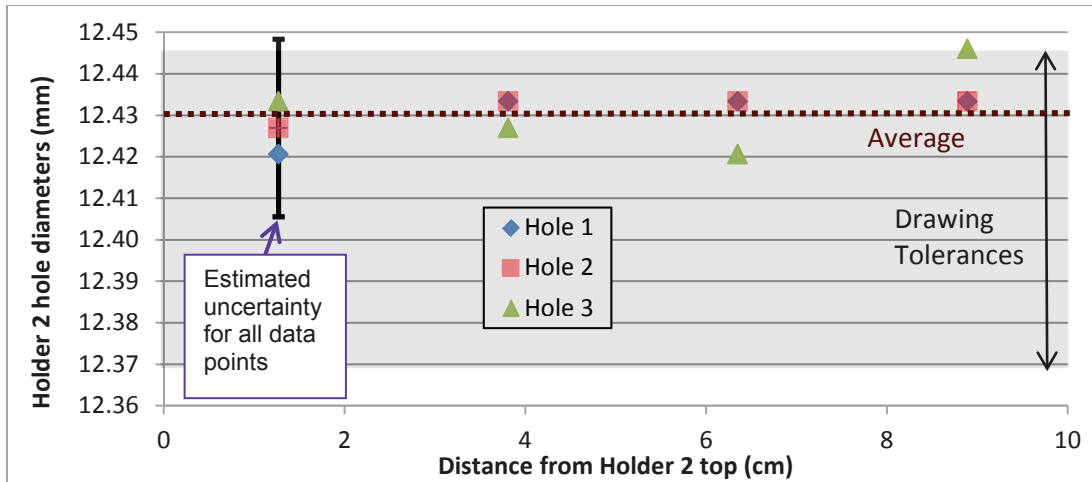


Figure 49. Hole IDs measured inside the Capsule 2 graphite holder (all ± 0.0214 mm).

4.5.3 Metrology Results from Capsule 3 Graphite Holder

OD results from a Holder 3 composite image (120° azimuth up) are summarized in Table 10 and plotted in Figure 50. The as-fabricated OD of Holder 3 was 30.35 mm. Positive change values in Table 10 denote expansion during the AGR-irradiation. ODs at the 0.041 and 1.22-cm elevations (at the level of the top three compacts in the capsule) were artificially enlarged by the crack that occurred when Holder 3 was loaded onto the pronged fixture for metrology imaging (see Figure 40), despite choosing the azimuth least affected by the crack for dimensional analysis. Consequently, these two OD values were excluded from Figure 50 and the averages in Table 10. Otherwise the substantial radial expansion is quite consistent along the length of Holder 3. The standard deviation among the remaining six measurements of 0.008 mm is considerably smaller than found along any of the other five AGR-2 holders.

Table 10. Exterior metrology results from AGR-2 Capsule 3 graphite holder.

Distance from Holder Top (cm)	OD (mm)	OD Change (mm)	% Change
0.41	30.816 ^a	0.466 ^a	1.535% ^a
1.22	30.793 ^a	0.443 ^a	1.460% ^a
2.82	30.490	0.140	0.460%
3.91	30.478	0.128	0.422%
6.05	30.466	0.116	0.383%
7.06	30.478	0.128	0.422%
8.79	30.490	0.140	0.460%
9.65	30.478	0.128	0.422%
Axial Average	30.480^b ($\sigma = 0.008^b$)	0.130^b	0.428%^b

a. Values enlarged by crack.

b. Excluding values influenced by crack.

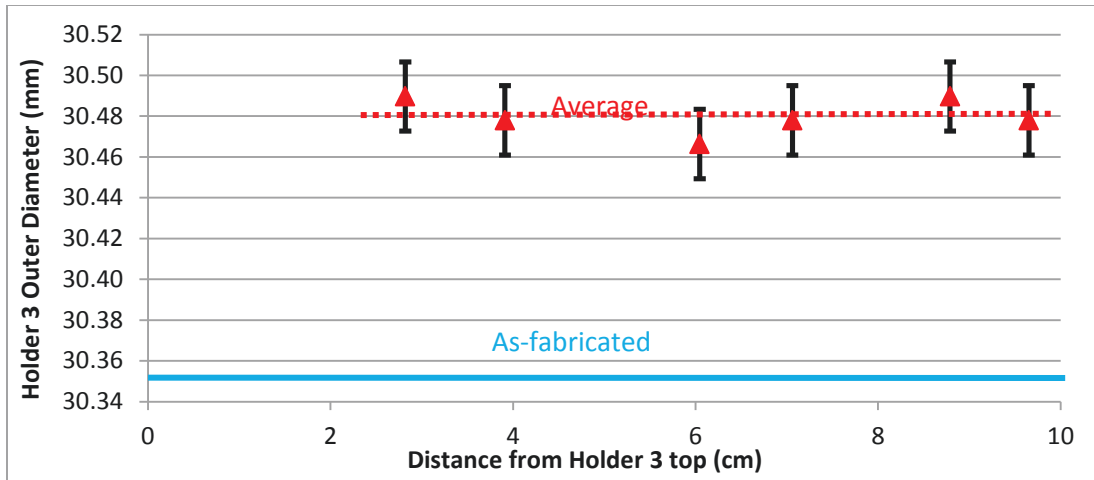


Figure 50. OD measurements from 120° azimuth image of the Capsule 3 graphite holder (excluding top two measurements enlarged by crack).

Hole diameters measured in Holder 3 are presented in Table 11 and plotted in Figure 51. All Hole 1 and Hole 2 values are larger than the drawing tolerances, generally by amounts exceeding measurement uncertainty. Thus these two holes definitely enlarged during irradiation, consistent with the OD expansion of Holder 3. Hole 3 diameter measurements are appreciably smaller (occasionally dropping into the drawing tolerance range), which may be related to the lower neutron fluence it received (see Figure 2).

Table 11. Hole diameters in Capsule 3 graphite holder (drawing tolerances 12.344 to 12.421 mm).

Axial Position (cm from top)	Hole 1 (mm)	Hole 2 (mm)	Hole 3 (mm)
1.27	12.459	12.459	12.427
3.81	12.440	12.433	12.408
6.35	12.446	12.446	12.421
8.89	12.459	12.465	12.427
Hole Averages	12.451	12.451	12.421
Grand Average	12.4407 mm ($\sigma = 0.0172$ mm)		

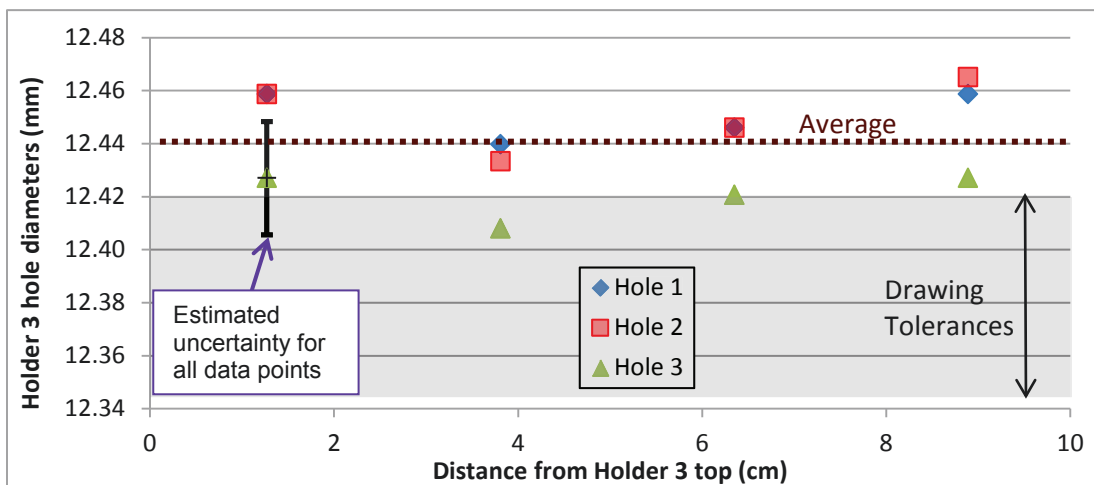


Figure 51. Hole IDs measured inside the Capsule 3 graphite holder (all ± 0.0214 mm).

4.5.4 Metrology Results from Capsule 4 Graphite Holder

OD findings from Holder 4 composite image (0° azimuth) are summarized in Table 12 and plotted in Figure 52. Holder 4 had an as-fabricated OD of 30.35 mm. Positive change values throughout Table 12 indicate radial expansion. More expansion occurred toward the ends by amounts beyond uncertainty.

Table 12. Exterior metrology results from AGR-2 Capsule 4 graphite holder.

Distance from Holder Top (cm)	OD (mm)	OD Change (mm)	% Change
0.33	30.501	0.151	0.499%
1.42	30.490	0.140	0.460%
2.82	30.455	0.105	0.345%
4.06	30.455	0.105	0.345%
6.10	30.443	0.093	0.306%
7.37	30.455	0.105	0.345%
8.94	30.490	0.140	0.460%
9.32	30.490	0.140	0.460%
Axial Average	30.472 ($\sigma = 0.021$)	0.122	0.402%

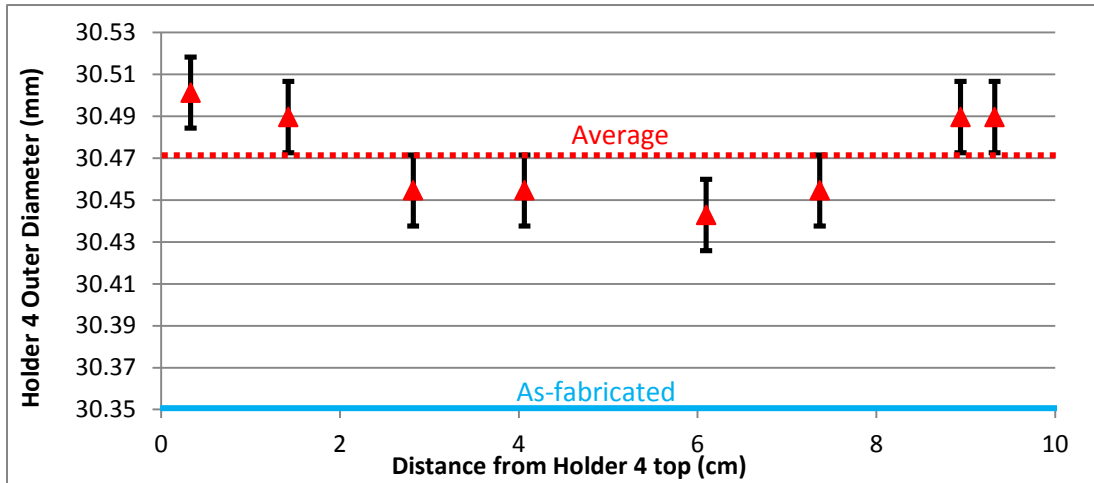


Figure 52. OD measurements from 0° azimuth image of the Capsule 4 graphite holder.

Hole diameters inside Holder 4 are presented in Table 13 and plotted in Figure 53. All values are substantially above the drawing tolerance range so all three holes expanded during irradiation.

Table 13. Hole diameters in Capsule 4 graphite holder (drawing tolerances 12.319 to 12.395 mm).

Axial Position (cm from top)	Hole 1 (mm)	Hole 2 (mm)	Hole 3 (mm)
1.27	12.454	12.454	12.403
3.81	12.428	12.416	12.403
6.35	12.416	12.416	12.416
8.89	12.428	12.441	12.416
Hole Averages	12.431	12.431	12.409
Grand Average	12.4240 mm ($\sigma = 0.0167$ mm)		

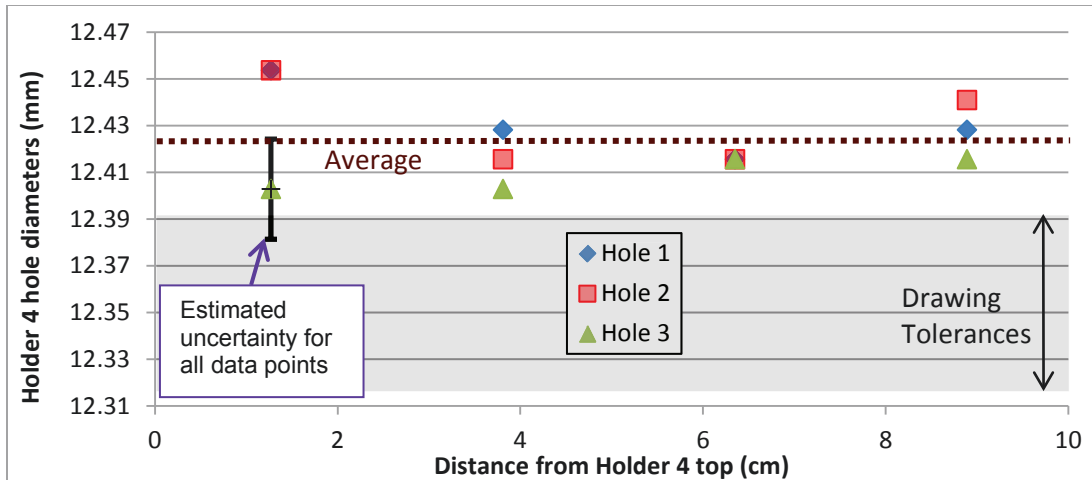


Figure 53. Hole IDs measured inside the Capsule 4 graphite holder (all ± 0.0214 mm).

4.5.5 Metrology Results from Capsule 5 Graphite Holder

Holder 5 ODs measured on the 120° composite image are summarized in Table 14 and plotted in Figure 54. Holder 5 had an as-fabricated OD of 31.11 mm. All diameter changes in Table 14 are positive, so Holder 5 expanded during the AGR-2 experiment. More expansion occurred near the ends of Holder 5.

Table 14. Exterior metrology results from AGR-2 Capsule 5 graphite holder.

Distance from Holder Top (cm)	OD (mm)	OD Change (mm)	% Change
0.97	31.259	0.149	0.480%
1.32	31.248	0.138	0.442%
2.90	31.201	0.091	0.292%
4.09	31.201	0.091	0.292%
6.15	31.236	0.126	0.405%
7.29	31.248	0.138	0.442%
8.92	31.248	0.138	0.442%
9.14	31.259	0.149	0.480%
Axial Average	31.237 ($\sigma = 0.022$)	0.127	0.409%

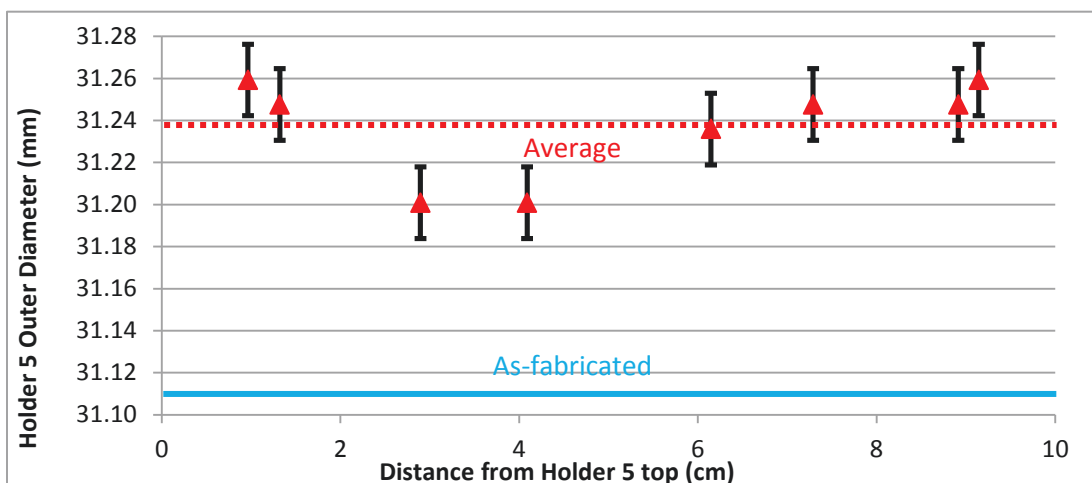


Figure 54. OD measurements from 120° azimuth image of the Capsule 5 graphite holder.

Holder 5 ID measurements are presented in Table 15 and plotted in Figure 55. All twelve values are larger than drawing tolerances, confirming expansion during irradiation.

Table 15. Hole diameters in Capsule 5 graphite holder (drawing tolerances 12.395 to 12.446 mm).

Axial Position (cm from top)	Hole 1 (mm)	Hole 2 (mm)	Hole 3 (mm)
1.27	12.471	12.478	12.465
3.81	12.459	12.478	12.471
6.35	12.471	12.478	12.459
8.89	12.465	12.488	12.484
Hole Averages	12.467	12.480	12.470
Grand Average	12.4723 mm ($\sigma = 0.0090$ mm)		

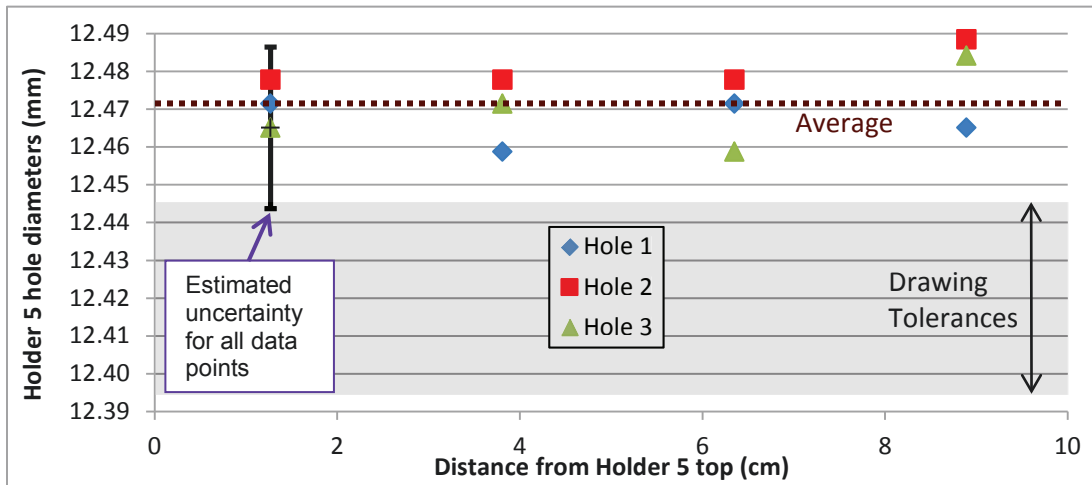


Figure 55. Hole IDs measured inside the Capsule 5 graphite holder (all ± 0.0214 mm).

4.5.6 Metrology Results from Capsule 6 Graphite Holder

Holder 6 ODs obtained by analyzing the 0° composite image are summarized in Table 16 and plotted in Figure 56. Holder 6 had an as-fabricated OD of 30.66 mm. All of the change values in Table 16 are negative, which indicates shrinkage over the entire length during irradiation. More shrinkage occurred toward the ends of Holder 6, especially near its top (top of AGR-2 test train).

Table 16. Exterior metrology results from AGR-2 Capsule 6 graphite holder.

Distance from Holder Top (cm)	OD (mm)	OD Change (mm)	% Change
0.33	30.455	-0.205	-0.670%
1.24	30.478	-0.182	-0.594%
3.00	30.548	-0.112	-0.366%
4.04	30.571	-0.089	-0.290%
6.15	30.595	-0.065	-0.213%
7.24	30.606	-0.054	-0.175%
8.94	30.571	-0.089	-0.290%
9.53	30.548	-0.112	-0.366%
Axial Average	30.546 ($\sigma = 0.050$)	-0.114	-0.370%

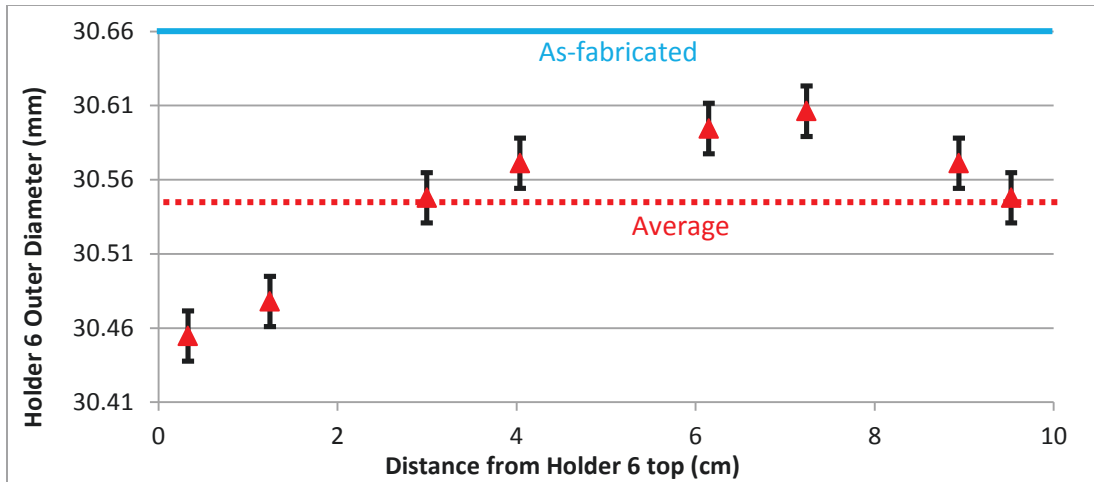


Figure 56. OD measurements from 0° azimuth image of the Capsule 6 graphite holder.

Holder 6 hole IDs are presented in Table 17 and plotted in Figure 57. Most values are within the tolerance range where no conclusions can be made as to irradiation-induced change. However, all three holes apparently shrank near the top of Holder 6 and the axial profile of Figure 57 strongly resembles the Holder 6 OD shrinkage profile in Figure 56. Assuming irradiation-induced hole deformation is related to OD deformation would suggest that the Holder 6 holes shrank over their entire lengths.

Table 17. Hole diameters in Capsule 6 graphite holder (drawing tolerances 12.395 to 12.446 mm).

Axial Position (cm from top)	Hole 1 (mm)	Hole 2 (mm)	Hole 3 (mm)
1.27	12.390	12.390	12.377
3.81	12.416	12.416	12.396
6.35	12.422	12.416	12.416
8.89	12.416	12.422	12.403
Hole Averages	12.411	12.411	12.398
Grand Average	12.4065 mm ($\sigma = 0.0141$ mm)		

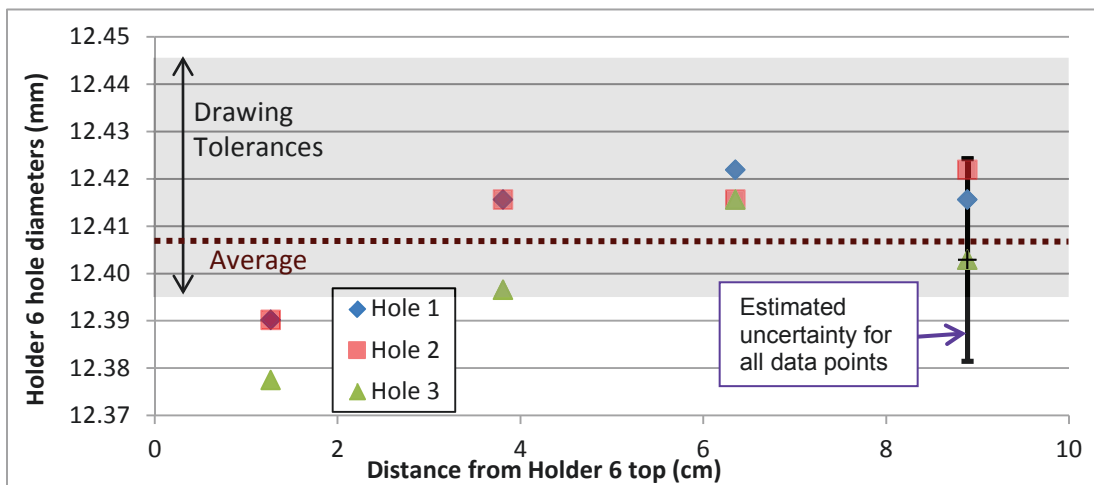


Figure 57. Hole IDs measured inside the Capsule 6 graphite holder (all ± 0.0214 mm).

4.5.7 Graphite Holder Comparisons

Absolute ODs for the AGR-2 graphite holders are displayed in Figure 58, excepting the crack-distorted values near the top of Holder 3. Comparing PIE ODs to as-fabricated ODs reveals that all four holders from inner capsules expanded while the outer two holders shrank. Holder 2 expanded the least among the four inner capsules, which may be related to its higher operating temperature. Comparing PIE results to Table 1 reveals no obvious relationship between holder deformation and B_4C concentration. Because as-fabricated ODs varied, relative OD changes are shown in Figure 59. Holder 6 shrank most at the top of the AGR 2 test train, while Holder 1 shrank most near its bottom. Meanwhile, Holders 5, 4, and 2 all exhibit a trough shape with more expansion toward their ends. Holder 3 might also have shown more of this configuration had not its upper region been distorted by the handling fracture. The origin of these holder end effects is currently not understood. Nevertheless, these effects are authentic because a nearly identical pattern is seen for AGR-1 holders in Figure 60 (although AGR-1 deformations were roughly twice as large).

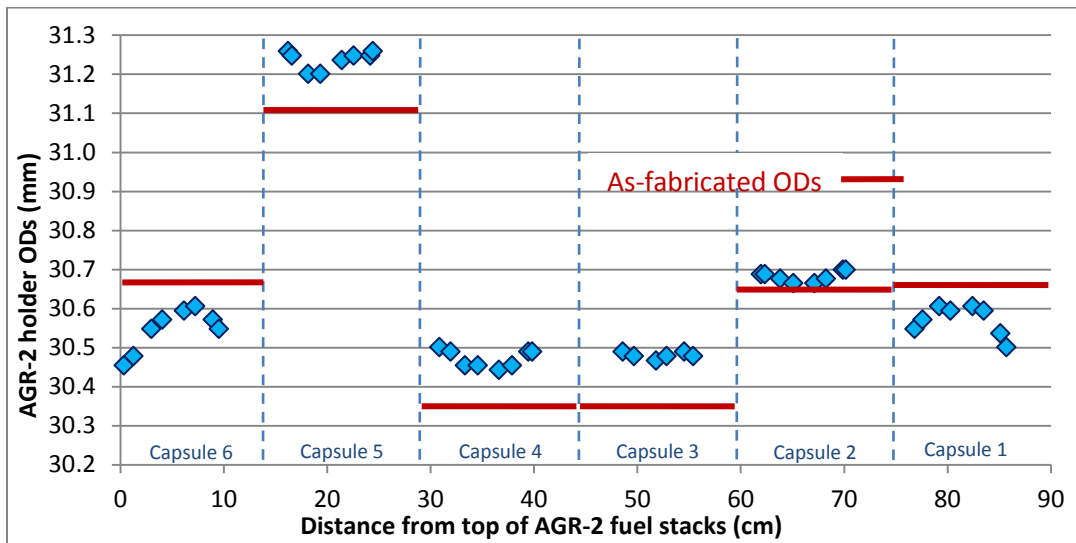


Figure 58. Graphite holder ODs as a function of elevation within the AGR-2 test train.

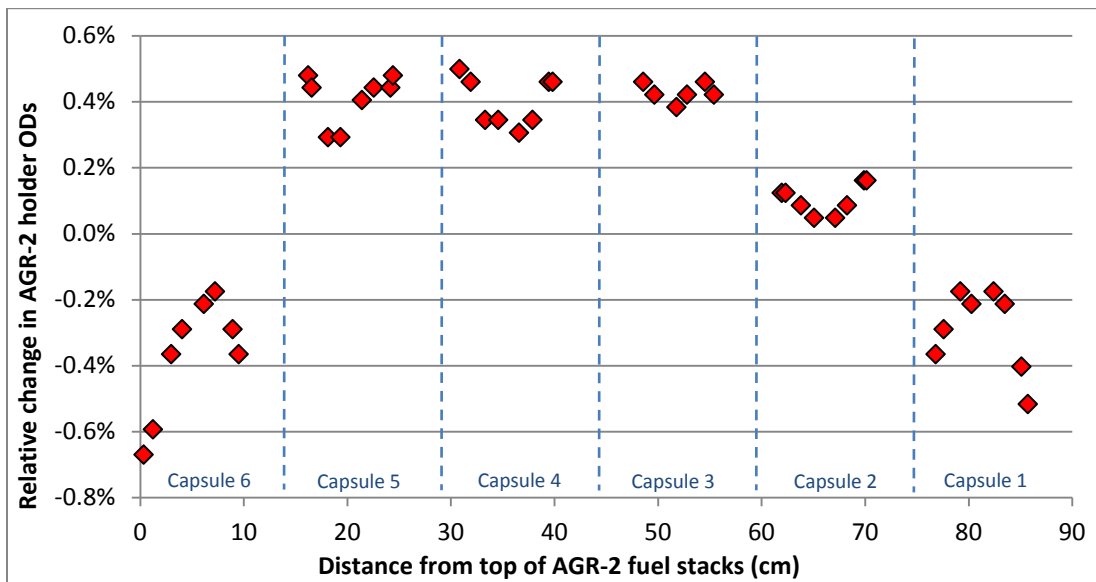


Figure 59. Relative changes in ODs of AGR-2 graphite holders during irradiation.

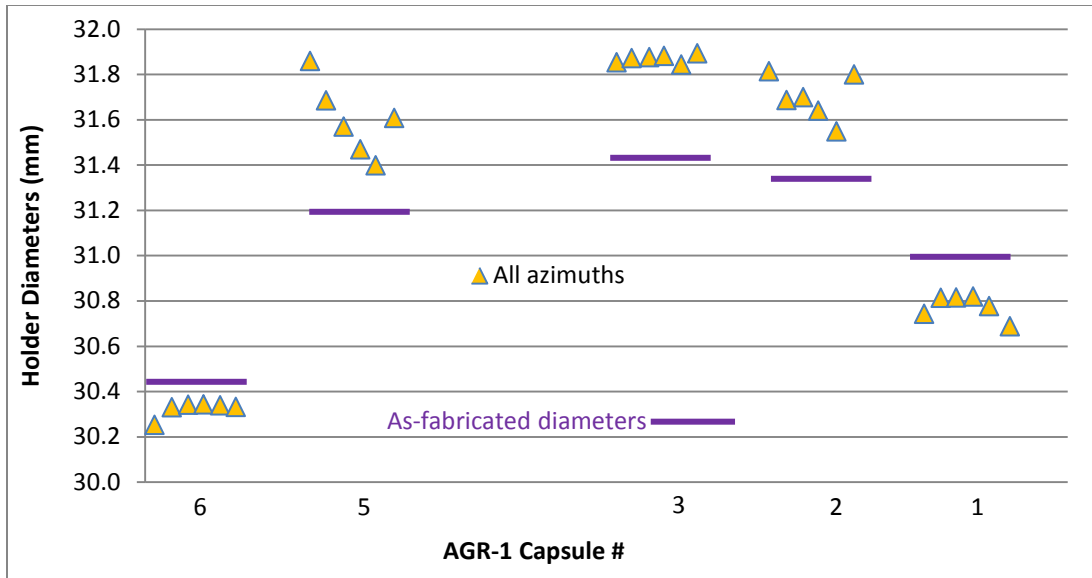


Figure 60. ODs of AGR-1 graphite holders after irradiation (Holder 4 broken during disassembly).

4.6 Capsule Shell Findings

IDs of capsule shells (interiors of their stainless steel liners) were measured with the three-anvil, self-centering bore gauge shown in Figure 61. This bore gauge is very similar to the one for graphite holder holes (see Figure 45) but has a larger diameter probe head and extension shaft. The probe was inserted into each shell according to fiducial marks on the bore gauge shaft. Depths were chosen to span the axial regions occupied by graphite holders. All large bore gauge readings were relative to the 32.004-mm (1.260-inch) ring gauge standard. Before any readings were taken on any AGR-2 shell, the bore gauge dial was rotated once to “0” with the probes extended inside the standard to null the gauge. The dial was then locked and not rotated again. However, readings were taken inside the standard before and after measuring each shell to compute an average bias (zero drift). Each absolute ID value was then calculated by adding the average bore gauge reading from each position to the standard value and finally subtracting the average bias value. AGR-2 shell ID results are presented in Table 18 and plotted in Figure 62. Each data entry represents an average of two measurements (sequence repeated after withdrawing probe head and wiping probe anvils). Negative change values indicate reduction from as-fabricated inner diameters.

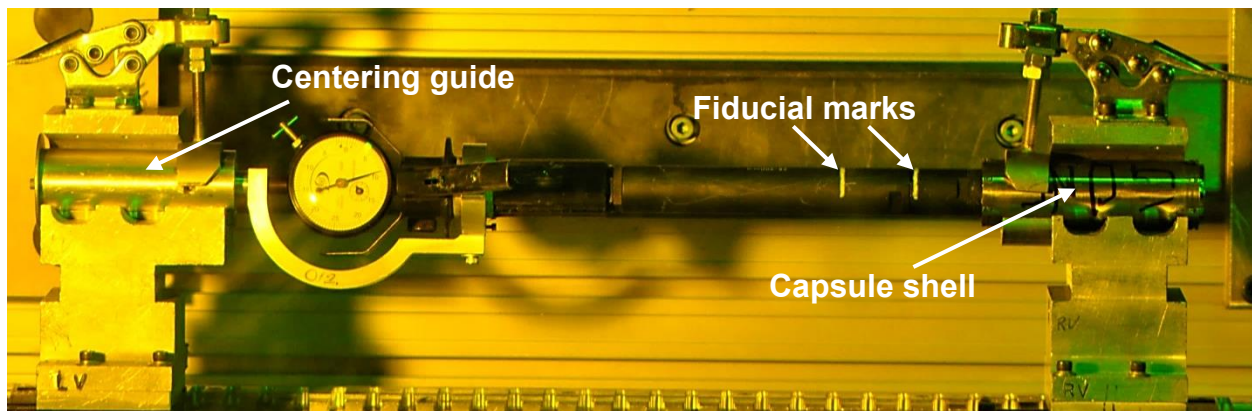


Figure 61. AGR-2 capsule shell ID being measured by large bore gauge.

Table 18. Capsule shell ID measurements and changes from as-fabricated values.

Shell #	As-fabricated ID (mm)	Bore Gauge Probe Depth (cm)	ID (mm)	ID Change (mm)	ID Change (%)
1	31.93	2.3	31.83	-0.10	-0.33%
		6.1	31.75	-0.18	-0.56%
		9.9	31.78	-0.15	-0.48%
		Axial Average	31.78	-0.15	-0.46%
2	32.03	2.3	31.86	-0.17	-0.54%
		6.1	31.77	-0.26	-0.81%
		9.9	31.88	-0.15	-0.48%
		Axial Average	31.83	-0.20	-0.61%
3	31.93	2.3	31.64	-0.29	-0.90%
		6.1	31.60	-0.33	-1.02%
		9.9	31.78	-0.15	-0.48%
		Axial Average	31.67	-0.26	-0.80%
4	31.93	2.3	31.74	-0.19	-0.60%
		6.1	31.62	-0.31	-0.96%
		9.9	31.78	-0.15	-0.46%
		Axial Average	31.71	-0.22	-0.68%
5	31.90	2.3	31.78	-0.12	-0.36%
		6.1	31.66	-0.24	-0.75%
		9.9	31.80	-0.10	-0.32%
		Axial Average	31.75	-0.15	-0.48%
6	31.93	2.3	31.70	-0.23	-0.72%
		6.1	31.65	-0.28	-0.88%
		9.9	31.66	-0.27	-0.84%
		Axial Average	31.67	-0.26	-0.82%

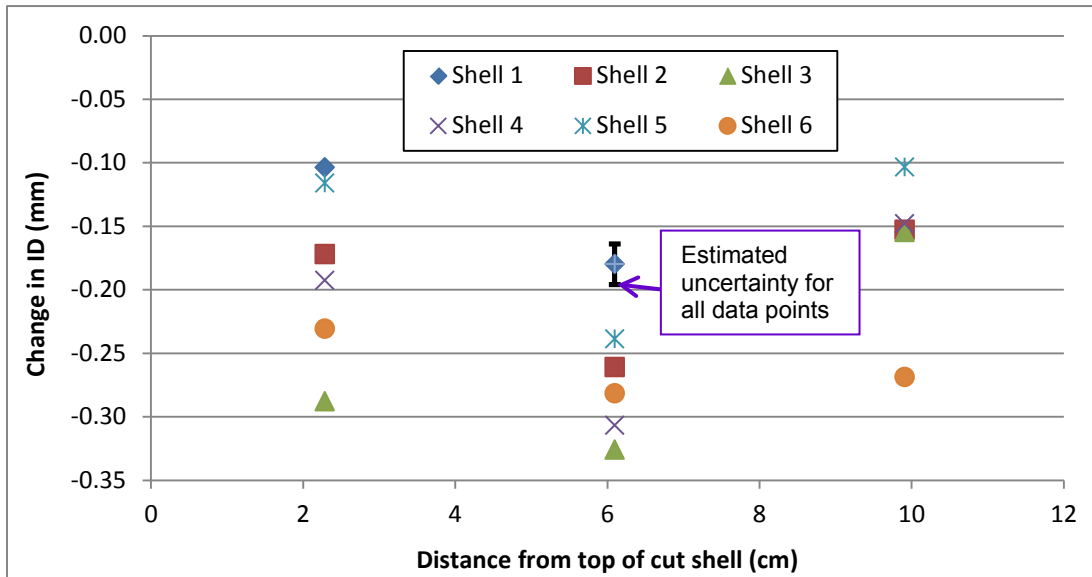


Figure 62. ID reductions (all ± 0.0160 mm) inside AGR-2 capsule shells.

The error bar in the middle of Figure 62 is a ± 0.0160 -mm combined standard uncertainty and applies to all 18 data points. It was estimated by root-sum-squaring a bias term and a repeatability term. The bias

term was chosen according to the bore gauge's resolution—the dial indicator's 0.0005-inch (0.0125-mm) graduation spacing. This value also represented the amount by which the ring gauge standard checks often changed before and after measurements were made on a given shell. The 0.0100-mm repeatability term is the standard deviation of ten independent readings in the ring gauge standard where the standard fixture was unloaded and reloaded between readings. Note that 0.0160 mm is appreciably less than the 0.0254-mm AGR-1 combined standard uncertainty requirement.

Examination of Table 18 and Figure 62 reveals substantial reductions from as-fabricated IDs at all three axial locations in all six shells. Shells 3 and 6 exhibited the largest average decreases while Shells 1 and 5 had the smallest decreases, so position within the AGR-2 test train was not a major factor in this regard. ID reductions were somewhat greater toward the middle of all six shells.

Visual inspection of shell interiors found no signs of inward buckling of the liners or failure of the tack welds that attached them to the shell bodies. Instead, unknown deposits of varying appearance were observed (except at through tube positions), as also seen inside AGR-1 shells (Demkowicz et al. 2011). Photographs were taken of all shell interiors through the hot cell window with the exception of Shell 5 (camera not available). Two examples are provided in Figure 63, where thicker regions with visible texture resemble patches found on some AGR-2 graphite holders (e.g., Figure 40). Loose fragments found on upper sides of some holders after shell removal may have been dislodged from shell interiors.

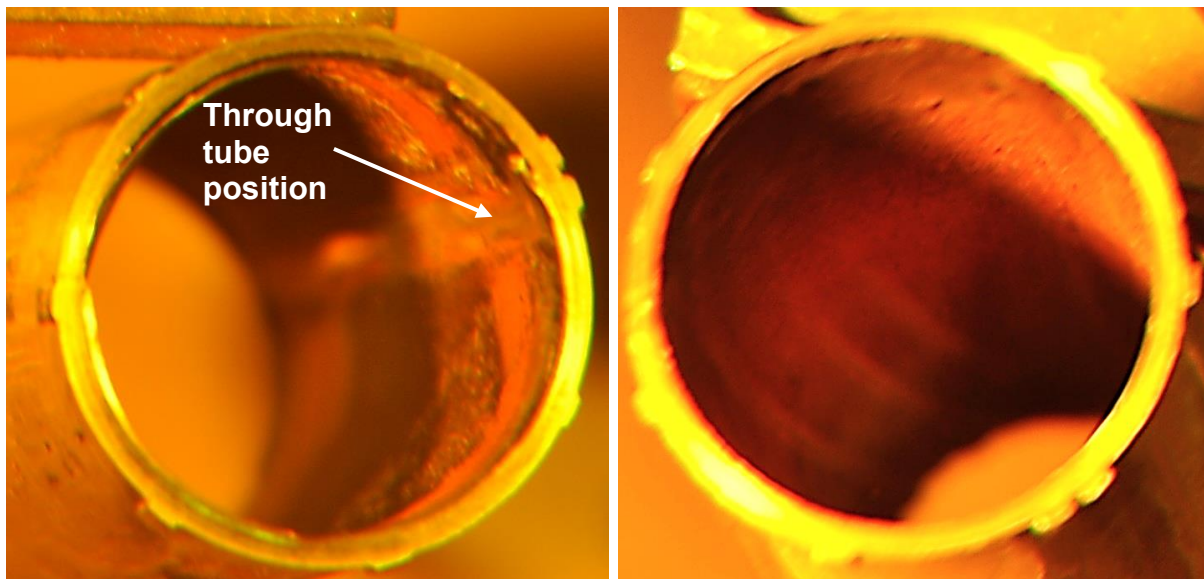


Figure 63. Deposits of unknown material throughout interiors of AGR-2 Shell 3 (left) and Shell 2 (right).

Such deposits were also conspicuous on the interior sides of AGR-2 capsule heads and capsule floors, as was also the case during AGR-1 PIE. Examples of both are shown in Figure 64.

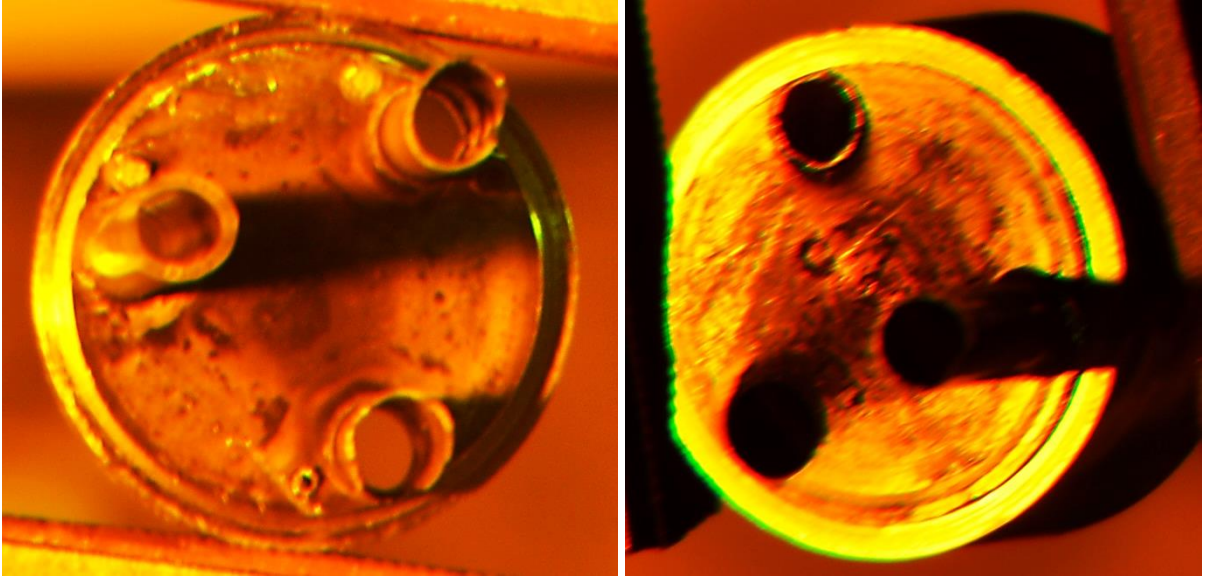


Figure 64. Dark deposit patches on insides of AGR-2 Capsule 2 head (left) and Capsule 6 floor (right).

5. CONCLUSIONS

- The AGR-2 disassembly and metrology campaign was completed rapidly and economically by reusing AGR-1 equipment and by employing basic approaches and tools that evolved during the AGR-1 campaign. The only major difficulty encountered in AGR-2 disassembly was related to larger TC wires than used in the AGR-1 test train, which was promptly overcome with new tooling.
- AGR-2 fuel compacts and their graphite holders were generally in better condition after disassembly than their AGR-1 counterparts, which reflects lessons learned during AGR-1 disassembly.
- Performing AGR-2 metrology imaging after all AGR-2 capsules had been disassembled successfully reduced radiation dose to the metrology lens and camera and permitted all AGR-2 images to be captured with a single camera (as compared to three cameras for AGR-1 metrology).
- No quantitative requirements on measurement uncertainty were imposed for AGR-2 metrology to allow for potential degradation between the AGR-1 and AGR-2 campaigns. Nevertheless, in-cell performance checks with in-cell standards established that the demanding AGR-1 uncertainty requirements were still satisfied during AGR-2 metrology.
- All fuel compacts from AGR-2 Capsules 2, 3, 5, and 6 shrank both radially (0.8% to 1.7%) and axially (0.1% to 0.9%) during irradiation. (Results from Capsules 1 and 4 are restricted proprietary information.)
- More shrinkage (especially radial) was measured on Capsule 2 compacts that experienced higher average temperatures during irradiation.
- Less axial shrinkage was measured on Capsule 3 compacts, which might be related to the larger size of particles and their lower packing fraction in this capsule.
- Capsule 6 compacts received much smaller fast neutron fluence than Capsule 5 compacts, but radial and axial shrinkage was nearly identical for these two batches of compacts. Thus fast fluence was not a major factor in AGR-2 compact deformation differences.
- AGR-2 graphite holders from bottom Capsule 1 and top Capsule 6 shrank radially during irradiation by amounts ranging from approximately 0.2% to 0.6%. Both holders shrank more toward their ends, especially at the bottom and top of the AGR-2 test train where neutron fluence was lowest.
- AGR-2 graphite holders from interior Capsules 2, 3, 4, and 5 all expanded radially during irradiation by amounts ranging from approximately 0.1% to 0.5%. All four of these holders appeared to expand somewhat more toward their ends. The Capsule 2 graphite holder expanded the least, possibly as a consequence of higher operating temperature.
- The substantial difference in holder deformation behavior between end Capsules 1 and 6 and interior Capsules 2 through 5 is not directly attributable to differences in B_4C concentration, which was very similar between the Capsule 6 holder and the holders from Capsules 3 and 4.
- Although reliable bore gauge measurements were made in all holder holes after unloading fuel compacts, conclusions on dimensional change were inhibited by the way as-fabricated measurements were made. Nevertheless, it is clear that the holes enlarged in the holders from Capsules 3, 4, and 5.
- A trend was observed for axial hole ID profiles to follow axial holder OD profiles.
- Bore gauge measurements inside lined capsule shells found significant ID reductions in all six shells. This was caused by deposit accumulations of unknown material that were somewhat thicker toward the middle of the shells. Similar material was also observed on interior surfaces of capsule heads and floors, as well as on outsides of graphite holders.

6. REFERENCES

- ANSI/NCSL Z540-2-1997, *U.S. Guide to the Expression of Uncertainty in Measurement*, NCSL International, October 9, 1997.
- PLN-3636, Rev. 3, "Technical Program Plan for the Very High Temperature Reactor Technology Development Office/Advanced Gas Reactor Fuel Development and Qualification Program," May 5, 2014.
- Collin, Blaise P., 2011, *AGR-2 Irradiation Experiment Test Plan*, Rev. 1, PLN-3798, October 2011.
- Collin, Blaise P., 2014, *AGR-2 Irradiation Test Final As-Run Report*, INL/EXT-14-32277, August 2014.
- Demkowicz, Paul, Lance Cole, Scott Ploger, Philip Winston, 2011, *AGR-1 Irradiated Test Train Preliminary Inspection and Disassembly First Look*, INL/EXT-10-20722, January 2011.
- Demkowicz, Paul A., 2013, *AGR-2 Post-Irradiation Examination Plan*, PLN-4616, December 2013.
- Hunn, John D., Fred C. Montgomery, and Peter J. Pappano, 2010a, *Data Compilation for AGR-2 UCO Variant Compact Lot LEU09-OP2-Z*, ORNL/TM-2010/017, Rev. 1, February 2010.
- Hunn, John D., Fred C. Montgomery, and Peter J. Pappano, 2010b, *Data Compilation for AGR-2 B&W UO₂ Compact Lot LEU11-OP2-Z*, ORNL/TM-2010/055, Rev. 1, March 2010.
- Hunn, John D., Traig W. Savage, and G.W. Chinthaka Silva, 2010c, *AGR-2 Fuel Compact Pre-Irradiation Characterization Summary Report*, ORNL/TM-2010/226, November 2010.
- Ploger, Scott A., 2010, *Qualification of AGR-1 Metrology System*, ECAR-900, Rev. 2, September 2010.
- Ploger, Scott A., 2012, *AGR-2 PIE Equipment for HFEF*, TEV-1650, November 26, 2012.
- Ploger, Scott A., 2014a, *Extracting Dimensions from AGR Component Images*, LI-463, Rev. 1, Oct. 13, 2014.
- Ploger, Scott A., 2014b, *AGR-2 Metrology*, HFEF-LI-0032, Rev. 2, November 4, 2014.
- Scott, Lester W., 2014, *AGR-2 Disassembly*, HFEF-LI-0031, Rev. 2, November 4, 2014.

Appendix A

Proprietary Results on Capsule 1 Fuel Compacts

Distribution of this appendix is restricted because of proprietary information constraints in the associated Cooperative Research and Development Agreement.

Appendix B

Proprietary Results on Capsule 4 Fuel Compacts

Distribution of this appendix is restricted because of proprietary information constraints in the associated Cooperative Research and Development Agreement.